Spring 4-27-2014

Oxygen Polarography in the Awake Macaque: Bridging BOLD fMRI and Electrophysiology

William Joseph Bentley
Washington University in St. Louis

Washington University in St Louis

Division of Biology and Biomedical Sciences
Neurosciences

Dissertation Examination Committee:
Lawrence Snyder, Chair
Joseph Culver
Timothy Holy
Steve Petersen
Marcus Raichle
Abraham Snyder

Oxygen Polarography in the Awake Macaque: Bridging BOLD fMRI and Electrophysiology

By
William Joseph Bentley

A dissertation presented to the
Graduate School of Arts and Sciences
of Washington University in
partial fulfillment of the
requirements for the degree
of Doctor of Philosophy

May 2014

Saint Louis, Missouri

Table of Contents

List of Figures:

Acknowledgments

My grandfather holds a PhD in education, my mother in business, and my father in physics. They supported both my personal and scientific development from day one. Dr. George Mandeville listened to my objection to high school science being taught as dogma and helped institute a curriculum focused on the empirical basis of scientific facts. Chris Olstad, the biologist for the Marinelab habitat, spent hours with me, underwater, in the habitat, discussing the balance of oxygen supply and demand in a closed system. Drs. David Williams, David Sheinberg, Jerome Sanes, James Simmons, Andrew Holowinsky and Stephen Sheinkopf helped guide my undergraduate education, clarify my scientific interests and point me to graduate school. Drs. Marcus Raichle and Avi Snyder played seminal roles in the inception of this project and my early graduate directions. Drs. Steve Petersen, Tim Holy and Joseph Culver, the other members of my thesis committee, provided exceptional guidance along the way. Jingfeng Li joined the project as a collaborator and injected new insight and energy. Finally, I don't think I could have found a better mentor than Dr. Lawrence Snyder.

My thesis represents the culmination of years of scientific training and would not exist without a long line of named and unnamed personal and professional collaborators and mentors. This list is too long and the support those on it have provided too great to describe in detail. I would like to thank all of you and hope that you know who you are. I would also like to thank the McDonnell Foundation, the National Institute of Health, the Washington University Division of Biology and Biomedical Science, and the Department of Anatomy and Neurobiology for funding my graduate studies.

ABSTRACT OF THE DISSERTATION

Oxygen Polarography in the Awake Macaque:
Bridging BOLD fMRI and Electrophysiology

by
William Joseph Bentley
Doctor of Philosophy in Biology and Biomedical Sciences
Neurosciences
Washington University in St Louis, 2014
Professor Lawrence Snyder, Chair

Blood oxygen level dependent (BOLD) fMRI is the predominant method for evaluating human brain activity. This technique identifies brain activity by measuring blood oxygen changes associated with neural activity. Although clearly related, the nature of the relationship between BOLD fMRI identified brain activity and electrophysiologically measured neural activity remains unclear. Direct comparison of BOLD fMRI and electrophysiology has been severely limited by the technical challenges of combining the two techniques. Microelectrode electrophysiology in non-human primates is an excellent platform for studying neural activity related to high order brain function similar to those commonly studied with BOLD fMRI in humans, i.e. attention, working memory, engagement. This thesis discusses the development of, validation of, and first results obtained using a new multi-site oxygen polarographic recording system in the awake macaques as a surrogate for BOLD fMRI. Oxygen polarography measures tissue oxygen which is coupled to blood oxygen. This tool offers higher resolution than BOLD fMRI and can be more readily combined with electrophysiology.

Using this new tool we evaluated local field potential and oxygen responses to an engaging visual stimulus in two distinct brain systems. In area V3, a key region in the

visual system and representative of stimulus driven sensory cortex, we show increased tissue oxygen and local field potential power in response to visual stimulus. In area 23 of the posterior cingulate cortex (PCC), a hub of the default-mode network we show decreased oxygen and local field potential in response to the same stimulus. The default-mode network is a set of brain regions identified in humans whose BOLD fMRI activity is higher at rest than during external engagement, arguing that they sub-serve a function that is engaged as the “default-mode” in humans.

Our results provide new evidence of default-mode network activity in the macaque similar to that seen in humans, provide evidence that the BOLD identified default-mode suppression reflects neural suppression and overall support a strong relationship between neural activity and BOLD fMRI. However, we also note that the LFP responses in both regions show substantial nuances that cannot be seen in the oxygen response and suggest response complexity that is invisible with fMRI. Further, the nature of the relationship between LFP and oxygen differs between regions.

Our multi-site technique also allows us to evaluate inter-regional interaction of ongoing oxygen fluctuations. Inter-regional correlation of BOLD fMRI fluctuations is commonly used as an index of functional connectivity and has provided new insight into behaviorally relevant aspects of the brain’s organization and its disruption in disease. Here we demonstrate that we can measure the same inter-regional correlation using oxygen polarography. We utilize the increased resolution of our technique to investigate the frequency structure of the signals driving the correlation and find that inter-regional correlation of oxygen fluctuations appears to depend on a rhythmic mechanism operating at ~0.06 Hz.

Chapter 1: Introduction

Overview

Since its initial demonstration by Ogawa et al, blood oxygen level dependent (BOLD) functional magnetic resonance imaging (fMRI), has provided an un-paralleled window into the active human brain. This technique provides a non-invasive near simultaneous view of activity in the whole brain and is used to study both task driven and ongoing intrinsic fluctuations in brain activity. Comparison of task driven brain activity under different carefully controlled conditions and the inter-regional interactions of task independent ongoing activity have both provided enormous insight into the functional structure of the human brain. [1-5]

However, BOLD fMRI is an indirect measure of neural activity. Fox and Raichle demonstrated that when neural activity in a brain region is increased by a task, there is commonly an increase in local blood oxygen[6], and thus in the BOLD signal. [7] Stimulus driven increases in neural activity increase metabolic demand, and thus consumption of oxygen. However, the increase in activity is also generally accompanied by an increase in blood flow. The increase in supply overwhelms the increased consumption leading to an increase in local blood (or brain) oxygen. This increase in local blood oxygen can be detected by BOLD fMRI. BOLD measures the hemodynamic changes (metabolic/vascular balance) accompanying neural activity. It is commonly expected that the BOLD response is a linear reflection of some facet of neural activity. [6-12]

Despite strong evidence that stimulus driven neural activity is commonly associated with hemodynamic changes there remains significant controversy about the neural BOLD relationship. The stability of the relationship across cortex, tasks, or response types is largely unknown. For example, the hemodynamic response efficiency, magnitude of a BOLD response to a given neural response, might vary across cortex. [13-19] There is also concern that BOLD responses may not always reflect neural activity or conversely that neural activity may not always result in hemodynamic changes detectable with BOLD.[20-23] Further, in contrast to BOLD increases discussed above, we know very little about commonly observed decreases in the BOLD signal. They could reflect increased neural activity without an increase in blood flow, or sustained neural activity in the face of shunting of blood flow to more active stimulus driven cortex, or they could truly reflect suppression of neural activity and coincident undershoot of blood flow. [24-26] Finally, although a relationship has been shown, almost nothing is known about the neural correlates of ongoing fluctuations in the BOLD fMRI signal or the mechanisms driving their inter-regional correlation.[24, 25, 27-30]

Efforts to evaluate the relationship between neural activity and BOLD, or between electrophysiological and hemodynamic measures of neural activity, have taken two paths. A large body of research, (reviewed in [25, 31]), has identified a long list of mechanisms through which neural activity can influence metabolism and or vascular tone and thus impact the BOLD signal. At present this set of potential neural-BOLD links has not produced a comprehensive model that describes the neural-BOLD relationship or can reliably predict one signal from the other. While this set of mechanisms strengthens the argument that BOLD fMRI and neural activity are tightly

related, it does not clarify the nature of the relationship. In fact it suggests that there may not be a direct relationship, with independent inputs driving neural and vascular responses in parallel. [25] Further, this work has been done primarily in anesthetized rodents, limiting its power to aid in interpretation of BOLD fMRI study of high order brain functions in awake humans. Tissue oxygen recording in the awake macaque in combination with drug manipulations of the mechanisms seen in rodents and task-state or behavioral manipulations would significantly extend this work.

A small body of work has directly compared electrophysiological and BOLD measurement of brain activity. Short of knowing the mechanistic link between neural activity and BOLD, direct comparison provides invaluable insight into the nature of the relationship. This small body of work is exceptional and provides strong support for a neural bold link. However, despite significant efforts, only a handful of papers directly comparing electrophysiological and BOLD data exist. Further, the details of how electrophysiological activity relates to BOLD fMRI vary across studies. [26, 30, 32-37]

Direct comparison of BOLD and electrophysiology has been severely limited by technical challenges. The powerful and changing magnetic fields of fMRI and sensitive, often metal and electrically active electrophysiological recording equipment fundamentally interfere with each other. To some degree this interference can be controlled for with active and passive shielding and its remaining impacts modeled and regressed from the data. However, interference driven artifacts result in substantial loss of data quality. ([37], personal communication Drs. Katy Chang and Linda Larson-Prior) Comparison of BOLD fMRI and electrophysiology is further limited by substantial mismatches in the resolution of the two techniques. Finally, with a few exceptions,

comparison of BOLD and invasive electrophysiology has been done in primary sensory cortex of anesthetized animals.[38] Anesthesia by definition alters brain function, and primary sensory areas may not be representative of the whole brain.[13]

The gold standard for directly studying neural activity supporting the high order behaviors studied with BOLD fMRI in humans, is microelectrode electrophysiology in awake behaving macaques. These animals are capable of learning complex behaviors similar to humans but do not appear to possess enough self-awareness to preclude invasive use. Awake macaque fMRI is possible, enabling potential serial comparison of BOLD and electrophysiology in response to tasks or stimuli.[39] However, awake macaque fMRI is exceptionally difficult and combining awake animal imaging with electrophysiology is exponentially more so. Of particular note, animal movement disrupts the stable magnetic fields needed for BOLD fMRI and can move electrophysiological recording equipment. Movement of electrical recording equipment in the strong magnetic field BOLD fMRI environment induces complex artifacts that cannot be easily shielded against or regressed out.

Given the importance of the awake macaque model and difficulties combining electrophysiology and BOLD fMRI in awake macaques and the resulting limitations on active study, an alternative less technically demanding platform for comparing BOLD fMRI related and electrophysiological signals in awake macaques would greatly facilitate our understanding of the relationship of these two measures of brain activity. Oxygen polarographic recording can provide this platform. Polarography is an electrode based technique that can be readily integrated into the standard macaque experimental setup and recorded alongside electrophysiology without interference. Since blood and

tissue oxygen are in equilibrium, oxygen polarography is sensitive to the same changes in oxygen supply and demand reflected in BOLD fMRI, and is a reasonable surrogate.

Oxygen polarography has a long and continued presence in neuroscience. Oxygen polarographic studies in neurosurgical patients in the 1960's may have been the first demonstration of task related increases in local oxygen now studied with BOLD fMRI. Recent work by the Freeman group has provided insight into differences in the spatial scale of neural and hemodynamic responses and into the role of synaptic vs. spiking activity in driving the neural activity related oxygen changes.[40-48]

Unfortunately, historical polarographic work was done with custom systems that cannot be recreated from published materials. Recent polarographic work and commercially available polarographic systems rely on specialized polarographic electrodes, Clark electrodes. These electrodes are suitable for acute experiments in small, anesthetized animals, however, they are too short and fragile for use in awake monkeys. In order to implement oxygen polarography in the awake macaque development of a monkey specific system was required. Development is discussed in chapter 2.

To provide a reasonable surrogate for BOLD fMRI an oxygen polarographic system must be able to allow study of both task-driven oxygen changes and long-range inter-regional interactions of oxygen fluctuations. The system I designed is based around microelectrodes conditioned for oxygen recording. Currently our hardware allows simultaneous recording from 4 oxygen sensitive electrodes with spacing of 0.5 mm and

greater. This is sufficient to study stimulus responses and inter-regional interactions of ongoing activity. Electrodes can be targeted anywhere in the brain.

Further, the system should provide easier implementation than awake animal BOLD fMRI and be readily combined with electrophysiology. This system can be integrated into the standard macaque recording setup and is robust to animal movement. Thus it allows standard macaque behavioral control. This system is far easier to implement under a range of behavioral conditions, including the resting state, in awake animals than BOLD fMRI. The system is capable of recording fluctuations in tissue oxygen with a temporal resolution of 20 samples/s and a spatial specificity of 30-100 microns.[49] This is dramatically closer to the resolution of electrophysiological recording than possible with BOLD fMRI, and much closer to the scale of neural architecture and activity, i.e. cortical columns. Higher resolution and improved location matching allows much more direct comparison of polarographic and electrophysiological recordings than is possible with BOLD fMRI.

Finally, electrophysiology and oxygen can be recorded from neighboring electrodes simultaneously without interference. For exact co-localization the microelectrodes utilized for this technique can also be used to record electrophysiology. Serial recording of electrophysiology and oxygen from the same electrode allows perfect co-localization of the two signals. In summary, with this system, awake macaque oxygen polarographic recording is far easier to implement in awake animals, provides higher resolution, and allows more direct comparison of hemodynamic and electrophysiological signals under a wider range of behavioral conditions than is possible with BOLD fMRI.

The primary drawback of this system compared to BOLD fMRI is loss of coverage. Coverage and resolution of our system is determined by how close and how many electrodes we can place. Four electrodes are sufficient to study most relevant phenomena, including inter-regional interaction. However, for increased coverage, the basic elements of the designed system, electrodes and electronics, could be readily replicated and the system expanded to more sites. For higher resolution, electrode placement hardware can be adapted to allow closer spacing.

Using this system we recorded visually driven oxygen and co-localized electrophysiology (serially from the same electrode) in two very different neural systems with very different task driven human BOLD fMRI responses, the visual system (area V3) and the default mode system (posterior cingulate). The default-mode network is a set of brain regions identified in humans whose BOLD fMRI activity is higher at rest than during external engagement, arguing that they sub-serve a function that humans engage as a "default-mode". Our results overall support a strong relationship between oxygen and neural activity in both systems and add to our understanding of the general relationship between neural and BOLD activity.

As expected for a visual area, in response to 15 s of stroboscopic illumination area V3 showed increased oxygen levels and overall increased neural activity. However, low frequency local field potential power was suppressed. Both the increase in neural activity and this suppression were strongly correlated with oxygen modulation suggesting that the neural oxygen relationship, while strong, is not always straightforward.

Consistent with human default mode network behavior, the posterior cingulated, (PCC), showed suppression of both neural activity and oxygen levels in response to the same stimulus. Our results provide new evidence that the macaque's default mode network behaves similarly to that seen in humans and are the first direct comparisons of electrophysiological and hemodynamic activity in the default mode network. Our results argue that the default mode network suppression identified with BOLD fMRI is reflective of suppression of neural activity. Local field potential, (LFP), power at all frequencies in PCC is suppressed and highly correlated with oxygen suppression. However, our LFP results also show multiple LFP timecourses in PCC and suggest multiple suppressed neural processes in PCC.

In addition, analysis of the mathematical relationship between oxygen and neural activity argues that the relationship differs between regions. The presence of multiple LFP waveforms, or neural processes, in both regions, the potential differences in the relationship of these processes to oxygen activity, and the apparent difference in the neural oxygen relationship between regions open many new lines of inquiry into the nature of the processes in V3 and PCC, the nature of the suppressed "default" processes in PCC, and which processes are best reflected in hemodynamic signals. These experiments are discussed in chapter 3.

We also evaluated inter-regional interactions of ongoing oxygen fluctuations. We confirm that we can measure the same inter-regional interactions studied with BOLD fMRI. These results are in large part a proof of concept and demonstrate that our technique meets a major design goal: the ability to study inter-regional interaction of ongoing fluctuations in tissue oxygen. Utilizing the greater spectral resolution of our

technique compared to BOLD, we demonstrate that inter-regional correlation of oxygen fluctuations only occurs in a band-limited frequency range, and argue that correlation reflects rhythmic activity at ~0.06 Hz. Further, since the spatial scale of our technique is much finer than commonly used with BOLD fMRI, we argue that inter-regionally related ongoing fluctuations reflect a moderately uniform and dominant regional signal. In contrast, it was possible that inter-regionally correlated activity was visible with fMRI due to averaging over larger volumes and would be overwhelmed by local activity at our spatial scale. These results are presented in chapter 4.

The results presented here are novel and compelling however, they are just the beginning. Having established the motivation for, validity of and power of our polarographic technique we conclude with discussion of the new experiments we have begun and future experiments that our new system enables. Before discussing the development of our system in chapter 2 and results in chapters 3 and 4, it is worthwhile to review a sampling of relevant background literature and to further elaborate the argument for and benefits of using oxygen polarography as a surrogate for BOLD fMRI.

Background

Bold:

Blood oxygen level dependent (BOLD) functional magnetic resonance imaging (fMRI) is a ubiquitous tool in systems neuroscience. This technique measures hemodynamic changes thought to be associated with neural activity. In general BOLD fMRI in humans provides images covering the whole brain with a spatial resolution of millimeters and a temporal resolution of seconds providing a well-localized, non-invasive view of whole brain function. [3] Due to these features, BOLD fMRI is our

primary window into the location and structure of brain activity related to human behavior. Its uses include real time biofeedback [50, 51], assessment of inter-regional interactions and information distribution among brain regions [52, 53], decoding of brain activity using multi-voxel pattern analysis to compare ongoing activity to classifiers identified under stimulated conditions [54], clinical applications [55], including identifying eloquent cortex before neurosurgery [56, 57], and identification of disease relevant distortions in organization or function. [2] Perhaps most prominently, BOLD fMRI has allowed significant progress in parsing the architecture and spatial location in the brain of neural processes underlying human cognitive behaviors (for example, [58]). (See below for deeper discussion of the origin of the BOLD signal, chapter 2, and its relationship to neural activity, below.)

BOLD fMRI studies can in general be split into two types [59]: studies that evaluate carefully controlled task or stimulus driven changes in the BOLD fMRI signal and studies that investigate structure in ongoing, task-independent, fluctuations in the BOLD fMRI signal. Careful comparison of the pattern of task driven BOLD activity under different task conditions has provided insight into both the localization of brain functions and the architecture of the brain itself. The pattern of brain activity can be used to adjudicate on whether or not two tasks depend on similar or different brain regions. This in turn has implications for whether or not similar processes are involved. In addition to clearly task driven signals, the BOLD fMRI signal also shows apparently un-driven fluctuations that are highly correlated among functionally related regions. The time-course of these fluctuations and the pattern of their inter-regional temporal dependence have both been linked to variability in continuous behavior, inter-individual

differences in ability and aberrant brain function with disease. The inter-regional relationships indicated by the correlation of these apparently un-driven fluctuations are thought to reflect the functional organization of the brain, or its functional connectivity. [1, 2, 7, 12, 60-73] Given the ubiquity of BOLD fMRI a full review is unwarranted. More to the point we will review electrophysiological measurement of neural activity, efforts to relate BOLD and neural activity, the history of oxygen polarography in neuroscience and as a prelude to chapters 3 and 4, the default mode of brain function and the significance of BOLD fMRI functional connectivity analyses.

Electrophysiological Measurement of Neural Activity:

Electrophysiology is the measurement of the electrical activity of neurons. The electrical potentials generated at synapses and along dendrites and the generation of action potentials result in both intracellular and extracellular electric fields that can be detected with a variety of techniques. The fundamental resolution of electrophysiology depends on the type of neural activity being measured. Action potentials are limited to a resolution of about 20 microns (1 neuron). Synaptic signals are limited to a single synapse or about 1 micron. The practical limits and nature of the electrical activity that can be recorded in vivo depend on the recording technique.

High resolution electrophysiological study relies on invasive techniques in animal models. Resolution of single synapses requires intracellular recording in slice preparations[74]. In vivo intracellular recording can record sub-threshold membrane voltage fluctuations and provide insight into activity of single dendrites[75]. Optical imaging of voltage sensitive dyes can simultaneously record the activity of multiple single neurons.[76, 77] Standard extracellular microelectrode recording can isolate

action potentials from single neurons. It is not possible to record single synapses using standard extracellular microelectrodes. However, local field potentials (LFP) recorded with extracellular electrodes can provide measures of population spiking and synaptic activity. High frequency (≥ 1 kHz) electrical activity is thought to reflect action potentials from multiple local neurons. These recordings are referred to as multi-unit activity (MUA). Local field potentials (lower frequency <300 Hz electrical activity) are believed to result from the spatial and temporal summation of potentials occurring at the synapses and along the dendrites of nearby neurons. The exact spatial and temporal organization of neural activity underlying LFPs is unknown. However, it is believed that LFP's recorded with standard microelectrodes represent concerted activity of neurons within a several hundred micron radius of the electrode[78]. This spatial sensitivity depends on the size and location of the electrode.

Non-invasive methods like EEG and MEG, the electrophysiological methods commonly available for human studies, record essentially the same phenomenon as LFP's, the summation of neural potentials. However, MEG and EEG record summation of neural potentials that reach the scalp. Due to the size of electrodes and the distance from the brain, the location and extent of the summed neural activity seen with these techniques can only be localized to very general brain regions. Electrocorticography in human patients in whom electrodes are placed on the brain surface for localization of epileptic foci can provide higher resolutions. This technique has greater spatial resolution and specificity than EEG. However, this technique is invasive, can only be used in an inherently small subject pool whose brain activity is known to be abnormal, is constrained to recording sites chosen by medical need without regard to experimental

value, and provides substantially less resolution than microelectrode recording in animals.

Of the possible tools and platforms for electrophysiological study of the brain, micro-electrode recording of extracellular electrical activity in the awake macaque continues to be the gold standard for studying the neural underpinnings of higher order brain functions. Due to technical constraints, intracellular and optical recording techniques cannot be readily implemented in awake macaques. However, unlike small animals in which these tools are available, macaques have brains that share substantial homology with the human brain and can be trained to perform complex tasks. These animals are not self-aware in the sense of apes or humans, or in such a way to prohibit invasive recording on ethical grounds. The awake macaque is a unique animal model allowing the closest link between invasive animal electrophysiology and human brain activity.

BOLD fMRI and Electrophysiological Measurements:

It should be clear from the above that BOLD fMRI has and continues to play an invaluable role in neuroscience and provides otherwise impossible insight into human brain function. However, since BOLD fMRI is a hemodynamic measurement and not a direct measure of neural activity, its interpretation is limited. Electrophysiological measurement can be directly tied to neural activity. However, electrophysiology often focuses on well identified electrical phenomena, like action potentials, and may miss more complicated aspects of neural population activity that are reflected in the hemodynamic signals. If one assumes that hemodynamic activity has a neural origin, linking hemodynamic measure like BOLD and electrophysiology might encourage exploration of and thus identification of relevant aspects of neural population behavior

often ignored with electrophysiology. Linking these two measures can validate and clarify the neural basis of BOLD fMRI findings in humans and may motivate greater understanding of electrophysiological activity.

Directly relating BOLD to electrophysiological measures of neural activity presents several methodological challenges. One must decide how to measure neural activity (MEG, EEG, eCOG, micro-electrode), whether or not simultaneous BOLD fMRI is possible, and whether or not to use an alternate measure of hemodynamic activity. Further, one must decide how to relate the two types of signals, and/or to what degree the signals must be transformed before comparison.

Several strategies have been employed. BOLD fMRI and micro-electrode recordings in animals, or electrocorticograpic signals from human patients, have been recorded serially in response to similar tasks and compared. BOLD fMRI and EEG have been simultaneously recorded in humans and a few labs in the world are able to simultaneously measure BOLD fMRI and electrophysiology in experimental animals including rodents and macaques. [13, 37, 79] Finally, other hemodynamic measurements that are related to BOLD fMRI can be recorded simultaneously with electrophysiology. [25]

Efforts to serially measure electrophysiology and BOLD fMRI are limited by an inherent time gap between recordings, difficulty matching recording location and stimuli, and changes in the state of the animals or patient. [22, 39] Movement of the subject in and out of the magnet and subsequent placement of recording equipment creates difficulty in co-localization of recording sites. Further, the fMRI and electrophysiological

environment have several substantial differences, including the loud sounds and movement of the fMRI environment, that lead to substantial changes in the recording environment and limit comparison. It is also often difficult to ensure that the subject's experience of stimuli used in and out of the fMRI environment is consistent. These issues are present in both animal and human serial comparisons of micro-electrode or eCog recordings and BOLD fMRI. Comparing eCog in human patients to BOLD presents further challenges. Patients with electrodes implanted for localization or epileptic foci are relatively rare and electrode locations and experimental access is limited by medical constraints. The presence of epileptogenic cortex near recording sites raises concerns about the generalizability of the results. Further, BOLD and electrophysiological recordings are at best several days apart and often before and after major surgery for implanting the electrodes.

Simultaneous BOLD fMRI and electrophysiology (EEG in humans or micro-electrode in animals) is limited by an inherent mismatch between the two techniques. The measurement techniques interfere with each other and fundamentally degrade the quality of both data types. Reliable BOLD fMRI signal detection requires stable magnetic fields and low electromagnetic interference. Standard electrophysiological recording equipment includes active electronics and can serve as an antenna for environmental noise. Both can introduce electromagnetic noise into the MRI recording environment, degrading data quality. Further, the metal hardware commonly used for electrophysiology disrupts the stability of local magnetic fields imaged with fMRI. For microelectrode recording in animals, the distortion of the BOLD signal around standard metal electrode makes tightly co-localized measurement effectively impossible.

Electrophysiological recording relies on reliable detection of millisecond order fluctuations in current and voltage. BOLD fMRI measurement utilizes strong magnetic fields, millisecond order changes in magnetic field, and microwave radio signals. The changing magnetic fields and radio signals of fMRI induce significant voltage and current artifacts in the electrophysiological measurement. Further, biological movement from heart rate and breath rate of the electrodes in the magnetic field induce current and cause artifacts. Active and passive shielding and data filtering can mitigate these issues. The interference and artifacts can be modeled and cleaned from the electrophysiological data. However, this data cleaning can significantly change the signal, and remove relevant features limiting comparison. Overall, there is a fundamental loss of signal quality compared to recording either signal alone. Signal averaging can overcome some loss of signal quality for stimulus driven BOLD fMRI electrophysiology comparisons. However, it is wholly unclear how substantial the impacts of signal distortions due to this technical interference on ongoing activity or its comparison are. [37, 80]

In a few labs EEG and microelectrode recording have been accomplished simultaneously with fMRI. [29, 30, 37, 81-85] However, even when the loss of signal quality is acceptable and electrophysiological and BOLD fMRI data are collected simultaneously, the results are not perfectly comparable. Differences in the spatial and temporal resolution of techniques limit the interpretation. Although band limited EEG power from multiple frequency bands has been shown to be related to BOLD fMRI (both stimulus driven and ongoing fluctuations), the specific neural origins of the EEG signals are generally unclear. EEG and MEG are poorly spatially localized. In contrast, the

spatial and temporal resolution of microelectrode recording is substantially greater than the resolution possible with BOLD fMRI. Relating microelectrode recording to BOLD fMRI requires substantial temporal smoothing, low-pass filtering and down-sampling, of the electrophysiological data. Smoothing blurs high frequencies differences among aspects of neural activity recorded that might otherwise be used to distinguish which aspects of neural activity best relate to BOLD fMRI.

Further, smoothing filter selection requires assumptions about the transform or nature of the neural bold relationship prior to direct comparison. In chapter 3 we provide evidence that the transform may vary between regions. Further, the transform may be different for different frequencies of neural activity. Comparison of electrophysiological and BOLD fMRI data after a transform is thus confounded. A particular relationship may appear artificially stronger or weaker depending on the accuracy of the chosen transform.

Since BOLD fMRI is distorted in the immediate vicinity of the electrode, assumptions must also be made about the spatial ubiquity of the electrophysiological data recorded from a single site. To date, microelectrode recording during BOLD fMRI has also been limited to single sites. Local electrophysiological fluctuations have been related to long-range correlated BOLD fMRI fluctuations. [27, 29, 30] However, single site recording does not allow identification of long-range neural relationships and thus limits identification of neural interactions underpinning long-range BOLD correlations. Overall, the fundamental mismatch in resolution and coverage of electrophysiological and BOLD fMRI measurements complicates comparison.

A few labs in the world have been able to perform simultaneous electrophysiology and BOLD fMRI in macaques. As a whole this work is exceptional and provides strong evidence that BOLD is generally related to neural activity. However, this work provides a complex and unfinished picture. This body of work is small, largely due to its extraordinary technical difficulty. Some argue that high frequency (gamma band, 30-150 Hz) local field potentials are the best neural correlate of BOLD fMRI. [26, 36, 37]. Some argue that low frequency LFP are a better predictor of BOLD fMRI behavior. [33] Some argue that the relationship between LFP and BOLD fMRI varies over time [30] or reflects complex features of the local field potential, multiple frequencies and cross frequency interactions. [27, 28]

With rare exception, [33, 36] direct comparison of BOLD fMRI and microelectrode electrophysiology has also been done in primary sensory cortex of anesthetized animals. Anesthesia by design interferes with neural processing of sensory input, and can influence vascular and metabolic activity. Awake macaque fMRI is possible, and in rare cases has been combined with electrophysiology. [36] However, awake macaque movement introduces complex artifacts into both electrophysiological and BOLD fMRI signals, making simultaneous awake macaque BOLD fMRI and electrophysiology even more prohibitively difficult than combing the measure in anesthetized animals.

The majority of human neuroimaging is focused on higher order cognitive processes of the awake brain. The gold standard animal model to study electrophysiological activity of higher order cognitive behaviors is the awake macaque. Awake macaque fMRI is possible. However, in addition to difficulties combining BOLD fMRI and electrophysiology, awake macaque fMRI is itself exceptionally difficult and only

performed by a handful of labs. The primary difficulty is controlling animal behavior. FMRI measurement requires subjects to remain still for extended periods. This is an unnatural task for the macaque, particularly in the loud and stimulating fMRI environment, and requires extensive training. Even with extensive training, long data recording sessions are required to get small amounts of “still” data[86]. Further, the small size of the macaque brain pushes the limits of fMRI. The animals are large enough that they cannot fit into the high field strength magnets used for rodent imaging, but at the edge of too small for human sized fMRI machines. This necessitates either custom fMRI machines, at several million dollars each, or low signal to noise. [87] These difficulties limit generalizability of awake macaque BOLD fMRI findings to human findings. The goal of awake macaque BOLD fMRI is to provide a serial link between high order behavior human BOLD and macaque electrophysiology findings. However, the difficulties of macaque fMRI raise concerns about the feasibility or validity of this approach. [88] (See below for difficulties identifying a default mode in macaques using BOLD fMRI)

Other measures of the metabolic and hemodynamic responses reflected in BOLD fMRI exist and can be used as a surrogate. Several optical imaging techniques exist for measuring blood flow and/or hemoglobin concentration. [89] Transcranial optical imaging is possible in awake humans and can be combined with EEG [90-92]. Brain surface optical imaging is possible in animal models, including awake macaques, and can be combined with micro-electrode recording of neural activity [93-97]. However, these methods are technically challenging, requiring substantial experimental setup,

and are only able to image superficial cortex. In the macaque, many areas of interest lie deep within sulci outside the reach of optical imaging.

Overall, serial or simultaneous comparison of BOLD fMRI and electrophysiology and or use of alternate hemodynamic techniques are prohibitively difficult to implement or compare. These tools so far provide an incomplete and conflicting picture of the neural BOLD fMRI relationship. Different studies argue for different neural features as the best correlate of BOLD (for a recent review see [13, 14]). Some even argue that they have identified behaviorally relevant hemodynamic activity without a neural correlate. [21] However, a negative finding is hard to justify and likely means that neural activity was inadequately estimated.

Given the importance of human BOLD fMRI the importance of the awake macaque model and the technical challenges of comparing electrophysiological and BOLD (or BOLD like) measures of neural activity; an alternative method that allows more flexible and active study of a hemodynamic surrogate in the awake macaque that can be combined with electrophysiology would be highly beneficial. Such a tool could provide a bridge allowing greater synthesis of human BOLD fMRI and macaque electrophysiological views of the brain.

Oxygen polarography is an electrode based electrochemical technique that can be readily integrated into the standard macaque electrophysiology setup. This technique has a long history in neuroscience, is far easier to implement on a recording by recording basis than optical imaging and is well matched in location and resolution to electrophysiology. Oxygen polarography records local tissue oxygen, which is highly

related to blood oxygen and BOLD fMRI, and allows recording of a hemodynamic signal alongside electrophysiology without interference. Despite its prior use in neuroscience, no commercially available system suitable for use in the awake macaque is available. As discussed in chapter 2, we developed our own system to allow high resolution study in the awake macaque of hemodynamic phenomena identified in humans with BOLD fMRI and to allow increased study of the neural BOLD relationship.

Oxygen Polarography in Neuroscience:

Oxygen polarography has a significant history in neuroscience beginning with Davies and Brink in 1942. [43] This technique is still used but fell out of fashion around the time of the advent of positron emission tomography (PET). The majority of oxygen polarography neuroscience was focused on average tissue oxygen under different conditions. Early work focused on conditions under which the brain was at risk for hypoxia. The bulk of available data concerns the partial pressure of oxygen in brain tissue under different conditions and in response to various surgically relevant manipulations. [41, 42, 98-106] A few early oxygen polarography studies explored task evoked changes in brain tissue oxygenation. These studies were in some sense the first observation of the phenomenon at the heart of the task BOLD response central to most fMRI. Currently the Freeman lab at Berkeley uses oxygen polarography as a surrogate for BOLD and examines the relationship of task evoked changes in tissue oxygenation to electrophysiological activity in anesthetized cats and a few other labs are using polarography to relate BOLD and electrophysiology in rats. [40-48, 105, 107-114]

Many of the early oxygen polarography studies remark on ongoing fluctuations in tissue oxygen as a fundamental property of the brain. However this variability was

generally orthogonal to the question of interest and was averaged out as noise. There was some interest in determining if tissue oxygen fluctuations represented fluctuations in systemic supply or were driven by a local process. Tissue oxygen variance was compared to variance in heart rate, arterial blood pressure, systemic oxygenation, respiration, and other physiological variables. Systemic variables explained a portion of tissue oxygen variance, however, the general consensus was that tissue oxygen variability was a under local control. A few studies asked whether tissue oxygen fluctuations were correlated across multiple sites in the brain. The majority of these studies observed tissue oxygen fluctuations to be uncorrelated across cortex. [40, 42, 115] This result was consistent with the local phenomenon/local control viewpoint and the issue was dropped. However, Burgess and Shallet [116] published an abstract in Stroke reporting correlation in matching areas in the right and left cortex of rats.

The “uncorrelated” finding of these older papers raises concerns about the use of polarography as a tool for studying the long-range correlated fluctuations studied with BOLD fMRI. However, determining the significance of an r value is not trivial. The correlation values we observe (chapter 4) and reported in these older studies are in the 0.3-0.5 range which could easily be discarded as measurement artifact. BOLD fMRI provides the ability to image the whole brain. The functional significance and network structure of inter-regional correlation of ongoing fluctuations only became apparent when the whole brain pattern of correlation was observed. However, since this pattern is now known, the significance of the correlation structure of oxygen fluctuations can be interpreted based on the correlation structure expected from BOLD fMRI results.

This prior polarographic work demonstrates the ability of this technique to study the phenomena of interest, stimulus driven and ongoing fluctuations in oxygen likely underpinning modern BOLD fMRI studies. Given the special status of the awake macaque model in neuroscience and in the study of the BOLD fMRI neural relationship, there is good reason to extend polarographic recording in the modern era into the awake macaque. This model allows investigation of both BOLD fMRI and electrophysiological correlates of higher order cognitive function. However, given the difficulty of direct comparison, polarography can provide a bridge connecting BOLD fMRI and electrophysiology in the awake macaque.

Oxygen Polarography vs. fMRI BOLD:

Oxygen polarography is an electrode based technique and allows high resolution study of tissue oxygen concentration anywhere in the macaque brain that electrophysiological recording is possible. Tissue oxygen is a reasonable surrogate for BOLD fMRI. [45] As discussed in chapter 2, oxygen polarography and BOLD fMRI are both sensitive to local brain oxygen levels. BOLD fMRI detects changes in local magnetic properties caused by changes in the concentration of para-magnetic deoxyhemoglobin. The concentration of deoxyhemoglobin is directly tied to the ratio of oxy- and deoxyhemoglobin and thus reflects oxygen concentration in the blood. Oxygen polarography measures the local availability of oxygen molecules in tissue, tissue oxygen concentration.

Polarography provides several advantages over BOLD fMRI. The electrodes used for polarography are also suitable for electrophysiological recording when connected to an appropriate recording system. This allows recording of electrophysiology during

electrode penetration to aid in targeting, and perfectly co-localized recording of stimulus responses. As shown in chapter 3, we recorded electrophysiology and oxygen serially from the same electrode in response to visual stimuli.

In addition, neighboring polarographic and electrophysiological electrodes have no effect on each other, allowing simultaneous recording. However, the degree of response variability with our 0.5 mm electrode spacing is not yet well characterized. In theory, polarographic and electrophysiological systems could both be connected to a single electrode and both signals recorded simultaneously. However, capacitance in the electrode introduces a risk of crosstalk. We chose serial recording to allow perfect co-localization and avoid any possible crosstalk between the systems or differences in response at neighboring electrodes. Multi-site recording allows us to investigate long-range correlation of oxygen fluctuations, functional connectivity, discussed in chapter 4.

The spatial specificity and temporal resolution (20-100 micron spatial specificity, 20 Hz temporal resolution) of our polarographic system is also well matched to the resolution of microelectrode recording. Local field potentials are thought to reflect a few hundred microns of tissue. [117] Spiking activity is restricted to a still smaller volume depending on the number of cells, ranging from a similar range as LFPs for multi-unit recording to 20-50 microns for a single cell. The resolution of tissue oxygen measurement is also well matched to the scale of neurons (~20 microns) and cortical columns (~100 microns).

Differences in peak, onset, and or rate of rise, of tens to hundreds of milliseconds are reasonable for neurally driven activity. [47, 118] 20 Hz temporal resolution provides

a much better platform than BOLD fMRI for comparing oxygen fluctuation differences at the scale of these neural timing differences. The higher temporal resolution of polarography compared to BOLD provides greater leverage in discriminating, or ruling out a difference in, the relationship between different aspects of either stimulus driven or ongoing neural activity and oxygen.

At the common temporal resolution of BOLD, oxygen fluctuations due to heart contractions or breathing will be aliased and can alter the observed BOLD fMRI correlation. [119] At the resolution of our tissue oxygen technique these fluctuations can be directly observed and their impact on the correlation pattern can be measured and removed. Further, we can evaluate much higher frequency relationships than possible with BOLD fMRI. In sum, the closer resolution match allows more direct comparison than possible with the widely different BOLD fMRI (3mm, 3s) and electrophysiology resolutions.

In addition to blood oxygen level, the BOLD fMRI signal is influenced by blood flow and volume. Blood flow and volume are highly correlated with oxygenation. However, while unlikely, it is technically possible that a particular BOLD observation reflects something other than blood oxygen. If tissue oxygen and BOLD fMRI results emerge that are in conflict they may provide insight into the hemodynamic mechanism driving those results. Further, both techniques are influenced by different noise sources. Since oxygen concentration is the common variable between the techniques, response similarity can inform interpretation of the source of signals recorded with BOLD.

The Default-Mode:

As discussed, task driven BOLD fMRI responses have been used to localize function or develop models of cognitive process architecture by comparing the pattern of neural activity underpinning different task conditions. Intriguingly, a set of regions, now known as the default mode network, have been identified not for their task specific activation, but for deactivation by the majority of tasks and stimuli[120]. This deactivation by task or external engagement has led to the idea of a "default mode." The "default-mode" of brain function is a hypothesized process or set of processes that is more engaged when subjects are at rest and not engaged with the external world, i.e. in a default state, and is suppressed (seen as BOLD fMRI suppression) when subjects switch from this default state to an externally directed state. [121, 122] The default-mode network consists of the posterior cingulate/retro-spenial cortex, the medial prefrontal cortex, lateral parietal cortex, the dorsal lateral prefrontal cortex, and sometimes includes medial temporal cortex. [68]

The nature of the default-mode function is a matter of ongoing debate. However, several lines of evidence point to an expectation modeling system [123] and roles in self-awareness and social cognition. Many of the default mode regions increase their activity during self-referential and autobiographical memory tasks. [124] There is also significant evidence that default mode network regions engage in social cognition, for example making judgments about others' mental states. [125-127] Intriguingly, the default network shows substantial distortions in topography and behavior in schizophrenia and autism. [123, 128-131] Both disorders show marked distortions in awareness of self and others. Recent work in humans has linked the level of concern

with one's thoughts, as opposed to the self-referential thoughts themselves, with activity in the default mode network. [132-134]. While such high cognitive functions remain possible in part in humans, the fact that external engagement suppressed default mode network activity in macaques, as discussed in chapter 3, argues for a more basic default mode network function. Evidence from macaque electrophysiology has shown neurons in default mode network regions that encode environmental uncertainty. [123, 135, 136] These results are consistent with a role for the default mode network in evaluating the importance of potential outcomes. Perhaps the default mode network is involved in modeling the future in the context of prior experience, and in humans such models have a substantial social component. [123]

The default mode network was first identified in analysis of PET imaging data and the majority of work supporting the default-mode has been done with BOLD fMRI. Hence, the neural underpinnings of default-mode network suppression are largely unknown. Suppression of neural activity could lead to increases or decreases in metabolic demand, depending on the activity of inhibitory neurons and to increases or decreases in blood flow. In some cases inhibitory neurons can inhibit blood flow. [24] Suppression of BOLD activity in the default mode network could reflect overall neural suppression or could reflect a complex set of increased and decreased neural activity and associated metabolic and hemodynamic activity that sums to an overall decrease in the BOLD signal.

A handful of papers in neurosurgical patients and two papers in macaques have examined the electrophysiology of default mode network suppression, in particular the posterior cingulate. [137-143] The responses reported were complex, and the tasks

used differed in structure from tasks used for BOLD fMRI. The studies in humans support an external engagement suppressed self-awareness process in PCC. However, as a whole, these studies, and our results shown in chapter 3, argue that there is more than one process in PCC. In these studies some apparent neural processes, often reflected in low frequency local field potentials, show increased task related activity while others, often reflected in high frequency LFP, show suppression. Unfortunately in these studies there was no direct way to relate the neural activity to prior BOLD findings. Chapter 3 presents the first direct comparison of hemodynamic and electrophysiological activity in the default mode network. We note highly correlated positive and negative LFP and oxygen responses in PCC when a resting macaque is engaged by visual stimulation. However, in contrast to prior studies we observe suppression at most LFP frequencies, albeit with different timecourses at different frequencies. Our technique provides a platform for future study disambiguating the functional role of the multiple processes suggested by multiple LFP timecourses and for relating those processes to oxygen suppression.

A “default-mode” has also been related to ongoing task-independent fluctuations in the BOLD fMRI signal. Task independent fluctuations in the bold signal apparently index intrinsic fluctuations in brain activity. However, intrinsic activity, though generally studied while subjects are at rest to disambiguate it from task driven activity, is not conceptually the same as a default mode. The brain could have many types of intrinsic activity that are not directly tied to a specific task. Importantly, these intrinsic fluctuations, as discussed below, are present and largely unchanged when subjects are at rest or engaged in a task. Further, these fluctuations are highly correlated among

functionally related brain regions. It is important to note that ongoing fluctuations are highly correlated among default-mode network regions.

Functional Connectivity:

In 1995 Biswal et al [73, 144] demonstrated that during periods of rest, in the absence of an explicit task or stimulus, fluctuations in the BOLD signal in right and left motor cortices were highly correlated. Ongoing BOLD fluctuations in several functionally related groups of regions or networks, have subsequently been shown to be correlated. [67, 68, 82, 145-147] For example, regions involved in spatial attention show correlated BOLD fluctuations. Right and left primary visual cortex, areas known to be functionally related but lacking direct anatomical connection, show correlated BOLD. [147] The general pattern of BOLD fMRI correlation is stable across and within individuals, across primate species, across levels of anesthesia, and largely unchanged from resting state to task conditions. [5, 147-150] However, the detailed spatial structure of the correlation patterns within individuals follows subtle anatomical functional differences between individuals. [151]

The above evidence argues that BOLD fluctuations and their correlation index functionally relevant elements of the brain's organization. The maintenance of correlation structure, or functional connectivity, across species and levels of anesthesia suggest that functional connectivity reflects a fundamental organizational principle of the brain. Vasomotion, or capillary cycling, is known to occur throughout the body with a frequency structure similar to BOLD fluctuations and it has been suggested that local fluctuations in BOLD may result from random fluctuations of capillary flow. However,

there is no known mechanism, other than neural architecture, that could organize activity in the observed correlation pattern.

In addition to functionally relevant correlation structure, BOLD signal fluctuations and their correlation can be directly tied to behavior. BOLD signal fluctuations have been related to and shown to be predictive of motor and sensory variance within subjects. [66, 69] The strength of correlation within a network has been related to: behavioral differences across subjects for example working memory ability and IQ, [64, 71, 72]; to prior and current experience; and to mood and arousal state. [152-154] Specific alterations in correlation structure have also been observed for several neurologic diseases. [5, 155-161] [2] Changes in correlation structure subsequent to brain injury also correlate with behavioral impairment.[162]

The relationship between ongoing BOLD fluctuations and behavior argue that they and their correlation structure in some way relate to functionally relevant neural fluctuations. Correlation among functionally related regions is believed to reflect the degree of functional coupling, or functional connectivity, between brain regions. It is technically possible that changes in local oxygen driven by vasculature, and not neural phenomena, could drive the relationship to behavior by impacting local metabolism. [163] However, it is far more likely that behaviorally relevant neural activity is driving local BOLD fluctuations and their correlation and thus their relationship to behavior.

Long-range correlated fluctuations of hemodynamic activity have also been seen with other techniques. Historically, Vern et al reported correlation from right and left visual cortex in rabbits using reflectance spectrophotometry. Golanov et al [164]

reported correlation of blood flow in between the frontal and parietal cortex of both hemispheres in rats, using laser Doppler flowometry. [116, 164, 165] Unfortunately these three studies report significantly different temporal and spatial properties of the correlated activity they identify. These differences could result from stated differences in anesthesia level, model species, measurement technique, or unknown differences between the conditions under which the data was acquired.[166] More recently, optical intrinsic imaging studies in humans have identified similar patterns of correlation as those seen with BOLD, and in other species functionally relevant patterns of correlation [93, 167-169]. These studies and the polarographic studies mentioned above support the ability to study functional connectivity with means other than BOLD fMRI.

Very little is known about the neural origin of hemodynamic fluctuations or the mechanisms orchestrating the inter-regional relationship. Three studies in monkeys and a handful in rats have attempted to directly relate neural activity to ongoing BOLD fluctuations. [27, 30, 32, 79, 84, 85, 170] These studies recorded electrophysiology from a single site simultaneous with BOLD fMRI in anesthetized animals. Since anesthesia is known to change baseline activity the relationships identified may not generalize to awake humans. Anesthesia is known to change the frequency and character of low frequency electrophysiological fluctuations. [171] Further, the aspects of neural activity found to best relate to BOLD fluctuations differs across studies. For example, Pan et al [172] find that a broad band LFP signal is the best correlate of ongoing BOLD fluctuations, Scholvinck et al [30] find that gamma band LFP power is the best correlate, and Magri et al [34] find that different LFP bands and phase relationships among LFP frequencies explain different aspects of BOLD fluctuation.

Finally, although all of these studies report strong relationships between neural activity and BOLD fluctuations they cannot directly address inter-regional relationships of neural activity.

Given its apparent significance to brain function, deeper understanding of functional connectivity and its neural underpinnings should provide insight into the relationship between brain function and behavior and brain dysfunction and disease. A platform that allows high resolution investigation of the oxygen fluctuations studied with BOLD fMRI that can be readily paired with electrophysiology would greatly facilitate reconciling the existing literature. In particular, it would of great benefit to be able to examine the relationships among neural activity at multiple sites and to compare those relationships to the hemodynamic activity relationship studied with BOLD. While our current results do not directly address the neural underpinnings of functional connectivity, chapter 4 shows a proof of concept that our technique allows investigation of functional connectivity, and sets the stage for simultaneous multi-site investigation of inter-regional correlation of hemodynamic and electrophysiological activity.

Aside from investigating the specific neural activity related to BOLD fluctuations and their inter-regional relationship, others have compared the network structure of BOLD fMRI correlation to known structural anatomy. [173] These studies find a strong relationship between structural connectivity and BOLD based functional connectivity. This relationship has led to the suggestion that BOLD fMRI functional connectivity arises from the interaction of ongoing fast neural activity within an anatomical network. In this view, correlated slow fluctuations, functional connectivity, do not reflect a unique form of slow inter-regional interaction but are simply an emergent epiphenomena of

stochastic positive and negative interaction of neural activity spreading through a structured network. Correlation then reflects the similarity of inputs to a region.

Supporting this idea local BOLD fMRI fluctuations have a $1/f^{\wedge\alpha}$, or scale free, power spectrum. This type of spectrum is expected from a large number of stochastically interacting elements. High levels of synchrony among elements are rare but lead to large (additive) effects while smaller degrees of synchrony occur more frequently but lead to smaller effects. Hence, fluctuations in the magnitude of activity in the system scale with its frequency in a $1/f^{\wedge\alpha}$ manner, and at any given scale fluctuations look similar (scale free). [174] However, the activity driving long-range BOLD correlation may not be identical with the local BOLD fluctuations. There is some suggestion that long-range correlation may depend on particular frequencies of fluctuation. [151, 175-179]

Our results, discussed in chapter 4, show that only a very slow frequency limited portion of the local oxygen fluctuations are correlated among regions. These results suggest that inter-regional correlation depends on a distinct, functional connectivity specific, rhythmic mechanism. Further the mechanism of long-range correlation is distinct from the mechanism driving local oxygen fluctuations. The band-limited nature of correlation is suggestive of a rhythmic or resonant process similar to bands of elevated EEG activity under certain states many of which have been tied to specific oscillatory features of neural membranes and networks. [180-187] Phase coupling of ongoing oscillatory activity is often proposed as a method of information binding and or segregation of information in the brain. [186, 188] Given the relationship of slow BOLD fluctuations and their correlation to behavior, it is intriguing to consider these fluctuations as possibly reflecting a slow oscillatory inter-regional binding mechanism.

Summary:

BOLD fMRI in humans and electrophysiological recording in awake macaques both provide invaluable insight into high order brain function. Linking these two views of the brain would provide much greater leverage in understanding brain function than either view alone. Given the difficulties associated with electrophysiology in humans or BOLD fMRI in macaques an alternative platform, or bridge, for comparing the two signals is highly desirable. Oxygen polarography in the awake macaque can provide such a platform. With multi-site recording, polarography allows study of stimulus driven and ongoing fluctuations in tissue oxygen that fundamentally relate to the blood oxygen related signals of BOLD fMRI. Chapter 3 demonstrates the ability of polarography to study stimulus driven and associated neural activity in response to stimuli. Visual stimuli were chosen and recordings were done in visual cortex, similar to prior sensory cortex comparisons of BOLD fMRI and electrophysiology, and in default mode cortex extending exploration to a new part of the brain. Chapter 4 discusses the long correlation structure of ongoing fluctuations in tissue oxygen and demonstrates our ability to measure and extend our understanding of the temporal details of functional connectivity. While there is no electrophysiology in chapter 4, it provides proof of concept and sets the stage for future exploration. Finally, chapter 5 provides overall conclusions and insight into the next steps being taken with our system.

Chapter 2: Technical Development

Overview

We have adapted an electrochemical technique, oxygen polarography, for use in the awake macaque as a substitute for BOLD fMRI. BOLD fMRI and tissue oxygen are highly related and reflect the same basic phenomena. The awake macaque is the gold standard animal model for directly studying the neural activity underpinning higher cognitive functions commonly studied in humans using BOLD fMRI. Direct comparison of BOLD fMRI and electrophysiological activity is exceptionally technically difficult.

Oxygen polarography in the awake macaque offers an alternative to BOLD fMRI that can be readily combined with electrophysiology. This tool can greatly facilitate our understanding of the neural underpinnings of the BOLD fMRI responses to higher order cognitive activities studied commonly studies in humans. Since no commercial oxygen polarographic system was available for use in the macaque we were motivated to design and construct our own.

This chapter discusses the mechanism of BOLD fMRI and oxygen polarographic recording in some detail, the benefits and limits of modern Clark electrode based polarographic systems, the need to develop a new system, that development, and system testing. Development of this new system required design of oxygen polarographic electrodes, adaptation and construction of recording electronics and system testing prior to use in macaque. In brief, we developed a glass insulated platinum iridium electrode for use as a polarographic cathode, identified a highly stable DC EEG Ag/AgCl electrode that performed well as a reference/anode, modified a

commercial polarographic amplifier, and constructed an optical isolation and battery power system to protect the polarographic system for ground instabilities and lab noise. We tested that the system displayed the expected electrochemical features of a polarographic recording system, its ability to detect respiratory modulation of oxygen in the mouse, and stimulus driven oxygen modulation in the macaque.

Related Measurements

Prior to accepting the substitution of an invasive measure of tissue oxygen for BOLD fMRI it is useful to consider the mechanism and resolution of each technique and their relationship.

BOLD FMRI:

All protons display tiny oriented magnetic fields, or spins. Neighboring protons in the nuclei of multi-proton atoms organize to have opposing spins. Thus, atoms with an odd number of protons display a net magnetic field. This field can be obscured by surrounding electrons. Electron shielding for a given atom is reduced in covalently bonded molecules in which the electrons spend a disproportionate amount of time around of the nuclei of the other atom. In water, the electrons cluster around the oxygen nuclei, leaving the single proton in each of the two hydrogen atoms essentially unshielded. This property of water and the abundance of water in the body provide a built-in mechanism to study the local magnetic properties of bodily tissues. By aligning the spins of water molecules magnetic resonance imaging generates a net magnetic field. MRI explores the local magnetic properties of tissues by manipulating the direction and alignment of these spins and measuring the resulting field.

BOLD MRI is possible due to differential magnetic properties of blood. Deoxyhemoglobin is paramagnetic and affects the local magnetic field. Oxyhemoglobin is diamagnetic and does not. BOLD MRI measures the impact of local magnetic field disruption caused by deoxyhemoglobin on the magnetic spin of protons in the surrounding water. [7] The magnitude of this disruption is proportional to the concentration of deoxyhemoglobin, i.e. the magnetic influence of deoxyhemoglobin is spread across all surrounding protons. The concentration of deoxyhemoglobin is inversely related to the concentration of oxyhemoglobin. ([oxyhemoglobin] = [hemoglobin] – [deoxyhemoglobin]) Thus the concentration of oxyhemoglobin in the blood is directly related to the BOLD signal. The concentration of oxyhemoglobin in the blood is directly (although non-linearly) related to the partial pressure of oxygen in the blood. The partial pressure of oxygen in the blood is in equilibrium with the partial pressure of oxygen in the surrounding tissue, tissue oxygenation. Hence the BOLD fMRI signal can be directly related to tissue oxygenation. Functional BOLD MRI is possible due to a link between neural activity, neural metabolism and the vasculature. Changes in neural activity in general lead to changes in deoxyhemoglobin concentration. [60]

The relationship between BOLD measurements and tissue oxygenation becomes significantly more complicated when the rate of oxygen diffusion becomes a limiting factor. Assuming a mean cortical inter-capillary separation of 50 microns a diffusion rate of oxygen in extracellular fluid (ECF) of 1 micron^2 per ms, and a maximal diffusion time from capillary to remote tissue of 67 ms, [189] changes in BOLD and tissue oxygen can be assumed to be well matched at frequencies below 20 Hz. [7, 12, 60]

The spatial and temporal resolution of BOLD fMRI is fundamentally limited by the physics of nuclear magnetic resonance, and is practically limited by the tools available to measure the fMRI signal. The theoretical spatial limit is the smallest vascular compartment, the tissue served by a single capillary, or approximately 50 microns. With currently available hardware, the maximal possible spatial resolution is hundreds of microns to millimeters. The theoretical temporal resolution is limited by the time necessary to establish a stable magnetic field and is on the order of hundreds of milliseconds. Field stability is required for reliable repeated measures. In some cases the practical limit approaches this theoretical limit. [190] However, due to both fundamental and practical limits as the spatial resolution becomes higher the temporal resolution must be reduced to maintain a similar noise level, and vice versa. The exact relationship between resolution and noise depends on the exact system and technique used to assess the BOLD fMRI signal. In common practice fMRI can provide whole brain coverage with a spatial resolution of 1-3 mm cubes and a temporal resolution of 2-3 s.[190, 191]

It is important to note that the mean BOLD fMRI signal can be influenced by several external factors (temperature, position of the measuring equipment, etc.) The BOLD fMRI signal is a relative, not an absolute, measurement. However, a relative measurement is entirely sufficient to measure changes in activity with time.

Polarography:

Polarography is an electrochemical technique used for the analysis of ions dissolved in solution. When two electrodes are placed in solution, and a polarizing voltage is applied, current can only flow if ions in the solution can accept electrons from the

cathode (Neg -) and release them to the anode (Pos +). The current that flows, charge per unit time, is limited by how fast the electron carrying ions can accept electrons from the cathode and deposit them on the anode. The charge transfer rate, i.e. current, is limited by the surface area of the electrodes on which the electron transfer can take place, the kinetics of the electron transfer reactions, and the concentration of participating ions.

The acceptance of electrons at a cathode and release at an anode are described as a pair of half-cell reactions. The half-cell reactions that occur depend on the ions in the solution, electrode material, and applied voltage. The set of ions in solution determines the set of possible half-cell reactions. The electrode material provides a surface on which the reaction occurs. Voltage, electrical potential energy, provides the activation energy for each half-cell reaction.

The electrode surface can be inert, can catalyze the half-cell reaction, or can directly participate in the half-cell reaction. Participation can result in intermediate products that are quickly reversed, it can release products into solution, or product can be deposited onto the electrode. Deposition can result in changing electrode characteristics over time. In the case of deposition the principles of polarography and electroplating become similar.

Any half-cell reaction has an associated activation energy. Available energy is distributed across the most efficient set of possible half-cell reactions. The total available energy, reflected in voltage, controls the set of half-cell reactions that can

occur. A given polarizing voltage, with specified electrodes and solution, results in a set of reactions that distribute the available energy between the anode and cathode.

The rate of electron transfer, current, for a particular reaction is limited by concentration. Given a fixed electrode surface area and reaction kinetics, a given reaction can only accept electrons from the cathode or deposit them on the anode at a specific rate. The rate of charge transfer is limited by how quickly the molecules on the electrode can be replaced after they have accepted or released an electron. This rate is dependent on concentration, essentially the pressure in solution of a given ion to push off the reactants on the electrode. Once the rate limit for a given reaction is reached, it cannot carry more charge and current is restricted until enough voltage is provided to recruit new reactions. New reactions can have different kinetics and ion concentrations and lead to abrupt changes in current. However, as voltage is changed, new reactions are not recruited instantaneously. Ions in solution have a distribution of energies, and thus, for the highest energy ions the activation energy for a given half-cell reaction is reached at lower voltages than for the lowest energy ions. Given a finite set of ions with fixed concentrations, the current voltage relationship in most solutions has substantial non-linearity (deviation from Ohm's law V=IR). As voltage is increased, current increases as new reactions are recruited and then plateaus during the voltage range over which the current carrying reactions are at peak capacity and then increases again as new reactions are recruited.

Further, after a voltage change, steady state current does not occur instantaneously. Each half-cell reaction can be thought of as a molecular capacitor. At the cathode, all of the ions in contact with the electrode have been reduced, (negative pole) and all of the

ions one molecular layer away remain un-reduced, (positive pole). Current flow occurs when reduced ions are replaced by un-reduced ions, like charge leaking through a capacitor, and an electron is transferred to those new ions. The rate that un-reduced ions can push through reduced ions is dependent on ionic pressure in the solution, i.e. concentration. Since ions are being consumed a concentration gradient is established from the bulk solution concentration to the zero concentration of the un-reduced ions at the electrode surface. The shape and extent of this gradient depends on the shape of the electrode and the mechanical stability of the fluid.

In the steady state, current is the leak of charge through the molecular capacitor, which is dependent on ion concentration. After a given voltage change, time is required for the molecular capacitors and concentration gradients to either be established or to decay. This appears as an instantaneous current jump after a voltage change followed by capacitive decay.

If the ions in a solution are known and the properties of the associated ion transfer reactions are known, the current resulting from a particular voltage with a particular pair of electrodes can be used to calculate the concentrations of those ions. If the ions present are not fully known, the profile of the current voltage relationship can be used to estimate the set of half-cell reactions occurring in a fluid, and identify the ions present. Prior work, begun by Jaroslav Heyrovsky in 1922, has established the half-cell reactions and the current voltage profile for a wide array of electrodes and solutions. [49, 192, 193]

Oxygen Polarography:

Oxygen polarography, and particularly oxygen polarography in the brain, represents a specialized application of the polarographic technique. Oxygen polarography requires a noble metal cathode, a non-polarizable anode and a polarizing voltage of between -0.7 and -0.9 V. A noble metal cathode is chosen so that it does not participate directly in the reactions occurring on its surface. In particular the electrode must not form and release oxides. It can serve as a stable catalyst.

A non-polarizable reference is chosen for control of the half-cell reactions. In high chloride concentration solutions like biological fluids, including extra-cellular fluid (ECF), a Silver/Silver Chloride (Ag/AgCl) anode works well. At this electrode electrons are accepted and new AgCl is formed. With a sufficiently large electrode, such that the total amount of AgCl or Ag isn't changed appreciably, there is essentially no concentration limit on charge transfer, the kinetics of this reaction are extremely fast, and its activation voltage is minimal. These electrodes are referred to as non-polarizable as they do not accumulate charge in relationship to the fluid. The half-cell reaction is fast enough that it presents virtually no resistance. Thus, regardless of flowing current (V=IR), infinitesimal voltage develops. Due to low activation voltage and no voltage accumulation due to the extremely fast kinetics, no other reactions form at this electrode. The current flowing between a noble metal electrode and an Ag/AgCl reference electrode is primarily dependent on the rate limit of the half-cell reactions at the cathode.

At a polarizing voltage between -0.7 and -0.9 the primary reaction at the cathode is the reduction of oxygen. Below -0.5 V other ions, such as hydrogen, accept electrons

from the cathode, however, by -0.5 V these have reached their current limit. Starting at ~0.5 V oxygen reduction begins, allowing a rapid increase in current, by -0.7 V oxygen reduction has reached its rate limit. No new reactions can be recruited until ~-0.9 V. Thus, the current voltage relationship in an oxygen polarographic system has a characteristic shape, a roughly exponential increase from 0 to -0.7 V, a plateau in the -0.7 to -0.9 range, and another exponential increase at voltages above -0.9. See Figure 1.

In ECF the concentration of ions in reactions other than the reduction of oxygen is essentially fixed and thus the current limit of those reactions is fixed. In the plateau voltage range oxygen reduction is carrying the bulk of the total current. Although oxygen reduction has a large activation energy it has relatively fast kinetics and is highly prevalent and thus has a significantly higher current limit. This limit is proportional to oxygen concentration, and thus total current is proportional to oxygen concentration. In brain tissue and ECF if a noble metal cathode is polarized in reference to an Ag/AgCl, (non-polarizable), electrode at a voltage in the plateau range, changes in oxygen concentration lead to linearly proportional changes in current (the level of the plateau). [49]

Due to the influence of and daily differences in electrode tip size, distance from capillaries, temperature and Ph., the mean current in a simple, bare metal cathode, polarographic system cannot be considered a measure of absolute tissue oxygen concentration. Mean current for any given recording reflects all of these variables, as well as current carried by ions other than oxygen with low activation voltages. Fortunately these effects are stable during a given recording. Fluctuations in current

around the mean are linearly related to fluctuations in oxygen concentration. Thus oxygen polarography in the manner described above is a relative measurement of oxygen, much like BOLD fMRI

Available Polarographic Systems:

Use of oxygen polarography in neuroscience began with Davies and Bronk in 1942, and continues in modified forms today.[109, 194, 195] Historically, oxygen polarography was done in the brain using systems similar to what we have designed here. However, the details of the custom systems used in the older studies were not published in a manner that could be copied. Further, changes in the basic layout for power supply and data acquisition in the modern laboratory introduced new constraints not present at the time of this prior work. Oxygen polarography is still widely used today in both science and industry; however, none of the available systems are suitable for use in an awake macaque. The majority of systems are simply too large to be used in the brain without substantial collateral damage. Further, most commercial and scientific oxygen polarography depends on variants of a specialized type of electrode, the Clark Electrode, which cannot be used in the awake macaque due to its fragility (see below). [45-48, 196]

In a Clark electrode, the anode and cathode are separated from the solution under measure by an oxygen permeable membrane. This allows the electrolyte between the anode and cathode to be fixed. With just a cathode and anode in the brain as discussed above, ECF serves as the electrolyte and its properties can vary. In a Clark electrode, a fixed electrolyte allows specific control of ion concentrations and half-cell reactions. Thus, current carried by all electrolytes other than oxygen can be explicitly

identified and current change due oxygen diffusing through the permeable membrane can be explicitly identified. With a known diffusion path from the membrane to the electrodes and known membrane permeability, current changes can be calibrated to absolute oxygen concentration in the solution of measure. This arrangement provides further benefit by electrically and chemically isolating the electrodes from the solution. Electrical isolation helps fix the current path between the anode and cathode and block stray currents or ground loops through the animal and other lab electronics that could destabilize the measurement. Chemical isolation further ensures that the anode and cathode do not interact with any molecules in solution. Platinum, the noble metal we chose for our cathode, does not interact with ECF. However, it does interact with blood. This interaction with blood and the desire to study blood oxygenation was the initial impetus for the design of the Clark electrode. [196]

Further, in an open polarographic system, fluid stability affects the shape of the oxygen concentration gradient from bulk solution to the tip of the electrode. In a Clark electrode the membrane permeability is much lower than fluid permeability, and thus diffusion through the membrane is much slower. The primary concentration gradient is thus from the membrane to the electrode, not the fluid to the membrane. This limits the effects of fluid stability or instability.

Clark electrodes can be made in a wide array of physical configurations including micro-electrodes and have been used previously to study brain oxygen concentrations in animal models. [45-48] In order to make a Clark electrode with a tip small enough to insert into the brain without substantial damage, the anode and cathode are placed in a glass pipette and the tip pulled into a micropipette. The tip is then covered with a

membrane. Unfortunately, this process leads to a short thin glass tip that cannot penetrate deeply into tissue and is easily broken. The tiny membrane is further easily clogged and broken. Finally, diffusion through the micropipette tip is slow and these electrodes have response time of 1s and greater.

Unfortunately commercially available Clark electrodes can thus not be used in awake macaques. Although awake macaque can be restrained, and are regularly head-fixed during micro-electrode recordings in the brain, they are still capable of some movement. This movement is in general beyond the tolerance of micro-pipette Clark electrodes. Further, the macaque brain is covered by thick dura mater. Micro-pipette Clark electrodes are not strong enough to pierce the dura; in particular the electrode membrane would be destroyed. In standard macaque microelectrode recording, the dura is pierced by a cannula, and a micro-electrode passed through the cannula into the brain. Unfortunately, the diameter of the body of the Clark electrode, including those with micro-pipette tips, is far too large to allow this. In theory a cannula could be fitted over the tip of a micro-pipette Clark electrode, used to pierce dura, and the Clark electrode advanced through it. Or the dura could be pierced by a needle, and the Clark electrode passed through it under a micro-scope. However, both of these techniques would require substantial mechanical development efforts before they could be incorporated into the standard macaque micro-electrode recording setup. Further, if a micro-pipette Clark electrode could be passed through dura, and handle the mechanical stresses of an awake macaque, the short length of the micro-pipette would limit recording to superficial gyri. The majority of the macaque cortex lays in sulci outside of the reach of micro-pipette Clark electrodes. Prior work in neuroscience with Clark

electrodes was done in anesthetized mice rats and cats in acute experiments in which the dura was removed.

Since commercially available oxygen polarography systems are either too large or too fragile for use in awake behaving monkeys, and have response times that limit comparison of oxygen and electrophysiological data, we have developed our own system for measuring local oxygen availability in the awake macaque based on principles of polarography. We use a bare noble metal cathode in the brain and a non-polarizable (Ag/AgCl) reference in direct contact with the macaque [196, 197], and ECF provides the electrolyte. Fortunately the benefits of a Clark electrode are either not necessary for a BOLD surrogate or can be achieved in other manners. BOLD is a relative measure and so the absolute calibration possible with a Clark electrode is unnecessary. The mechanical properties of the brain provide minimal fluid motion concerns. ECF is in general already moving and well mixed. Further, when an electrode is inserted into the highly membranous brain, a small fluid pocket generally forms around the tip. Oxygen diffusion is faster in this fluid than across the membrane. Thus much like in a Clark electrode the diffusion path is restricted. Together these effects lead to a short and already moving oxygen gradient that is robust to further movement. Thus, there are minimal fluid stirring effects. [44] Chemical isolation in ECF is not necessary and electrical isolation can be accomplished with other means. Optimization and testing of this system required substantial development efforts: see below.

Awake Macaque Oxygen Polarographic System

In order to provide a useful surrogate for BOLD fMRI our system had to meet several design constraints. To provide maximal compatibility with macaque electrophysiology our technique had to be implemented in the standard macaque electrophysiology setup. Further, to allow a better match between our oxygen signal and electrophysiology than is possible with BOLD fMRI our technique needed a spatial specificity and temporal resolution that was more compatible with the scale of electrophysiological measurement. Further, to allow use in the awake macaque our technique also had to be robust to animal behavior. Macaques are generally head-fixed during standard electrophysiological recording. However, they are still capable of small movements. Further, the brain pulsates, in particular, when there is an open chamber through the skull to allow electrode penetration, these pulsations can cause substantial movement. These movements contribute to the exceptional difficulty of awake macaque BOLD fMRI and combined BOLD fMRI and electrophysiology. Our system had to be robust to these movements.

Further, macaques are not commonly electrically isolated from their environment. (Small animal electrophysiology preps are commonly electrically isolated). Since polarography is an electrochemical technique and dependent on control of voltage drops and current flow, we also had to develop electronics that could isolate our polarographic circuit from other electrical connections to the monkey.

Our final system consists of platinum iridium microelectrode cathodes designed in collaboration with FHC (Bowdoin Me), high quality DC EEG Silver/Silver chloride anodes (Grass Electronics), a specialized polarographic amplifier that provides the

polarizing voltage and measures the resulting current (Unisense PA 2000), and custom designed optical isolation circuitry to allow control of stray current paths. Placement of electrodes was accomplished with a standard micro-electrode multi drive (NAN) and data was digitized and recorded using the Plexon MAP system.

The final microelectrode cathode design (FHC-UELS3) can be seen in appendix 1. It consists of a 20 mm long, 75 micron diameter platinum iridium wire, to serve as the cathode tip, bonded to a 90 mm stainless steel shank for length and mechanical strength. This design is within the general parameters of an electrophysiology recording electrode. However, the details are relevant to polarographic recording. The platinum wire is insulated with glass. During development we found that other insulating materials provided unstable recordings. Current would change suddenly, in either direction, suggesting that thin insulation near the tip was being oxidized. Oxidization of insulation carries current. The oxide can then become inert, blocking current and increasing resistance, or the oxide can slough off, dropping resistance and increasing oxygen reduction current. Platinum iridium is stronger than pure platinum, however, it is a soft metal. The stainless steel shank, in place of a pure platinum electrode, provides strength necessary for the macaque environment and reduces cost. However, the stainless steel must be well coupled to the platinum to avoid potential voltage drops in the electrode and be very well insulated so that it does not have any electrical contact with the solution.

Since these electrodes are in the general form of standard macaque electrophysiology electrodes they can be easily integrated into the standard electrophysiology environment. In macaque electrophysiology, electrodes are

commonly acutely placed for each recording session. To accomplish this, a chronic recording chamber is attached to the monkey's skull and dura exposed. For each session, dura is penetrated with needle, and the recording electrode is passed through this needle or, guide tube, into the brain using a microdrive.

Our electrodes fit into 23 gauge extra thin wall tubing, a common guide tube material, and can be positioned with a standard microdrive. Our system employs two 4 electrode microdrives to allow placement of multiple electrodes in both hemispheres. (NAN systems) However, any microdrive suitable for macaque electrophysiology would work. Currently we are able to place electrodes at 0.5 mm spacing. Thus our point-to-point resolution is 0.5 mm. However, this could easily be modified.

Finally, the exposed tip size must be controlled. Tip size directly translates to the spatial specificity of the electrode. In general the resolution is between 1 and 5 times the diameter of the exposed cathode tip. [49] To control tip size, the electrode is passed through a molten a glass bath stopping just short of the tip. The stopping point is adjusted to leave only enough metal remains exposed to provide 1 MOhm impedance at 1 KHz. Although not a direct measure of tip size, this criterion reliably results in exposed tip size of 20-30 microns and thus a spatial specificity of the electrode of 20-100 microns. This spatial specificity is similar to the tissue volume thought to be reflected in local field potentials, and similar to the scale of neural architecture: neurons are about 20 microns across, cortical columns are on order of 100 microns, etc.

The temporal resolution possible with these electrodes is theoretically only limited by the time required for the oxygen concentration gradient (or oxygen pressure) at the tip

of the electrode to change. This is in principle the same as the time to change the oxygen concentration itself, thus theoretical temporal resolution is near infinite. In practice, temporal resolution is limited to 20 Hz by capacitance in the electronics required for the polarizing electronics. See below. This limit on temporal resolution is also significant for matching to BOLD fMRI. The average cortical inter-capillary spacing is ~50 microns, and oxygen diffuses through ECF at ~1 micron^2 per ms. Above 20 Hz (50 ms periods) oxygen could be non-uniformly distributed in tissue and our technique would be sensitive to phenomena not visible with BOLD fMRI. 20 Hz is the upper limit for diffusion matching of blood and tissue oxygen. In theory this system could distinguish timing differences in a response or ongoing activity between regions of ~50 ms, which is comparable to neural transmission delays between distant regions. Both the spatial specificity and temporal resolution are thus orders of magnitude greater than possible with BOLD fMRI and far better matched to electrophysiological recording and neural phenomena.

Prior to use, new electrodes or electrodes that have been sitting unused for a long period of time must be conditioned. The electrode manufacturing process can leave small amounts of oil on the electrode tip, or very small cracks in the glass. Oxidation of oil can cause issues similar those discussed for insulation above. Small glass cracks can become hydrated or open further changing the oxygen diffusion path to the electrode or its surface area and destabilizing recording. Conditioning electrodes is done by placing them in a solution of de-ionized water and NaCl, and polarizing them at -0.8 V relative to an Ag/AgCl reference. Current is monitored until there is less than a 1% fluctuation over 5 minutes and no linear trend. Conditioning usually requires 3-5

hrs. During conditioning, the current occasionally jumps as cracks are opened or hydrated, and falls as oxidizable oils are burned off. Conditioning allows these processes to be exhausted and stable recording to commence.

Additionally, although designed for polarography, our electrodes can also be used to record local field potentials and multi-unit activity. Currently, electrophysiology can be recorded serially from these electrodes by switching the system they are connected to. Serial recording required construction of a small switching adaptor that allowed us to switch systems without disturbing the electrode. Serial recording allows exact co-localization of oxygen and electrophysiological responses to stimuli. Further, recording electrophysiology during electrode placement allows for confirmation of tissue type before recording oxygen.

Electrophysiology can also be recorded simultaneously with oxygen from a neighboring electrode. In theory, if each system was referenced to a different isolated ground, an ammeter (polarography) and voltmeter could be simultaneously connected to the same electrode, allowing simultaneous polarography and electrophysiology. However, capacitance in the electrode allows some capacitive coupling between systems despite ground isolation. We are developing circuitry to prevent crosstalk such that electrophysiology and polarography can be recorded from the same electrode simultaneously.

For use as an anode we chose a commercially available DC EEG electrode (Grass Electronics). These electrodes are known for stable EEG recording, are large (10mm diameter) and have a substantial coating of AgCl. They provide a large enough source

of AgCl, a broad and thus stable physical connection to the monkey, and are inherently electrically stable. They provide a stable non-polarizable reference electrode. In order to use these electrodes in a macaque, an area of the head that is free from movement must be identified. Macaques have substantial musculature on their heads, and movement of the anode can disrupt the recording. Further, the head must be shaved and the skin abraded to provide stable electrical contact with tissue. Variability of the resistance over the cutaneous layer of the skin due to changing amounts of perspiration can add small amounts of noise. The effects of these noise sources at the anode are small. However, since one of our goals is to establish a system that can study the ongoing fluctuations in tissue oxygen, control of nuisance fluctuations is desirable.

Based on prior literature, we chose a commercial polarographic amplifier, the Unisense PA2000. [45-48] This amplifier consists of a highly stable voltage source with substantial capacitive buffering to handle changes in current without changing voltage, and a high fidelity current to voltage op-amp. This amplifier is designed for use with micro-pipette Clark electrodes (see above) and required some adaptation for our use. In order to handle the higher current observed in an open metal polarographic system, the range of the amplifier had to be increased. Due to the greater oxygen availability in tissue as opposed to the diffusion limited availability within a Clark electrode, and due to larger surface area, we observe currents ~2 orders of magnitude greater than those reported in prior literature using Clark electrodes with this amplifier. Making this change required changing the value of a resistor and capacitor in the input current to voltage converter of the amplifier.

Further, since Clark electrodes are by design electrically isolated from the solution under study, the PA2000 was not designed with integrated ground isolation. Polarography assumes a specific current path: from the amplifier to cathode and back via the anode. Alternate current paths invalidate the basic assumptions of polarography. For example, a ground loop in which current flows from the cathode to earth ground and back to the amplifier via power ground or amplifier output ground instead of via the anode adds the potential for several uncontrolled half-cell reactions along this alternate loop. In order to block alternate current paths in an open, bare metal electrode, polarographic system, the entire system must be isolated from earth or other lab electronics. Since we intend simultaneous electrophysiological measurement, isolation also limits the potential for crosstalk between recording systems.

Isolation can be accomplished by isolating the fluid, or animal, under study from earth or other electronics as is commonly done in small animal preparations. However, this is not feasible for macaques. In the macaque the polarographic circuit must be isolated so that current can only leave the amplifier via the cathode and return to the amplifier via the anode. Transformers isolation is the most common form of ground isolation. However, transformer isolation can allow fluctuations in ground voltage or ground loop resistance to interfere with recording. Ground loop fluctuations can be introduced by fluctuating ground voltage due to other lab systems delivering or drawing current from the ground. In addition to the potential for stable ground loops in macaque recording, macaques move and change their coupling with ground, and ground loop resistance, during recording. Since fluctuating energy can be transferred through transformers in either direction they cannot isolate the polarographic circuit from fluctuating ground

noise. To provide a surrogate for BOLD the system must be sensitive to both stimulus driven and ongoing fluctuations in oxygen. Thus both stable, DC, ground loops and fluctuating, AC, ground activity must be blocked from returning energy to the amplifier.

To accomplish AC isolation we designed and built a custom analogue optical isolation system. Optical isolation transmits the signal from the isolated circuit to external systems (like the digitizing system) via light emitted from and LED and received at a photodiode. The change of signal type and unidirectional transmission completely block both AC and DC current from flowing to the amplifier from ground. Commonly, optical isolation is done after digitization. Light output from LED's, and current drive through the receiving photodiode are not linear with voltage. Hence, optical isolation is commonly only used in digital applications where only event detection, and not measurement of absolute event magnitude, is required. However, we needed to isolate an analogue polarographic circuit directly. Thus we adapted the optical isolation method. Reliable analogue optical signal transmission is possible if the LED and photodiode are under feedback control. This is accomplished by a specialized chip that contains 1 LED and 2 photodiodes (Vishay IL300). One diode serves as a feedback controller to the voltage source driving the LED. The voltage driven in this photodiode is compared to the input voltage and current to the LED adjusted. This allows the LED luminance/photodiode drive pair to be linearized and the voltage output to be matched to the input voltage. The second photodiode has no electrical connection to the input and is the isolated output of the system. System tuning with variable resistors allows the response of the feedback and output photodiodes to be matched. See appendix 2 for circuit schematics.

The final step in isolation is independent power. Also shown in appendix 2, included in the optical isolation device, is a battery and recharging circuit to provide power to the PA2000 and isolation system. Between recordings this system is connected to building power and earth ground via a relay to allow battery charging. During recording, the connection to earth and building power is mechanically severed at the relay. The entire polarographic circuit runs on battery power optically isolated from all other lab circuitry and earth. Weak capacitive coupling with earth ground is still possible. However, this is unlikely to drive meaningful fluctuations.

In summary our system consists of customized platinum iridium micro-electrodes as cathodes (FHC, Bowdoin ME), high quality Ag/AgCl EEG electrodes as anodes (Grass Technologies, Warwick RI), customized electronics to provide the polarizing voltage and measure the resulting current (Unisense, Aarhus Denmark) and purpose built isolation circuitry to allow control of the polarographic current path (in house). This system provides a spatial resolution of 0.5 mm with a spatial specificity of 20-100 microns, and a temporal resolution of 20 Hz. However, the spatial specificity is dependent on the tip size of the electrode and could be altered. Currently both the temporal resolution and spatial specificity are orders of magnitude greater than possible with BOLD fMRI. While the systems current four-site coverage is far less than the whole brain coverage of fMRI, it is sufficient to study multi-regional stimulus driven activity, and inter-regional dependencies of ongoing activity. Further, the number of sites is only limited by the ability to place electrodes in the brain and the electronics for applying the voltage and measuring current. These are not hard limits and the system could be readily expanded. This system provides a high resolution surrogate for BOLD fMRI that is

easily integrated into the standard macaque electrophysiology environment, providing access a wealth of tools for controlling animal behavior, and is easily combined with electrophysiological measurement.

System Testing:

During development we tested our system in several ways to confirm that it was recording oxygen and could provide a surrogate for BOLD fMRI. As discussed above, a hallmark of polarographic is nonlinearity in the current voltage relationship. In particular, in an oxygen polarographic system current in -0.7 to -0.9 V range is primarily carried by, and thus restricted by, the concentration of, oxygen leading to a plateau in the current voltage relationship. We confirmed the presence of this plateau in our system in vitro in saline and artificial CSF, in the live mouse brain, and in the awake primate brain. In general we tested for the plateau by randomly varying voltage between 0 and -1.2 V. For simplicity, figure 1 shows the effect of increasing voltage from -0.2 V to -1.2 V by 0.05 V steps. Note the capacitive transients at voltage transitions as the new chemical equilibrium and molecular layer capacitor are formed (see above) and the current restriction in the plateau range, specifically around -0.8 V (the polarization we used during recording). In a small subset of experiments we also bubbled nitrogen, air, and pure oxygen into a beaker, and confirmed by eye a rough linearity of oxygen concentration with current.

Beyond confirming that our system showed the basic hallmarks of oxygen polarography we also evaluated whether our system was sensitive to physiologic changes in oxygen. Figure 2 shows the impact of changing the breathing gases while recording oxygen in the mouse brain. Oxygen was recorded from the somatosensory

cortex of an anesthetized artificially ventilated mouse. When the ventilation gas was changed from air to carbogen, tissue oxygen concentration increased nearly 300%. Carbogen is 95% oxygen and 5% CO2. This mix increases oxygen and CO2 concentration in the lungs and blood. . Since the respiratory rate is fixed by the ventilator, respiratory rate cannot be increased to compensate. Increases in blood CO2 drive vasodilation. The combination of these effects disrupts normal homeostatic mechanisms and leads to the observed increase in tissue oxygen concentration. These results demonstrate that our system behaves as expected for a polarographic circuit and is sensitive in general to changes in oxygen in the brain.

In addition to these basic features we assessed whether our technique was safe for use in the brain, provided high enough signal to noise, and was robust enough to the brain environment to provide a surrogate for BOLD fMRI. Based on the observed currents in our system and known reactions we calculated that the oxygen consumed in the cathode reaction is insubstantial compared to the quantity of oxygen available to the brain tissue and does not pose a health threat. [49, 198] Further, the current observed in the brain using our system is between 3 and 50 nA (mode ~ 10 nA) and will not stimulate cortex. The variability in current is related to distance from the capillaries and variation in size of the electrode tip.

Prior observation has shown that platinum-iridium electrodes are not corroded by CSF. However, blood can corrode Pt/Ir electrodes. [197] In general our electrodes will not be in contact with blood. However, penetration of dura can result in minor bleeding. In general, this bleeding will be short lived and given a few minutes to clear will not affect our electrodes. If the electrode does come in contact with blood, this will lead to a

layer of material being deposited on the electrode tip and a slow linear decrease in mean current. We did not regularly observe this, and if observed, recordings showing such a trend can be discarded.

Since the brain is electrically active we also assessed whether electrical activity of the brain could influence our electrochemical measure. The -.8V polarizing voltage we use is 3 orders of magnitude greater than electrical potentials normally recorded from brain tissue. Current in this voltage range is limited by oxygen concentration and thus should be independent of voltage. Minor physiologically driven fluctuations in voltage should have virtually no effect on observed current. Further, our system is electrically isolated. Local neural voltage fields cannot affect the primary voltage drop between the isolated anode and cathode. However, fluctuating voltage fields in the brain (local field potentials) could induce fluctuations in current flow, like waves in a flowing stream.

To test this we recorded the polarographic current in a saline filled beaker while applying external electric fields. Since the electrode has some capacitance, and current must flow through a solution in which ions are being moved by external fields, high powered external fields can slightly influence our measurement. We used field ranging from 50 mV to 2 V at frequencies from 4-10 Hz and evaluated the magnitude of current fluctuation at the frequency of the field. These experiments demonstrated a linear relationship between external field voltage and induced signal, with a peak of ~20 picoamps of induced signal at 2 V. Extending the applied voltage induced current fit to the few mV range of the brains local field potentials, we estimated that the brain electrical could drive only a few picoamps of artifact current compared to the 1-5 nanoamps fluctuations we observed and attribute to oxygen modulation driving current.

Since the magnitude of oxygen fluctuations scales with frequency we estimated the maximal variance an LFP scale field could drive and compared the estimated variance to the variance in the oxygen signal filtered into the frequency band of the applied field. LFP's could drive less that 3% of the observed variance. Further, the applied fields were uniform in the fluid between the cathode and anode, brain potentials are not uniform in the current path between the anode and cathode and their effects likely cancel.

Further, we are able to record significantly different LFP and oxygen responses simultaneously. We assessed whether we could detect stimulus driven changes in oxygen and electrophysiology simultaneously. Figure 3 shows the oxygen and LFP responses from neighboring electrodes to 4 s of 5 Hz stroboscopic illumination in area V3. These results show that our oxygen polarographic system can detect stimulus-driven changes in local brain oxygen similar to what would be expected from BOLD fMRI recording under the same conditions. In addition to confirming that our system was sensitive to changes in brain oxygen concentration driven by ventilator gas, insensitive to electrical fields, and showed the basic characteristics of a polarographic system we confirmed that we could detect the phenomena of interest studied with BOLD: stimulus driven and ongoing fluctuations in oxygen in the presence of the brain's electrical activity. Chapter 3 discusses serial recording of tissue oxygen and electrophysiological stimulus responses in detail.

Chapter 4 discusses oxygen fluctuations and our ability to assess their inter-regional dependence. Initially, as discussed above regarding conditioning, we determined that we could measure a nearly flat (less than 1% modulation) signal in a beaker. In vitro

recording confirmed that the inherent signal to noise of our system was fairly high (low noise). Once recording in the brain we further noted that we observed large fluctuations, as was reported in prior polarographic literature. However, the magnitude of these fluctuations was location dependent. In some cases we even noticed nearly flat recordings in the junction of the lateral occipital and intra-parietal sulci where a pocket of CSF can form. Position dependence of fluctuations implies that they are brain driven and not simply an artifact of recording in the macaque.

Daily use of this system has proven to be similar to standard macaque electrophysiology. One must choose electrode locations, load electrodes into a microdrive for placement in the brain, condition or train a macaque for recording, and engage recording equipment. Somewhat more electrode maintenance is required to keep conditioned electrodes available, and combining polarography and electrophysiology requires knowledge of two sets of recording hardware. However, this system is far easier to deploy than BOLD fMRI or optical measures of hemodynamic activity and far easier to combine with electrophysiology.

Development and testing of this system was done in collaboration with Illya Tolokh and Tim Holy, who provided mice, gases, and small animal recording space for system testing during development, and Gerald Gusdorf with whom we collaborated in the design and customization of recording electronics. In particular, the design and construction of the optical isolation and charging systems were done in collaboration with and under the mentorship of Gerald Gusdorf. Illya performed all mouse surgery.

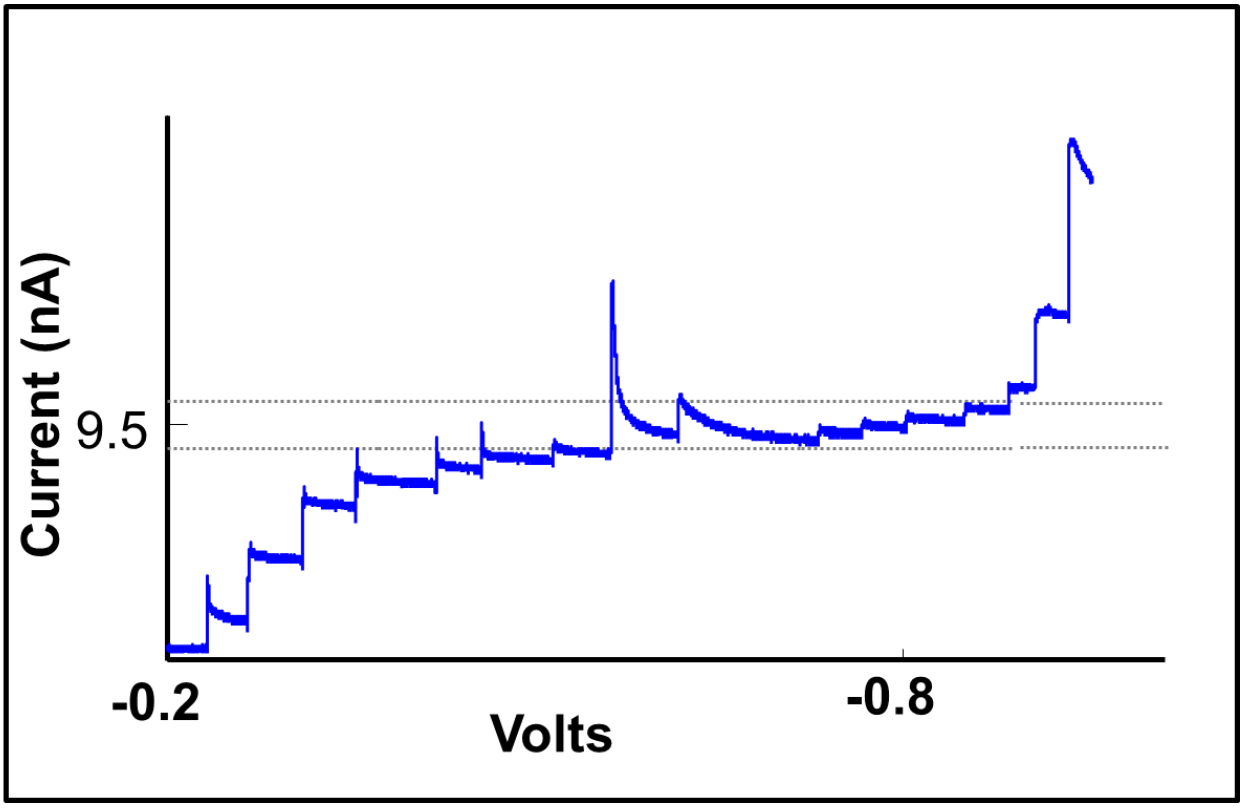

Figure 1: Oxygen Polarographic Plateau. The blue line shows current (y-axis) driven in our oxygen polarographic system at the indicated voltage (x-axis). Voltage was adjusted in 0.05 V increments from -0.2 to -1 V. Note the plateau in the current voltage relationship around -0.8 V. The plateau shown here, or deviations from a linear (Ohm's law V=IR) current voltage relationship, reflects oxygen concentration restriction of current and is a hallmark of oxygen polarographic measurement.

Oxygen polarography is an electrochemical technique that allows measurement of oxygen concentration in a fluid. In an oxygen polarographic system, oxygen concentration is proportional to current at a specific polarizing voltage. In the -0.6 to -0.9 voltage range current is restricted by the rate of charge transfer at the cathode. Oxygen reduction at the cathode is known to be the primary half-cell reaction carrying charge (or current) through solution. The rate of charge transfer, current, depends on how frequently this reaction can occur which in turn depends on oxygen concentration. Thus current is limited by oxygen concentration. At lower and higher voltages other half cell reactions contribute significantly to charge transfer.

The height of this plateau, or current at -0.8 V is proportional to oxygen concentration, in the remainder of the document, changes in current at this voltage are considered changes in oxygen concentration. The capacitive transients reflect adjustments of the micro scale capacitor of reduced ions on the electrode tip and unreduced ions one molecular layer away. This recording was obtained in a saline filled beaker. However, we confirmed current restriction in CSF in vivo and linearity of the plateau height with oxygen concentration in other experiments.

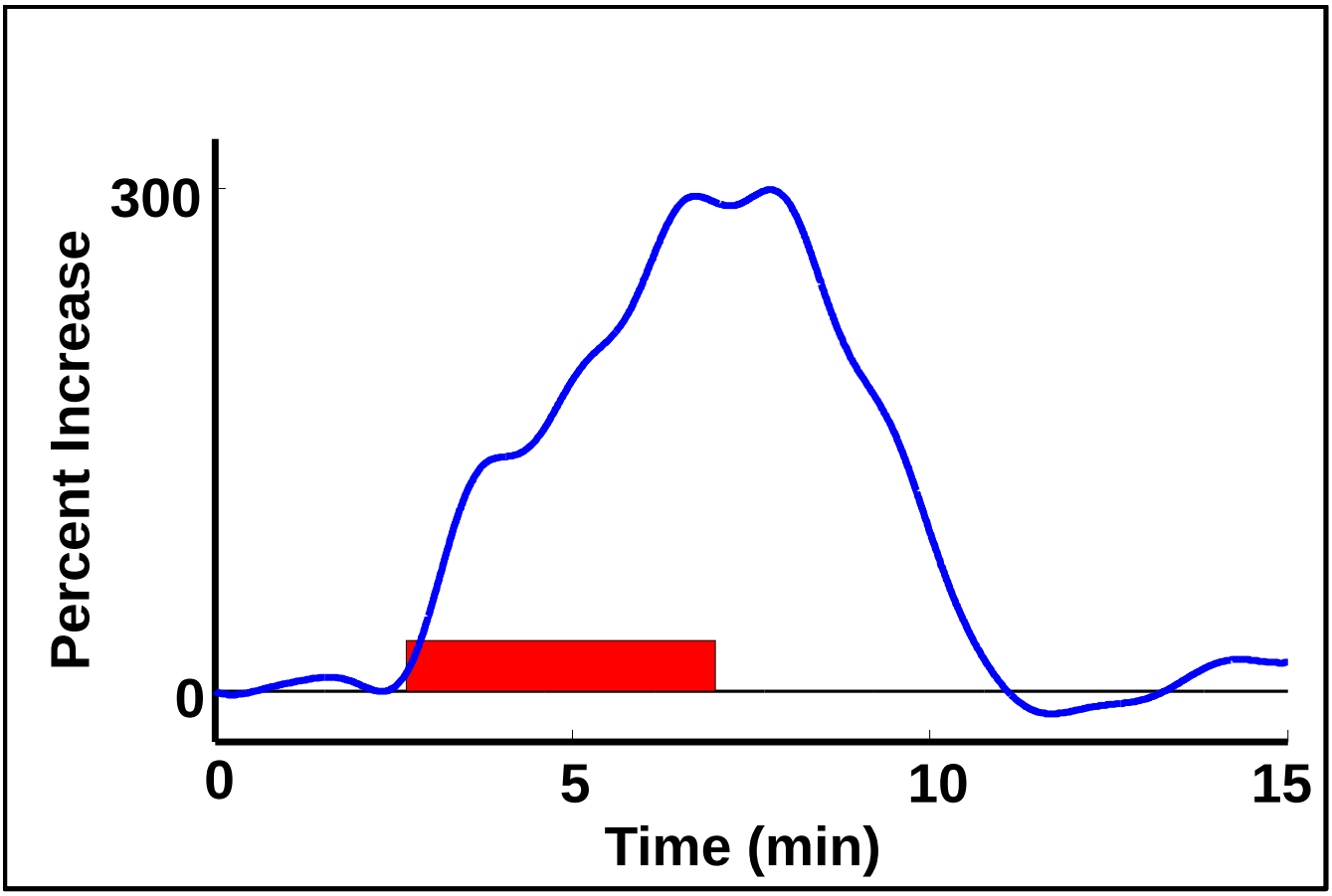

Figure 2: Carbogen Response: The blue line depicts changes in oxygen concentration (current at -0.8 V) recorded in cortex of an anesthetized artificially ventilated mouse. When the ventilation gas is switched from air to carbogen (95 %O^2 5% CO^2, red bar) systemic vasodilation is induced by the increased $CO^{2,}$ and oxygen saturation is increased by the elevated O^2 concentration. Vasodilation in the face of increased oxygen concentration caused by carbogen disrupts normal homeostatic regulation and leads to a dramatic increase in tissue oxygen. This increase in local oxygen levels can be detected by our system as a near 300% increase in polarographic current and/or oxygen. These results demonstrate that our technique is sensitive to in vivo changes in oxygen concentration.

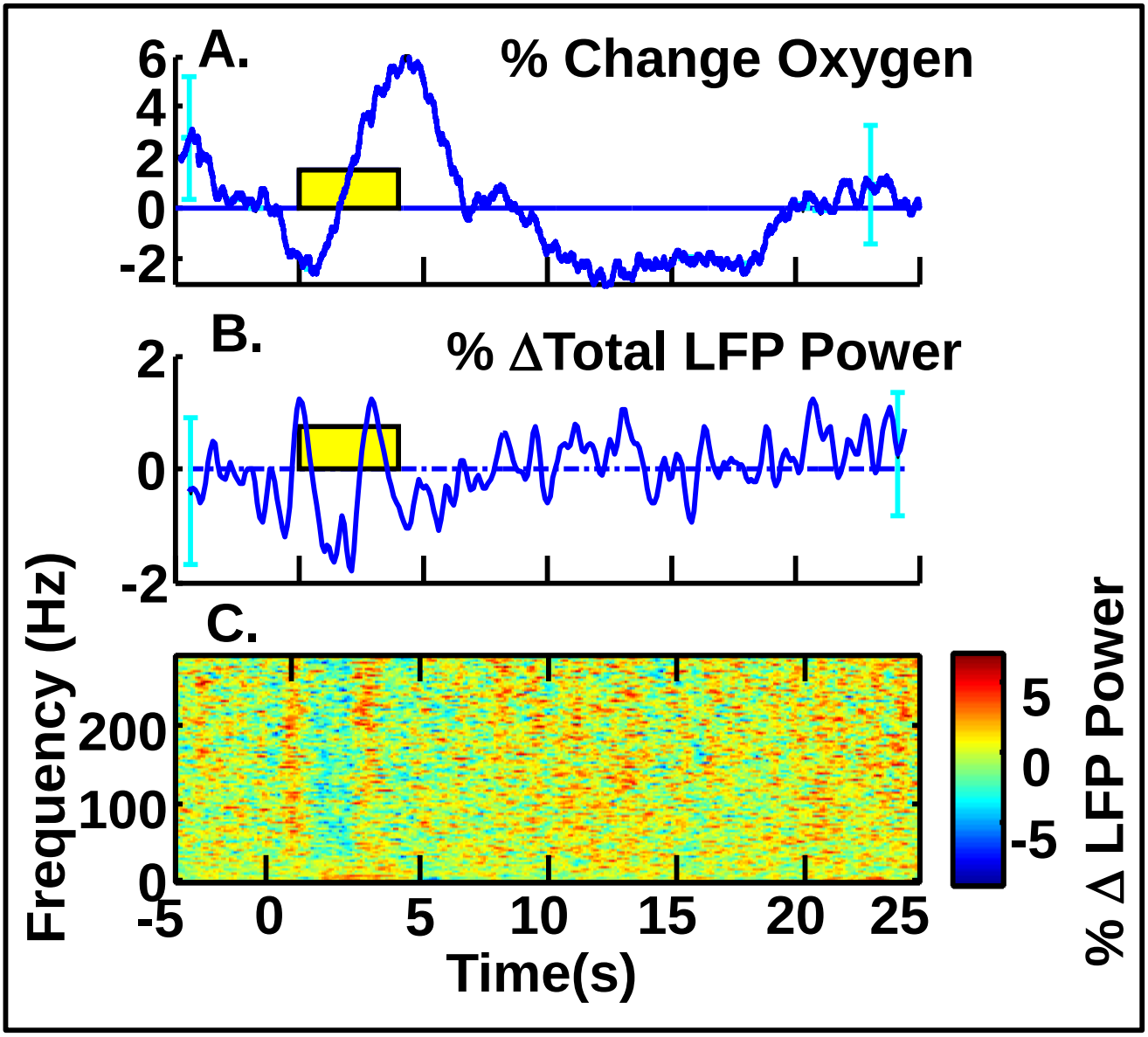

Figure 3 Simultaneous local field potential and oxygen stimulus response: Panel A shows the oxygen, polarographic current, response to 4s of 5 Hz stroboscopic illumination recorded from area V3 of the awake macaque. Panels B and C show the local field potential response recorded simultaneously from an electrode 1 mm away also in area V3. These recordings demonstrate that we are able to record normal physiological fluctuations in oxygen. Recording with our system matches what we would expect to see with BOLD fMRI recording under the same conditions. Further the substantial difference in the oxygen and LFP responses demonstrates our ability to record oxygen and electrophysiology simultaneously without substantial interference, a major design goal.

Chapter 3:

Stimulus Driven Tissue Oxygen and Local Field Potential Responses.

Overview:

This chapter discusses stimulus driven tissue oxygen and local field potential responses in representative regions of the default mode and visual/attention networks, (posterior cingulate, PCC, and area V3) to 15 s of 1 Hz stroboscopic illumination. These results extend the system testing discussed in chapter 2. The presented polarographic oxygen results are consistent with prior BOLD fMRI results validating our technique. Further, these results provide novel evidence that macaques show external engagement suppressed default mode network activity and provide insight into the electrophysiological behavior of the default mode network. Finally, these results allow comparison of the neural activity related to oxygen and by proxy to BOLD fMRI responses. This comparison supports a strong neural BOLD relationship. However, it suggests that the nature of the neural activity BOLD fMRI relationship, or at least BOLD's relationship to LFP power, varies across regions and suggests caution in making specific claims about neural activity from BOLD data. Here we briefly re-introduce the relevant issues, discuss experiment specific methods, results, and conclusions.

V3 and PCC have very different, task-positive vs. task negative, BOLD fMRI responses to externally engaging stimuli in humans. As expected both LFP and oxygen

increased in V3 and decreased in PCC. However, in addition to this primary behavior oxygen and LFP showed substantial nuance. In V3, oxygen showed greater responses to the onset and offset of the stimulus and a reduced sustained activation during stimulation. In PCC, oxygen showed a prominent activation to stimulus onset followed by sustained suppression. In V3, most LFP bands showed an increase, however, LFP power decreased in the 4-16 Hz range. In PCC, all LFP bands showed an onset transient followed by sustained suppression. However, the time-course of suppression varied across frequencies. In both regions the LFP showed positive responses to each flash of the stroboscopic stimulus. These phasic responses rode on top of the primary tonic behavior and were 10 times greater in V3 than in PCC. Both regions showed a strong relationship between LFP and oxygen.

This work will be submitted for publication by myself and Jingfeng Li in a format similar to what is presented here. Data collection and writing (publication version) were done collaboratively and authorship will be shared. As the senior member of the team I in general took the lead and coached Jingfeng through much of his involvement. I designed the study, did the analyses and wrote what is presented here.

Introduction:

Blood oxygen level dependent (BOLD) fMRI in humans and electrophysiological recording in animal models have both provided enormous insight into the functional architecture of the brain. It is generally accepted that BOLD relates to neural activity. However, the majority of work comparing BOLD and neural activity has been done in primary sensory areas in anesthetized animals. The specifics of the relationship

between BOLD fMRI and neural activity remain unclear and may differ between states, between positive and negative responses, and across areas. [13, 14, 24-26, 33-37, 85, 194, 199, 200]

A unique set of regions, the default-mode network, show decreasing-“task negative”, responses to a wide range of stimuli or tasks. These areas are thought to sub-serve a function that is engaged when subjects are at rest and not engaged with the external world [121]. Our understanding of these task-negative responses comes primarily from human BOLD fMRI and the nature of the relationship between the studied task-negative BOLD fMRI responses and neural activity is unclear.

Direct comparison of neural and task negative BOLD responses in the default mode network faces several serious technical complications. Simultaneous BOLD fMRI and electrophysiology is nearly impossible in humans, and, when possible in macaques, is exceedingly technically demanding. [37]. Comparisons of BOLD and electrophysiological recordings are further confounded by signal interference and difficulties in matching the location and spatial coverage of the two signals. In addition, to examine task negative default-mode responses in the macaque a baseline resting state must be established. Collection of BOLD fMRI in monkeys requires the animal to sit still in the loud and potentially frightening fMRI environment. While sitting still and ignoring the fMRI environment are easy tasks for humans, they are unnatural and effortful actions for monkeys that require extensive training. It is unclear whether the effortful, “sitting still” baseline state used in macaque fMRI can be considered a resting state that is directly comparable to the human resting state. In contrast, monkeys left

alone in a quiet dark room with minimum restriction, naturally enter a drowsy state that resembles the resting state used in human BOLD fMRI studies.

We implemented, oxygen polarography, an electrode-based, MRI-independent, oxygen measurement, in the awake macaque to allow comparison of oxygen (a BOLD fMRI surrogate) and electrophysiology when a macaque is woken from this resting state by stimulation. This electrode-based technique has few limits beyond those of standard micro-electrode electrophysiological recording. In addition, oxygen polarography can be readily combined with electrophysiology and allows the comparison between neural and oxygen responses.

We recorded oxygen polarography and local field potentials (LFP) in the posterior cingulate cortex (PCC, a core default mode, or task negative, region) and area V3 (a visual task positive area) of awake monkeys. When a macaque sitting restfully in the dark is engaged by stroboscopic visual stimulation, oxygen levels and LFP power are primarily suppressed in PCC and increased in V3. However, we also note substantial activations to stimulus onset in both oxygen and LFP, and positive, phasic LFP responses to the individual flashes in both regions. Finally, comparison between LFP and oxygen responses shows that LFP and oxygen responses are highly related across a wide range of LFP frequencies in both regions, but the relationship appears to differ between regions.

Methods:

Oxygen Recording:

Oxygen polarography is an electrochemical technique. At a highly controlled voltage the current flowing between a noble metal cathode and a non-polarizable reference

electrode across a fluid bridge, in this case the brain/ECF/CSF, becomes proportional to oxygen concentration. In this arrangement, the primary half-cell reaction receiving electrons at the cathode is the reduction of oxygen. This reaction is rate limited by oxygen concentration and thus the rate of charge transfer, current, is proportional to oxygen concentration[49, 196]. This technique has a long and well-validated history in neuroscience. [109, 195].

We utilized specialized platinum microelectrodes suitable for both oxygen polarographic redox control and electrophysiological recording (FHC instruments) as a cathode, polarized at -0.8 V compared to a high quality Ag/AgCl reference (anode) (Grass Technologies). A high quality purpose built ammeter (Unisense PA2000) supplied the polarizing voltage and measured current.

Control of stray current paths was achieved by electrically isolating the entire system using a custom built optical isolator. The anode was placed on the back of the head in an area that showed little visible movement and skin was abraded to avoid sweat and movement potentials. Oxygen signal response time was limited to 50 ms (20 Hz) by capacitance in the system and was thus filtered at 20 Hz just prior to digitization (Frequency Devices). Our system allows simultaneous recording at 4 sites in awake macaques with a temporal resolution of 50 ms and a spatial specificity of 30-100 microns.

Animals, Behavior, Stimulus:

2 macaques participated in this study. Animals were cared for and handled in accordance with the public health service guide for animal use and all procedures were approved by the Washington University Animal Studies Committee. During recording

macaques were fully hydrated and sat head-fixed in a dark room facing a wide field textured screen with no expectation of a task or reward. Behavior was unconstrained and macaques naturally settled into a resting "default" state operationally similar to the resting state used in human fMRI. This state was interrupted by 15 seconds of dim 1 Hz stroboscopic illumination presented at 30 s intervals. Eye tracking and behavioral monitoring demonstrated that macaques engaged with this stimulus but found it only mildly arousing and entered a natural resting state during darkness.

Recording:

The brain was accessed via bilateral 15 mm chronic recording chambers (Crist instruments). MRI images (Siemens Trio MPRAGE .5 mm isotropic voxels) were obtained including a specialized phantom that allows visualization of the chamber and projection of a chamber based coordinate system into the brain. In one monkey, 2 small MRI lucent manganese chloride injections were placed using this coordinate projection and he was reimaged to confirm and refine its accuracy. For each recording session 4 specialized platinum microelectrodes were inserted using the MRI projection into bilateral PCC and V3, using twin multi-electrode microdrives (NAN instruments). During penetration electrophysiology was recorded from the advancing electrodes. Placement in gray matter was confirmed by multi-unit activity.

We recorded from 23/21 sites and 1025/942 trials in PCC and V3 respectively for oxygen, 605/607 trials for LFP, across 15 sessions. In order to allow precise co-localization, oxygen and LFP responses were recorded serially from the same electrode. Our oxygen polarography technique allows simultaneous recording from neighboring electrodes, however, given the tiny volumes that generate LFP and from

which we record oxygen, we were concerned that neighboring electrodes would not reflect overlapping response fields. Data shown in figures 6 and 7 reflects 19 sites in V3 and 22 in PCC from which both oxygen and LFP were successfully recorded from the same electrode at the same site. Data from both monkeys was similar and thus combined. LFP was measured and all data was stored at 1 kHz using the Plexon MAP system (Plexon Inc.).

Analysis:

All analyses were done in Matlab (Matlab Inc. Natick Ma). LFP data was decomposed into amplitude by frequency using the complex wavelet transform with the morlet wavelet. LFP power fluctuations were normalized to the inter-trial interval (ITI) mean by frequency to overcome the roughly 1/f power spectrum of raw LFP and allow comparison of LFP responses across frequency. Oxygen recordings were converted to percent deviation from the mean ITI value. The ITI was defined as the last 5 s of each trial. Oxygen and frequency decomposed LFP responses were averaged across trials, days, and, since results were very similar, monkeys.

In order to compare LFP and oxygen, correlation between and transforms from LFP to oxygen were assessed. Lagged Pearson's r correlation was assessed between LFP and oxygen at each LFP frequency. For statistical analysis Pearson's r values were converted to a normal distribution using the Fisher's z transform. Three methods of evaluating the LFP oxygen transform were assessed. We fit two assumed shape transforms and directly estimated the transform using FFT de-convolution. Fitting each transfer function minimized mean squared error between the predicted oxygen response (convolution of the fit kernel with LFP) and the recorded oxygen response.

The SPM 5 transfer function was generated using the default settings of the SPM 5 fMRI toolbox (http://www.fil.ion.ucl.ac.uk/spm/software/spm5/). This function was chosen due to its prior use in the literature relating LFP and hemodynamic signals. Generic hemodynamic response functions were fit using the SPM 5 toolbox. The parameter space for both transforms was searched to minimize the squared deviation of the convolution of the fit TF with the LFP response and the oxygen response. (The SPM5 function has one free parameter, scale; the generic hemodynamic response function has 8 parameters: length of the kernel, onset delay of the kernel, ratio of the two gamma functions, time to peak and dispersion of the two gamma functions and scale).

Data driven transfer functions estimates were calculated using standard linear systems theory. In brief, the average oxygen and LFP response at each frequency were whitened, zero padded and converted into the frequency domain using the fast Fourier transform. The transform was limited to values at frequencies less than 20 Hz (the high-cut of the oxygen system) to remove non-physiologic effects and the transformed oxygen was divided by LFP. To remove idiosyncratic effect of white noise, this process was repeated 500 times and the division result averaged in frequency space. The result was then converted back to the time domain using the inverse Fourier transform and remaining idiosyncratic high-frequency results of the Fourier division removed by smoothing with a ½ s Gaussian kernel.

Results:

We recorded local tissue oxygen and LFP in bilateral V3 and PCC in response to 15 s of 1Hz stroboscopic illumination in two monkeys. Each stimulus was separated by 30 s of darkness to allow the macaque to return to the resting state. Figure 1 shows approximate recording sites and the stimulus paradigm. Animals were head-fixed and sitting in a primate chair but were otherwise unrestrained. No rewards were delivered. Visual monitoring and eye tracking confirmed that during the 30 s of darkness macaques were relaxed and drowsy. Oxygen and LFP recordings were acquired serially from the same electrodes. Each signal, oxygen or LFP, was recorded simultaneously in all four regions. V3 is visually responsive and is representative of stimulus driven "task-positive" brain regions. PCC is the most common default or task-negative region cited, and is often thought of as a hub of the default mode network.

Oxygen polarography and BOLD fMRI both reflect changes in local brain oxygen levels. However, there are substantial differences in resolution and oxygen contrast mechanisms. Nevertheless, the integral of the oxygen response during the stimulation period is positive in V3 and negative in PCC (0.77 ±.075%, V3, -1.82 ± .21%, PCC, $p<.005$ across sites in both regions). Oxygen activation in V3 and suppression in PCC by a visual stimulus is consistent with the BOLD fMRI results and demonstrates that our technique captures the stimulus driven phenomena of interest. (Figure 2)

In addition to the main effect our design allows direct assessment, by trial averaging, of the time-course of the response. Oxygen signals in both regions exhibit a strong positive response to the onset of the stimulus (onset response) and are indistinguishable for the first 3.5 s. In V3, the amplitude and timing of the onset

response (peak of 2% at 6 s) are highly consistent with BOLD fMRI results in both humans and macaques. Onset responses in PCC are not commonly noted, potentially due to the focus on suppression of default-mode activity. However, several human BOLD fMRI studies report onset activations in PCC that are consistent with our observations, peak response of 1% at ~4 s. [201]

Following the onset response, oxygen behavior in PCC and V3 diverges. In V3, oxygen falls to a sustained ~0.3% by ~10 s, and shows a response to offset of ~0.7% at ~3 s relative to the last flash. After the offset response, there is a notable undershoot, with oxygen reaching a negative maximum of -0.6% at ~10 s after stimulus cessation. The time-course in V3 is highly consistent with both human and macaque BOLD fMRI responses. In PCC, the oxygen response quickly reverses sign and reaches a nadir of -2.7% at ~11 s after stimulus onset. Throughout stimulation, oxygen levels in PCC remain suppressed at ~ -2% and do not return to the resting level until 17 s after stimulus cessation. The time-course in PCC is highly consistent with human BOLD fMRI results. In the macaque, there is only limited evidence of BOLD suppression in PCC and no reported time-courses. Our results provide the best evidence to date of default activity suppression in the macaque and the first characterization of the time-course of suppression in the macaque.

Despite contrast differences and dramatically higher spatial specificity and temporal resolution of our technique compared to BOLD fMRI (30-100 microns vs. 2-3 mm and 20 Hz vs. .3-.5 Hz) the valence and time-courses of the responses we report are highly consistent with human BOLD fMRI and argue that our technique is a valid surrogate. Further, our results provide addition evidence of a stimulus onset response in PCC in

general, and new oxygen suppression evidence of a default-mode in the macaque.

Serially recorded local field potentials (LFP), from the same sites in response to the same stimuli shows qualitatively similar responses to oxygen. Figure 3A shows that, like oxygen, LFP power is overall increased in V3 and decreased in PCC. LFP modulation is highly significant and is presented in standard error units (Z-score) with green transitioning to yellow (+) or blue (-) at Z-scores of ± 2. Figure 3B shows the mean (± SEM) percent change by frequency of LFP power during visual stimulation (5-15 s). In PCC, LFP power is suppressed across the whole frequency range (1-150Hz), though the magnitude of the suppression varies across frequency. In V3, LFP power is significantly increased at most frequencies, with the notable exception of 4-16 Hz. Both heat maps and mean modulation are relative to the mean ITI (last 5 s) power across all trials.

The LFP response shows substantial temporal and spectral details that are not visible in the oxygen responses. In order to examine these details of the LFP response, we collapsed the LFP response into the common EEG frequency ranges (Figure 4): Delta: 1-4 Hz, Theta: 4-8 Hz, Alpha: 8-14 Hz, Beta: 14-30 Hz, low Gamma: 30-50, and high Gamma: 50-150 Hz. These bands were chosen for consistency with the existing literature.

In both V3 and PCC, like oxygen, there is a significant LFP onset response across all bands. The magnitude of this onset response is similar between the two regions. However, the waveform varies across regions and frequencies. After the onset response, the LFP time-courses can be separated into tonic baseline modulation and

phasic responses to each flash of the strobe stimulus. Baseline is defined as the 100 ms before each flash and is compared to the ITI resting level. In V3, the gamma and delta range baseline is elevated, theta and alpha range baseline is suppressed, and beta range baseline is unchanged. In PCC, all bands show sustained baseline suppression. Baseline modulation in both regions in all bands is significant at $p<<.001$.

The temporal dynamics of baseline modulation also differs across frequency bands (Figure 4). In V3, gamma band elevation occurs immediately following stimulus onset and is maintained at a constant level until ~1 s after the end of stimulation. Baseline suppression in the alpha and theta bands increases slowly over the first several flashes and is much slower ~2 s to return to the resting level after the end of stimulation. The delta band baseline increase occurs rapidly and, in contrast to the sustained baseline elevation in the gamma band, decreases immediately after the end of the stimulus. Delta band LFP also shows a prominent post-stimulation undershoot. In PCC, baseline suppression in all the bands increases slowly and does not return to the resting level until ~15 s after the last flash. The timing and magnitude of suppression varies across bands. One way ANOVA of time to peak suppression (time at max suppression) across frequency by trials shows a significant effect of frequency in PCC, with a trend for longest peak times in the beta and low-gamma range, 14-50 Hz ($df = 74,59850$ $F= 4.16$, $p = 3 \times 10^{-30}$).

In addition to the sustained activity, figure 5 shows that there are significant (p at peak < .0001) phasic responses to each stimulus (prominent in V3, less visible in PCC). To highlight the phasic response, we averaged the LFP responses across flashes 4-15. (Flashes 1-3 were not used to prevent confounds from the onset response). Sustained

responses were removed by subtracting the mean of the 100 ms before each flash. Phasic responses are present in both regions at all frequencies; however, they are approximately 10 times larger in V3 than in PCC. There is a strong phasic response to the onset of each flash, with additional smaller structures just before and after the offset of each flash. At low frequencies (Delta, Theta and Alpha) the response is distorted largely due to blurring in time inherent to estimation of power at these frequencies and not shown. Note that in V3 the strongest phasic response occurs in the high Gamma band, while in PCC the strongest phasic response is in the Beta band.

Overall, the LFP response contains substantial high frequency detail, multiple time-courses across frequencies, and shows phasic responses. The different LFP time-courses across bands and between regions are suggestive of multiple processes with distinct responses to the stimulus onset, sustain, and offset. The reflection of the high frequency LFP details in the oxygen signal is unclear and the apparent multiple LFP processes may each have a unique relationship to the oxygen response. With only a single stimulus we cannot disassociate the roles of these features.

However, despite these details, the oxygen and LFP responses are qualitatively very similar and highly related. Both oxygen and LFP show onset responses followed by sustained activation in V3 (except for Theta and Alpha LFP) and sustained suppression in PCC. Given matched LFP and oxygen recordings (recorded from the same cortex during the same task) and qualitatively related but distinct responses it is reasonable to evaluate the quantitative relationship between them. Quantification can be broken into two questions: how strong is the relationship between two signals, and what is the nature of the relationship, or shape of the transform, between two signals? These two

questions are in principle confounded as the apparent strength of the relationship will change if a transform is applied to either signal.

In order to quantify the first order linear similarity between the oxygen and LFP signals we evaluated lagged linear correlation shown in figure 6. Lagged correlation was used to account for the substantial delay between LFP and oxygen responses. Since linear correlation could be impacted by substantial differences in frequency content between the LFP and oxygen responses or across LFP frequencies, (higher frequency LFPs are able to represent higher frequency detail in the response), we also evaluated linear correlation after low-pass filtering the LFP responses below 1 Hz. Low-pass filtering is a mathematical transform and could artificially distort the relationship between oxygen and LFP. We do not imply that it reflects the actual transform between LFP and oxygen. However, low-pass filtering provides a control for potential frequency confounds of the raw linear correlation.

In V3, absolute correlation has a mean of 0.58 across frequencies and ranges from a minimum of ~0.3 at 4 and 16 Hz where the response changes valence to a maximum of ~ 0.7 in the delta and low gamma ranges. Note that in the 4-16 Hz range, correlation is negative. After low-pass filtering, in V3 the mean and minimum correlation are slightly but significantly increased (r_{mean} = 0.63 r_{min} = 0.55 p<.0001). However, the maximal correlation is slightly decreased, (r_{max} = 0.65 p<.0001). In PCC, correlation ranges from ~0.45 in the 20-30 Hz range to ~0.8 in the 1-6 Hz range with a mean across frequencies of ~0.6. After low-pass filtering, mean min and max correlation in PCC are all significantly increased. (r_{mean} = 0.82 r_{min} = 0.66 r_{max} = 0.86 p<.0001). In V3 the mean lag at peak correlation is 3.1 ± .3 s with a minimum of ~1.5s in the 4-16 Hz range and a

maximum of ~7s in the 3-4 Hz. In PCC the mean lag is significantly longer at 4.5 ± .3s ($p <<< .0001$) and has a minimum of 3.8s in the 20-30 Hz range and a maximum of 7.1s at 10 Hz. Filtering does not significantly change lags. Lagged linear correlation without low-pass filtering is shown in figure 6.

Overall, with or without filtering, LFP and oxygen responses are highly correlated at all LFP frequencies and no one LFP frequency range, in either region, is clearly the best correlate of oxygen. Comparing V3 and PCC, there are significant differences between regions in both time lag at peak correlation and in the profile of correlation strength across LFP frequencies. (Permutation, Two way ANOVA of *time lag* X region X frequency, df = 74,1,74,2700 F = 1064, 2.1e5, 1736 P<<<.0001, Two way ANOVA of *correlation* X region X frequency, df = 74,1,74,2700 F = 7e3, 2.8e4, 7.6e3 P<<<.0001) At most frequencies, lags are significantly longer in PCC. Correlation primarily differs in the 4-16 Hz range, where correlation in V3 is negative, and in the low gamma range, where correlation in V3 is slightly greater than in PCC. These differences in correlation pattern demonstrate that the first order relationship between oxygen and LFP differs between regions.

To directly evaluate the nature of the relationship between LFP and oxygen in V3 and PCC we fit three classes of transfer functions. Figure 7 illustrates the relationship between the gamma-band (50-100Hz) LFP and oxygen responses. Prior literature has suggested that the gamma band is the most consistent LFP frequency range correlated with BOLD fMRI[27, 28, 36, 37, 202], thus we chose to use it to illustrate the transfer function effects in detail. However, the primary findings can be extended to our full frequency range (1-150 Hz).

Figure 7 shows the fit kernels for each class of transfer functions and the result of convolving the gamma band LFP with each of the kernels shown: the canonical SPM 5 hemodynamic response function (HRF) with 1 free parameter (scale), a generic HRF or sum of two gamma functions with 8 free parameters (scale, amplitude of both functions, delay of both functions, ratio of the two functions, total delay and total width of the kernel), and a kernel calculated from the data using Fourier de-convolution. All three methods generate reasonable kernels, (figure 7, column 2), reflecting a delayed temporal smoothing of LFP into oxygen and increase in the strength of the relationship between oxygen and gamma band LFP above that found with linear correlation. The standard SPM 5 HRF increases the correlation between transformed LFP and oxygen from a linear correlation of 0.54 to 0.7 in V3 and from .47 to 0.92 in PCC (figure 7, column 3, rows 1, 2). Across recording sites, the increase is significant at $p < .005$. Using the generic HRF the fits again improve significantly to a correlation of 0.92 in V3 and 0.96 in PCC respectively, as is expected with more degrees of freedom, $p < .0005$ (figure 7, column 3, rows 3, 4). The calculated kernel fits are statistically similar to the generic HRF fits, though slightly better, 0.94 and 0.98 in V3 and PCC (figure 7, column 3, rows 5, 6). These results argue that in both regions gamma band LFP and oxygen have a very strong linear relationship.

However, closer inspection argues that the relationship in V3 and PCC may not be the same. Most notably, the scale of the kernel is significantly larger in PCC for all 3 function classes: SPM 5, 3.5 times $p = .0004$, generic HRF 3.5 times, $p = .0026$, calculated kernel, 2.5 times $p = .0007$. Further, it appears by eye that the shapes of the kernel are different in the two regions. Note the initial negativity in the generic HRF fit for

PCC. These observations are suggestive that for our stimulus the reflection of neural activity in tissue oxygen may be different in PCC and V3. In the least, magnitude of neural response should not be assumed to directly correspond to magnitude of oxygen (or BOLD) response. However, these results may also indicate the LFP power modulation isn't the best correlate of BOLD activity.

Further, for all three kernels the fit of transformed gamma band LFP to oxygen is significantly better in PCC, $p<.05$. For the canonical SPM 5 HRF and the generic HRF, this suggests that these models are closer to the ideal relationship in PCC than in V3. One might note that Fourier de-convolution should provide perfect fits in both regions. This is essentially true in PCC. In V3 the reduced fit is due to limited frequency content and a restriction to positive time. The kernels shown and used for fitting are restricted to frequencies actually present in the data, and further smoothed. The raw FFT de-convolution kernel includes some high frequency elements related to transforming the large phasic responses. Further, FFT de-convolution identifies a transform with some negative time elements (portions of the kernel before time zero). Inclusion of the negative portion increases the fit to near perfect. Negative time violates causality and in a pure sense indicates mathematical over-fitting. Since we are fitting the mean LFP response to the mean oxygen response, and the ITI right before the trial starts has a mean of zero, negative time does not reflect anticipation. Negative time values in a Fourier derived kernel can reflect feedback. Essentially this mathematical result suggests that the relationship between LFP and oxygen changes over time. This is reasonable in V3 where the oxygen response to onset and offset is much greater than during sustained stimulation. Negative time in the Fourier derived kernel suggests that

the oxygen onset/sustain/offset profile isn't fully explained by differences in LFP response to onset, offset and sustained stimulation. Including negative time does not have a significant impact in PCC.

The basic findings from analysis of the gamma band LFP to oxygen kernel can be extended to our full frequency range. For this analysis the transform from the single frequency LFP response at all frequencies in1 Hz and 2 Hz steps from 2 to 150 Hz was assessed. At all frequencies the canonical SPM5 and generic HRF's provide a better fit in PCC than V3. However, the effect is mild in the gamma band, as seen in figure 7, and pronounced at low frequencies (below 20 Hz), where generic and SPM5 models offer minimal improvement in fit over linear regression in V3. The inability of these functions to fit V3 LFP to oxygen at low frequencies further argues that the LFP oxygen relationship differs in V3 and PCC. The FFT fitted functions also differ substantially. If the estimated kernels at a given frequency are compared, region-to-region kernel correlation is less than 0.4 at all frequencies. Further, the peak amplitude of the estimated kernel is greater in PCC than V3 in the gamma band, and greater (and negative) in V3 in the theta and alpha bands. Finally, the importance of negative time increases significantly at low frequencies (<20 Hz), in which the LFP response is primarily monotonic positive, and adaptation appears to be required to fit the onset sustain difference.

Overall, these results validate the use of oxygen polarography as a surrogate for BOLD. Further, they demonstrate task driven suppression of oxygen and LFP in a default mode area in the macaque and its time-course. Finally, in both regions they

demonstrate a strong neural oxygen relationship, though for this comparison the relationship differs between V3 and PCC.

Discussion:

Using a novel implementation of oxygen polarography, we recorded local field potentials and local tissue oxygen responses to visual stimulation in visual/attention (V3) and default mode (PCC) regions in the awake macaque. Our observations argue that: oxygen polarography in the awake macaque is a reasonable, high resolution, surrogate for BOLD fMRI; the macaque default mode network shows the same characteristic suppression of high resting activity by external engagement; suppression of BOLD fMRI activity in the default mode network relates to neural suppression; and that neural and hemodynamic responses to stimuli are highly related although the nature of the relationship may differ between V3 and PCC.

Oxygen Polarography as a BOLD Surrogate:

Oxygen polarography and BOLD fMRI should, in principle, measure the same phenomena. Blood and tissue oxygen are in equilibrium and physiologic changes that alter blood supply or oxygen consumption (metabolism) should be well represented in both measurements. Since our results show that task driven hemodynamic responses recorded with oxygen polarography are near identical to what we would expect to see with BOLD fMRI we argue that, to a first order, oxygen polarography can be considered a BOLD fMRI surrogate.

As a BOLD fMRI surrogate, oxygen polarography provides several advantages and is more readily combined with electrophysiology. Oxygen polarography provides higher spatial and temporal resolution than commonly available with BOLD fMRI (30-100

microns vs. 2-3 mm and 20 Hz vs. 0.3 Hz). This resolution is much closer to the scale of neural architecture (i.e. cortical columns), to the scale of local field potential recording[203], and to the timing of neural activity. Thus, oxygen responses recorded with oxygen polarography are more naturally relatable to neural phenomena or recordings. In the present study, this increased resolution also provided better characterization of the time-course of oxygen responses than is commonly reported in BOLD fMRI literature.

Further, macaque fMRI requires significant training specific to controlling animal behavior in the fMRI environment and comes with substantial constraints on the experiments that can be performed. Simultaneous BOLD fMRI with electrophysiological recording requires the use of specialized non-magnetic mechanical systems to place and target electrodes in the cramped high magnetic field fMRI environment. Oxygen polarography is an electrode based technique and can be implemented in the standard macaque electrophysiology setup. Implementation of oxygen polarography in the standard electrophysiology setup makes it a more practical measurement that can be used under a wider range of conditions and more easily mechanically combined with electrophysiology.

Finally, Oxygen polarography has no direct interference with AC coupled electrophysiological recording. The strong fluctuating magnetic fields of fMRI interfere with electrophysiological recording. Although these effects can be measured and filtered or regressed out they cause inherent loss of signal quality. Oxygen polarography can, in principle, provide much cleaner simultaneous oxygen and electrophysiological recordings. Additionally, the electrodes used for polarography can

be used for electrophysiological recording. We are capable of recording oxygen polarography and standard electrophysiology simultaneously from neighboring electrodes. However, in the present study we capitalized on the ability to record local field potentials (serially) from the same electrodes used to record polarography. This provides spatial localization and resolution match of the two signals that is impossible with BOLD fMRI.

There are differences in the mechanics, resolution, and noise sources for the two measurement techniques. For instance, total blood volume can have effects on BOLD fMRI that are orthogonal to oxygen concentration. Since both techniques are sensitive to brain oxygen levels at different scales, in different tissue compartments and with different noise sources, detailed comparison of measurements with the two techniques might provide insight into the vascular or metabolic details of a particular response or cross validation of either technique. In this case comparison simply supports the well-established concept that BOLD primarily reflects oxygen concentration.

A Macaque Default Mode Network:

In the present study we capitalized on the benefits of oxygen polarography to investigate the task negative behavior of the macaque default mode network. Our understanding of the default-mode of brain function, [122] rests on a large body of human BOLD fMRI literature. This work has identified a group of regions in which activity is consistently suppressed by a wide range of tasks and stimuli. Most of the brain, like the visual system, (or area V3 here), is responsive to specific classes of stimuli. In contrast, the default-mode regions, or network, are specifically active when

subjects are at rest compared to when they are engaging with the majority of tasks or stimuli, implying a resting or default-mode function.

BOLD fMRI functional analyses have shown that functionally associated brain regions have correlated un-driven fluctuations. In humans the default-mode network is one of the clearest and most strongly correlated networks, further arguing that it supports a common function. In the macaque, functional connectivity analyses have identified a set of regions showing correlated ongoing fluctuations homologous to the human default-mode network. However, the functional definition of this network, suppression of resting state activity by external engagement has been harder to demonstrate.

The primary obstacle to identifying “default mode” suppression in the macaque has been behavioral control in the BOLD fMRI setting. Conducting fMRI requires subjects (monkeys) to ignore the noise and vibration caused by the scanning apparatus, remain still, and minimize movement. This represents an unnatural and effortful state for a macaque and requires extensive training. It is unclear whether the effortful, “sitting still” baseline state used in macaque fMRI can be considered a “default” state that is directly comparable to the human resting or “default” state. Polarography allowed us to study naturally resting macaques. Monkeys were left alone in a quiet dark room, (the standard electrophysiology setup) with minimum restriction (other than head fixation), and entered a naturally drowsy state that is highly analogous to the human resting state. When this natural resting state is disrupted by visual stimulation our technique allows us to identify clear and fairly straightforward task-related deactivation of resting state activity.

One PET study and one fMRI meta-analysis report task related suppression of activity in default mode network regions. In these studies it is hard to distinguish activity modulation due to differential demands of the baseline and target tasks, (for example foveal vs peripheral fixation), from suppression of an actual default mode.[82, 204, 205] Nevertheless, combining these studies with the clear suppression of resting activity we report, makes a compelling argument for a classically defined, hemo-dynamic suppression of resting activity by a wide variety of tasks, a macaque default mode network.

A macaque “default-mode” has relevance to interpreting the nature of the default-mode network function. In humans, activity in default-mode areas is increased during self-referential thinking, autobiographical memory, and social cognition. [123] Since macaques are not thought to engage in high order self-reflection, at least in the same way as humans, the presence of activity in macaque PCC activity that is higher at rest suggests that a more basic process, perhaps related to modeling the future in context of prior events at whatever level the animal can represent the past. [135]

Suppressed “Default” Neural Activity:

Since the task-negative default mode network activity has primarily been studied with BOLD fMRI its neural underpinnings are unclear. BOLD decreases could represent an increase in neural activity (metabolic demand) in the face of constant supply, or could reflect decreases in neural activity (decreased demand) and a concomitant overshoot in decreased supply.[24, 25] A handful of studies in humans and one study in macaques report suppression of high frequency field potentials, (electrocorticography in human neurosurgical patients, microelectrode LFP in macaques), in default mode areas during

some conditions compared to others. [138-143] However, these studies also often report increases of low frequency LFP and report strong onset or offset transients across frequencies[26, 33]. Further, they use short tasks which might not allow distinction of hemodynamic responses to onset and offset from sustained activity. These studies tie their high frequency LFP results to default mode BOLD fMRI suppression and argue for suppression of a neural default-mode. However, it is unclear whether BOLD fMRI measured under the same conditions would be dominated by the onset and offset transients and show activation, or if suppressed, would be better related to high or low frequency LFP. Positive and negative modulation of activity by task is common throughout the cortex. For example, as we report, V3 shows suppression in the 4-16 Hz range by a visual stimulus. Since these studies have no way to compare their neural activity to BOLD activity under the same conditions, the relationship of the results reported in these studies and BOLD fMRI results is unclear.

We report highly correlated onset activation and sustained suppression of oxygen and LFP across all frequencies. Our results provide a clear demonstration of suppression of resting-state neural activity in a default-mode network area that can be clearly tied to BOLD fMRI. Together our LFP and oxygen results provide a compelling argument for both a hemodynamically and a neurally defined resting “default mode” in the macaque.

However, neural activity in the PCC shows substantial nuance arguing that more than simple disengagement of a single process is occurring. Suppression is slow to engage and increases during stimulation. Further there is a clear activation to onset and phasic responses to each flash of our stroboscopic stimulus. The onset activation clearly

indicates excitatory input; the phasic responses argue that this input is not fully cut off during default mode suppression. Further, we note different time-courses (timing and magnitude) of LFP suppression across frequencies and different magnitudes of onset and phasic response. Differences in response characteristics of timing, shape, and amplitude, across frequencies are highly suggestive of multiple processes. In the previous human and macaque electrophysiological studies in PCC, substantial differences across frequencies are evident. For example, the macaque study mentioned above reports increases in low frequency (<20 Hz) LFP power. These studies required actions from subjects and thus required routine engagement of more brain systems than our simple externally orienting stimuli. Our results argue for blanket suppression of multiple processes by external engagement. However, this is likely an oversimplified story due to our simple stimulus. Disambiguating the nature and/or default character of distinct responses, and apparent multiple processes, in PCC will require further study under different conditions. Further, it is unclear which of these possible processes is best reflected in the widely observed BOLD suppression. Understanding the BOLD identified default mode will require further comparison of hemodynamic and neural measurements. Finally, the presence of an onset response and graded suppression suggests that disengagement of the default-mode might best be studied with longer tasks. Since polarography allows direct comparison of neural and oxygen activity and ready access to macaque behavioral control tools, our system represents an excellent platform for this study.

Comparing Neural and Oxygen Responses in the Default and Visual/Attention Systems:

Visual inspection, linear correlation, and transfer function analysis all argue that stimulus driven tissue oxygen modulation is highly related to local field potential modulation at all frequencies. However, it is also clear that there is substantial detail in the LFP response that is not clearly represented in the oxygen response. In V3 the character of the oxygen and overall LFP responses is activation. In PCC the character of the oxygen and overall LFP responses is suppression. However, in both regions differences in LFP time-course across frequencies suggests multiple neural processes contributing to the bulk LFP response. Linear correlation analysis demonstrates that LFP at all frequencies, in either region, is reasonably related to the oxygen response. Notably, V3 LFP power between 4-16 Hz is suppressed. This suppression is highly, though negatively, correlated with the oxygen response. Certain forms of neural activity, in particular activity of inhibitory interneurons, can drive vasoconstriction. [24] It is thus plausible that the decreased 4-16 Hz LFP power reflects a reduction in vasoconstrictive neural activity and thus is directly related to the increase in oxygen. Further, the LFP response in both regions contains phasic responses to each flash of the stroboscopic stimulus. At this level it is not possible to determine whether one LFP frequency, or one of the neural processes reflected in the LFP, is best reflected in the oxygen response.

Evaluation of the transform from LFP at each frequency to the oxygen response demonstrates that LFP at all frequencies can be transformed to a near perfect prediction of the oxygen response with a reasonable linear filter. These results further support a strong neural source for the oxygen response. However, since the

relationship of these filters to the actual mechanisms linking neural activity to metabolic and vascular activity is unknown, this method cannot disambiguate which aspect of the LFP responses are best reflected in oxygen.

This analysis does suggest some important considerations when extrapolating neural activity from BOLD fMRI activity. Primarily the relative magnitude of the neural response between regions, at least a single frequency LFP reflection of a neural response, cannot be assumed or compared based on an oxygen response. Further, the standard hemodynamic response function performs differently in both areas, with better fit in PCC. This specific difference and the apparent shape difference of the ideal estimated kernel either from the generic hemodynamic model or with Fourier de-convolution are relevant to studies directly comparing neural activity to BOLD fMRI. In these studies to account for the low sampling frequency of BOLD fMRI, neural responses are often filtered and then down-sampled to the fMRI sampling frequency. Our results indicate the filter used may impact the apparent strength of the relationship between LFP at different frequencies or LFP in different regions and BOLD fMRI responses. Further, in V3, estimation by Fourier de-convolution of the exact mathematical transform from the LFP to oxygen response identifies a kernel containing negative time. This is reasonable if one compares the relative magnitude of the LFP onset and sustained responses, to the relative magnitude of the oxygen onset and sustained responses. The differences between the onset, sustained and offset neural responses does not appear to fully explain differences between onset, sustained and offset oxygen responses. This may help explain why BOLD fMRI responses in visual cortex to long stimuli cannot be modeled as a linear superposition of responses to

shorter stimuli. [206] In contrast, kernels in PCC only contain positive time and are fully causal.

Our comparison of LFP and oxygen responses so far has focused on relating single LFP frequency bands to oxygen. However, correlation results do not imply that a single LFP frequency range is clearly most related to oxygen. In fact, our results are more consistent with a multi-frequency mapping of LFP into oxygen. However, in the current dataset we do not have enough free parameters to truly explore the multi-frequency space. In principle, there is an infinite set of possible transforms and a mathematical transform can always be found that perfectly matches the LFP signal at any frequency or combination of frequencies to the oxygen signal. Given an infinite search space, a single multi-frequency high order transfer function could be found that perfectly matches the LFP and oxygen signals in both areas. However, interpretation of this transfer function would be difficult and more likely reflect a mathematical artifact than a property of the brain. Our correlation results suggest that the multi-frequency mapping of LFP into oxygen differs between regions, but without multiple task conditions we cannot discern among the set of possible multi-frequency functions. Further, we only examined a subset of neural responses, and it remains readily possible that BOLD reflects lower or higher LFP frequencies, cross frequency interactions.

Our current results provide further validation of the strong relationship between neural and hemodynamic responses and some insight into first order nature of that relationship. However, understanding the actual mechanics of the relationship between LFP and oxygen responses is beyond the scope of the current study. Further experiments in which the different processes reflected in the LFP response can be

disassociated will be required to clarify how the processes are distinctly reflected in oxygen. Further, utilizing our polarographic setup in conjunction with pharmacological and behavioral manipulations we may be able to add to the literature directly testing the mechanistic link between LFP and oxygen.

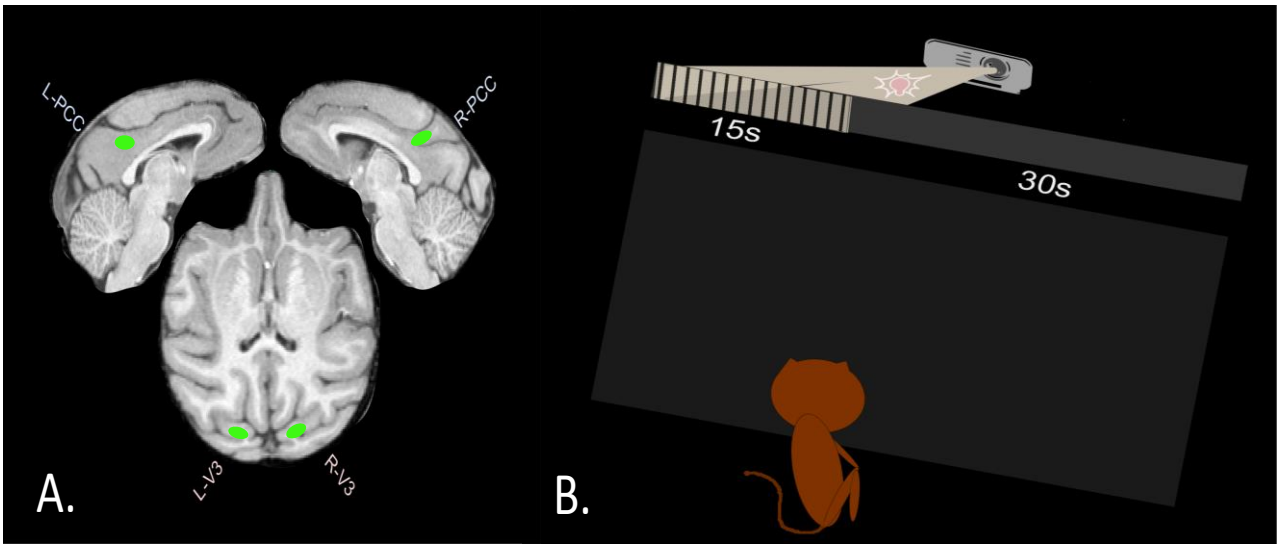

Figure 1 Recording Location and Stimulus Paradigm. Panel A shows the approximate recording locations in green, bi-lateral PCC and V3, overlaid on an MPRAGE T1 weighted anatomical image. Panel B shows the stimulation paradigm. Macaques sat head fixed in front of a wide field textured screen in the dark. During darkness the screen was not visible. Every 45 s, 15 s of stroboscopic 1 Hz illumination was generated with a projector. This resulted in both luminance and, by illuminating the screen, textured visual image changes. During the 30 s period of darkness eye tracking and infrared video monitoring confirmed that macaques were resting comfortably in a natural “default” state.

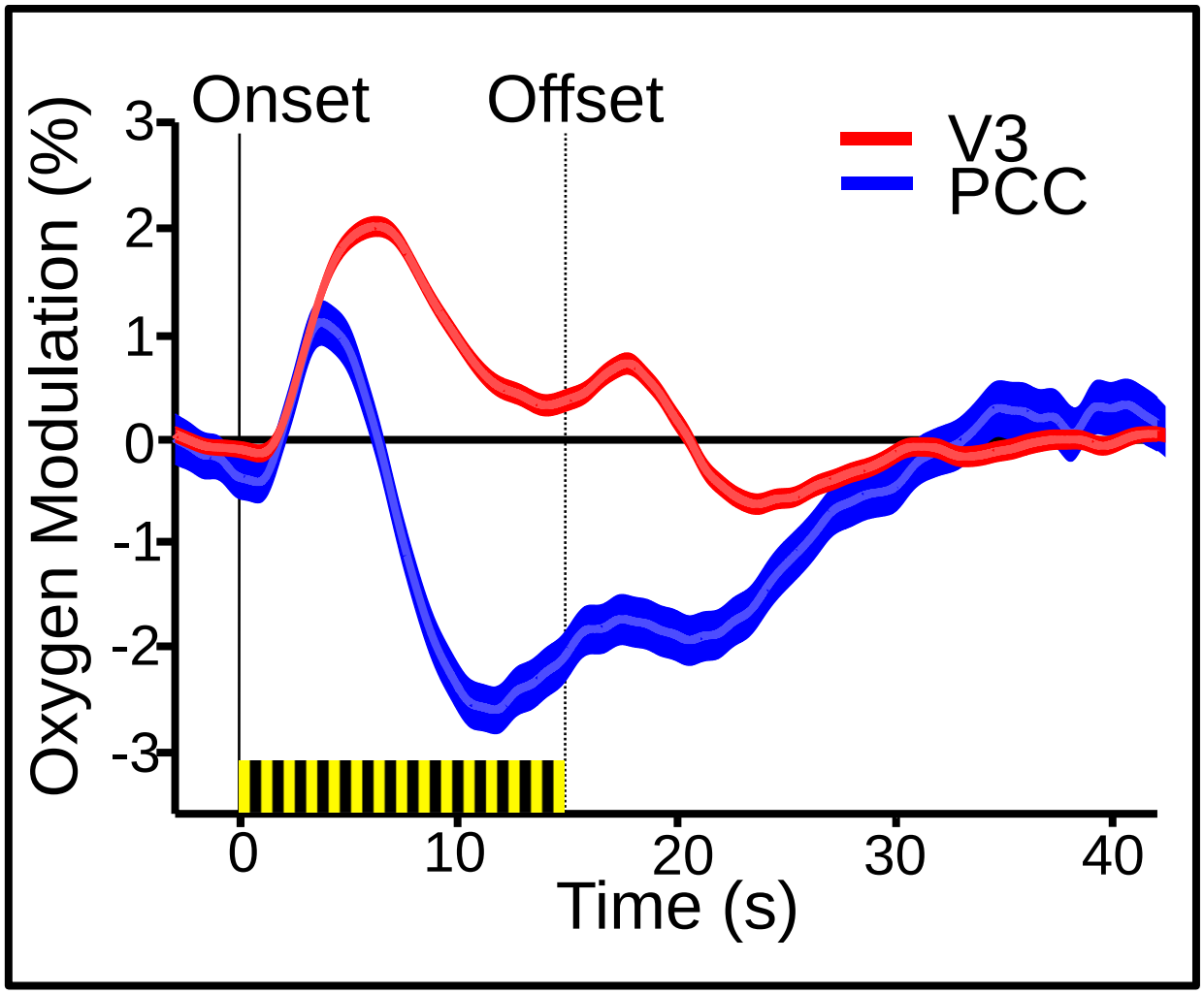

Figure 2 Oxygen Stimulation Response. Blue and red lines indicate oxygen modulation in posterior cingulate (PCC) and V3 respectively in response to 15 s of 1Hz stroboscopic illumination (yellow/black bars indicate each flash/dark cycle of the stroboscopic stimulus). Error bars show 1 S.E.M. across recording sites. When a macaque sitting in the dark, in a default resting state, is awoken by stimulation, oxygen increases in area V3 (red) and decreases in the PCC (blue). These oxygen responses strongly resemble what would be expected from human BOLD fMRI results, validating our technique and supporting the use of oxygen polarography as a surrogate for BOLD fMRI. The increased temporal resolution of oxygen polarography allows clear visualization of stimulus onset activation in PCC. This activation is occasionally observed but rarely discussed in human imaging. Further, these results present novel evidence of default-mode suppression by external engagement in the awake macaque.

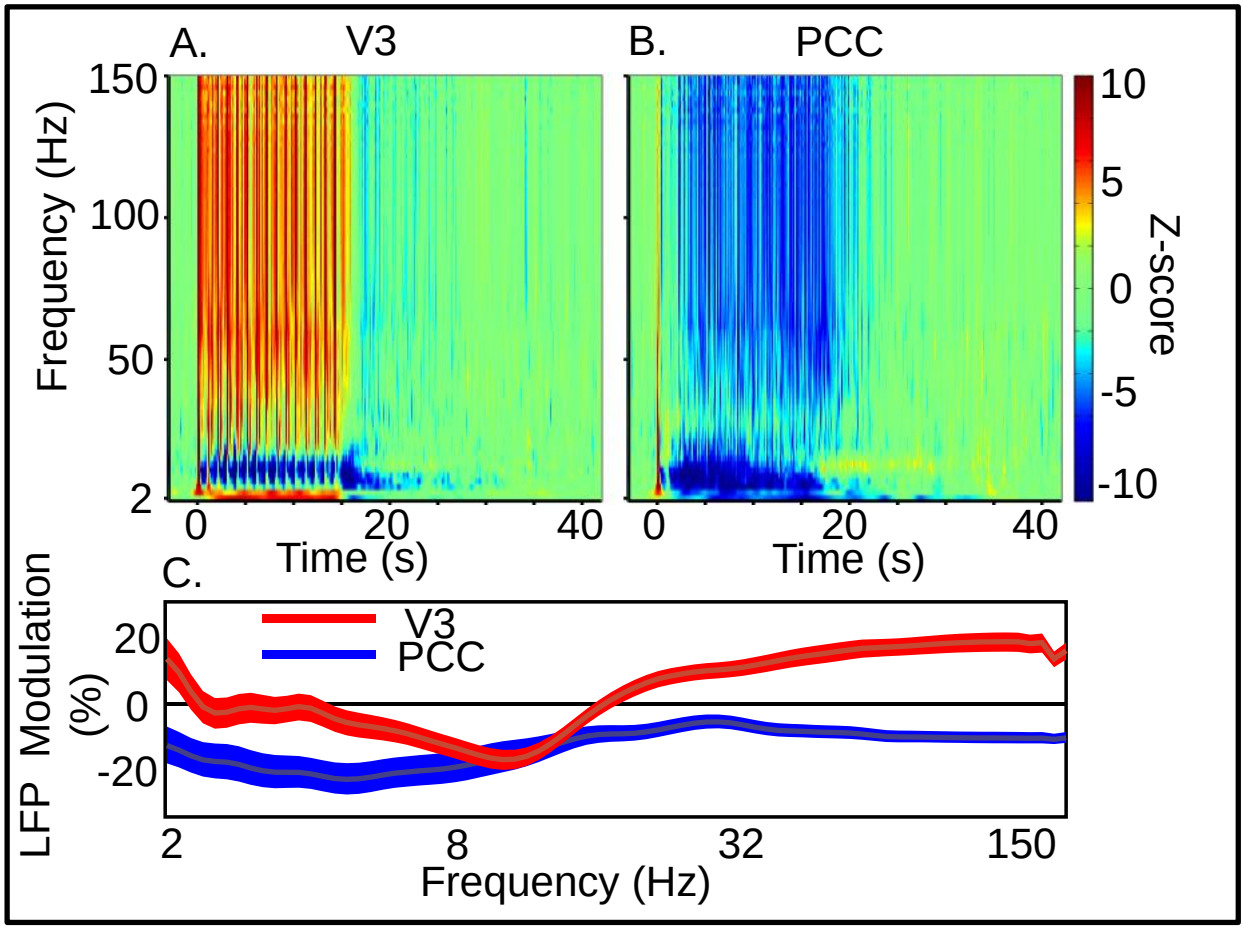

Figure 3 LFP Stimulus Response All. Panels A and B show heat maps of the full power modulation X frequency X time LFP response to the same stimulus shown in Figure 2. The LFP responses were recorded serially from the same electrodes used to record the oxygen responses shown in figure 2 and are thus reflect exactly the same cortex. The colormap shows modulation of the LFP from its inter-trial interval (ITI) level in standard error units, and reflects the significance of the LFP modulation. The Y-axis shows frequency in 2 Hz steps. The x-axis shows time. The LFP responses are qualitatively very similar to the oxygen response with onset activation responses in both regions and sustained activation in V3 and suppression in PCC. However, note the suppression of LFP in the 4-16 Hz range in V3 and the variable suppression across frequencies in PCC. Panel C shows the mean LFP modulation during stimulation in percent deviation from the ITI level. The intent is to allow visualization of the magnitude of the response and to quantify the main activation/suppression effects. The x-axis is shown in logarithmic units from 1-164 Hz, to allow better visualization of low frequency behavior.

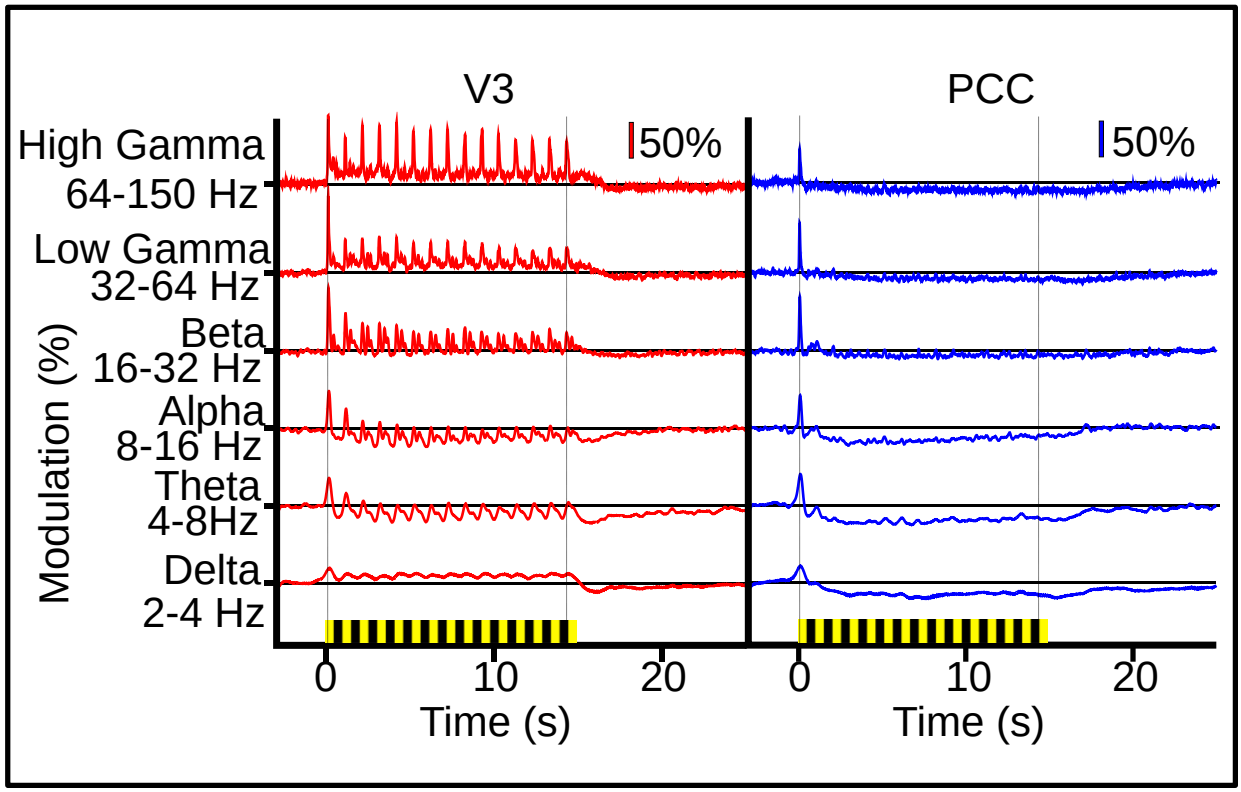

Figure 4 LFP Stimulus Response by Bands. For V3 (left, Red) and PCC (right, Blue) the LFP responses to stimulation is shown averaged across to indicated frequency bands. Line width reflects standard error. Stimulation is the same as in Figures 2 and 3. Each flash of the stroboscopic stimulus is indicated by the yellow/black bar. This view allows clearer visualization of the time-course of the LFP response. Note the onset activation in both regions, the large in V3 and subtle in PCC responses to each flash of the strobe stimulus, the different ratio of onset to sustained activity across frequency bands, and the different baseline modulation and time-courses of the LFP response across bands. For example, in V3 Gamma band power remains elevated for ~1 s after stimulation ends whereas in the Delta band power falls to a suppressed level immediately after stimulation ends. In PCC Alpha band power reaches an early negative peak and then trends towards baseline whereas Gamma band power suppression slowly increased throughout stimulation.

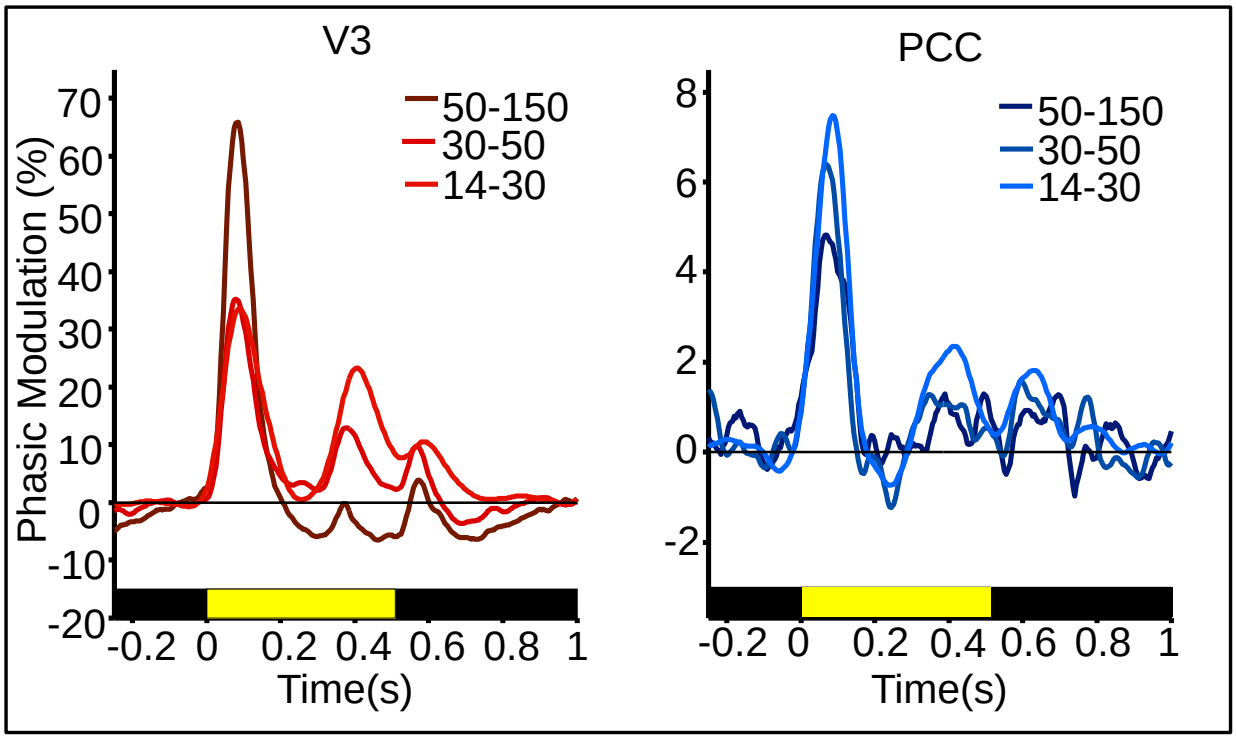

Figure 5 Phasic LFP Response. For V3 (left, Red) and PCC (right, Blue) LFP modulation to each flash of the stimulus is shown for 3 frequency bands. Percent LFP power modulation relative to the ITI following flashes 4-15 was averaged for each frequency band. The average of LFP responses to flashes 4-15 of the 15 flash (15s 1 Hz) stimulus were used to avoid contamination from the onset response. Baseline modulation was removed by subtracting the mean LFP response in the 100 ms prior to each flash. High and mid gamma are collapsed due to similarity, lower frequencies are not shown due to distortion of the response by the length of the wavelet required to assess LFP power at those frequencies. Note that there are significant phasic modulations in both regions with a primary response at flash onset and another effect just before and after offset. Also note that the frequency of peak modulation is different in the two regions, Gamma in V3 and Alpha in PCC, making it unlikely that this is an artifact. The presence of phasic modulation, activation, in the face of primary suppression in PCC is relevant to conceptualization of the default-mode process in PCC.

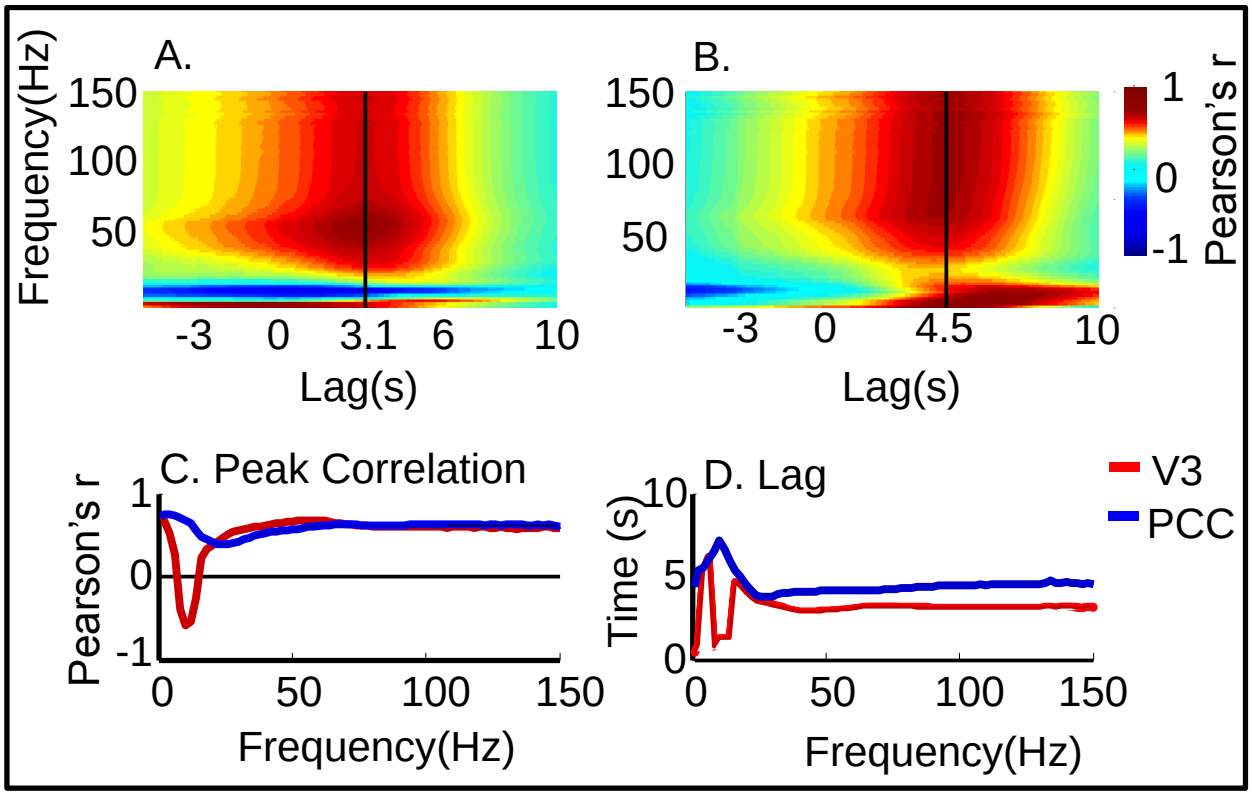

Figure 6 LFP Oxygen Linear Correlation Panels A and B show the full lagged linear correlation of mean LFP and oxygen responses at each LFP frequency. Color denotes correlation, y-axis LFP response frequency, and x-axis the shift in time or lag between the oxygen and LFP responses for the corresponding correlation value. Panel C shows the peak correlation by frequency for each region and panel D shows the lag at which peak correlation occurs. Note that LFP responses at all frequencies are well correlated with the oxygen response in the same region. Line width in C and D reflect 95% confidence interval of correlation evaluated by permutation. These results quantify the strength of the linear relationship between the clearly qualitatively related oxygen and LFP responses in both regions. Though it is negative, the correlation in the 4-16 Hz range in V3 is strong and significant. However, the different correlation profile and optimal time lag between regions suggests that the first order linear mapping of LFP into oxygen differs between the two regions.

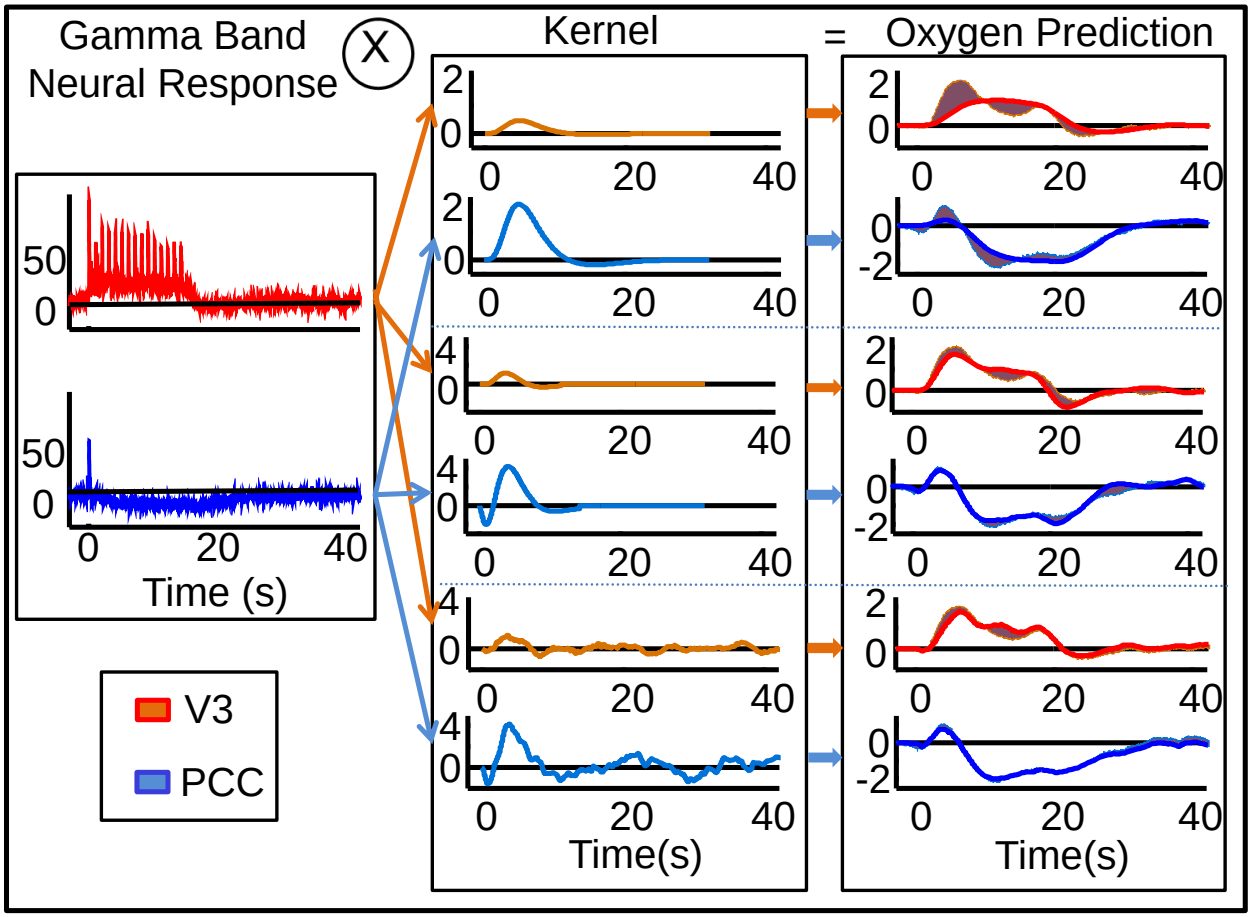

Figure 7 Gamma Band LFP to Oxygen Transfer Functions Column 1 shows the gamma band (50-100 Hz) LFP response in both regions. Column 2 shows the estimation of an optimal transform from the gamma band LFP to oxygen responses with 3 methods. Rows 1 and 2 show the canonical SPM 5 hemodynamic response function scaled to provide the best match (after convolution) of the LFP to oxygen. Rows 3 and 4 show an 8 parameter fit of a generic hemodynamic response function to optimize the match between LFP and oxygen. Rows 5 and 6 show a mathematically derived (FFT de-convolution) estimate of the kernel that best relates gamma band LFP and oxygen. Column 3 shows the results of convolving the LFP response with the kernels shown, gray shows where the prediction misses the measured oxygen response. Note that for all methods the kernel is much larger in PCC than in V3 and for all methods the shape of the kernel differs between regions. Further, the fit of LFP to oxygen possible with the SPM and generic hemodynamic response is significantly better in PCC than in V3. These results support the idea that oxygen is highly related to LFP and that oxygen reflects a lagged and smoothed linear transform of LFP. However, the exact shape of that transform may vary across cortex. Different magnitude shapes and fits are also found at all other frequencies. See text. These results suggest that the common practice of convolving electrophysiological signals with an a priori kernel prior to evaluating the relationship with BOLD fMRI may be confounded by different accuracy of that transform in different regions.

Chapter 4:

Inter-Regional Correlation of Ongoing Oxygen Fluctuations

Overview:

BOLD fMRI functional connectivity analyses are based on inter-regional temporal dependencies of fluctuations in the resting state BOLD fMRI signal. In this chapter we demonstrate the ability of our polarographic system to investigate the long-range temporal dependencies of oxygen fluctuations. We argue that this technique provides a higher resolution surrogate measure of the same phenomena studied in BOLD fMRI functional connectivity. This chapter does not contain electrophysiology. However, since polarography can be readily combined with electrophysiology, demonstration in this chapter of oxygen polarography in the awake macaque as an alternative for the study of functional connectivity, establishes a platform for future study of the neural underpinnings of functional connectivity.

We capitalize on the temporal resolution and long recording possible with our technique to explore the temporal structure of the long-range correlated oxygen signals. The fluctuations underlying functional connectivity are slow, and readily detectable with BOLD fMRI. However, these fluctuations have a $1/f^{\wedge\alpha}$ power spectrum and are not periodic. Thus, in the presence of noise Fourier and nyquist limit assumptions about sampling rate, length and frequency resolution are not wholly valid. Due to slow sampling frequency and short sample durations, BOLD fMRI cannot fully assess the waveform or frequency content of the fluctuations or their correlation. We find that inter-regional correlation is present in a specific frequency range with peak correlation at ~.06

Hz. Further, while we confirm the power spectrum for local oxygen fluctuations is well described by a $1/f^{\wedge\alpha}$ fit, we note deviations from the $1/f^{\wedge\alpha}$ behavior at the same frequencies driving correlation. These results imply distinct mechanisms orchestrating long-range correlation and driving local fluctuation. In contrast it was possible that correlation was simply a result of local activity passively propagating through an interconnected network.

The work discussed in the chapter will be submitted for publication with myself and Jingfeng Li as co-authors. Jingfeng and I collaborated on all stages (data collection, analysis, and write up for publication) of this work. However, I designed the project and impetus for the majority of the analysis came from me. As the senior member of the team I often played the role of mentor for Jingfeng in establishing understanding of the concepts and methods utilized. The text presented here was written by me.

Introduction:

Long-range correlations of ongoing fluctuations in the BOLD fMRI signal, functional connectivity, have provided enormous insight into the functional architecture of the brain. Analysis of the pattern of correlation strength has been used to describe the topology of functional networks, their evolution over time and with training, behaviorally relevant topology differences between subjects, and network disruption in disease. However, the mechanism driving inter-regional correlation remains unknown. [2-4, 64, 66-69, 71, 72, 145-147, 150, 207, 208]

It is clear that anatomic connectivity plays a large role in shaping the pattern of functional connectivity. Graph theory analyses of structural (tracer based) and

functional (activity correlation based) network topologies show substantial similarities. [173, 209, 210] However, there are prominent correlations between regions that do not have direct structural connection, for example, left and right V1 are correlated. These correlations may depend on multi-step but nonetheless unusually strong connections. [211] However, the differences between anatomical and functional connectivity networks are suggestive of an additional organizing principle.

Modeling efforts have shown that in networks with brain like topology, random input can lead to patterned long-range correlation across nodes, comparable to functional connectivity. [173, 212] Modeling efforts predict that activity in the network would show a $1/f^{\wedge\alpha}$ power spectrum. [213-217] This type of spectra is common in complex systems and reflects the low probability of activity in the system being synchronized, and therefore large, or increasing probability of activity being desynchronized, and thus smaller, to varying degrees over time. Large events occur rarely and appear as high power low frequency fluctuations while small events occur frequently and appear as lower power high frequency activity. Local BOLD fMRI and oxygen fluctuations have a primarily $1/f^{\wedge\alpha}$ power spectrum. It has been suggested that the local $1/f^{\wedge\alpha}$ power spectrum arises from network interaction.

It is possible that functional connectivity simply represents passive propagation and integration of activity in a structured network. However, it is equally plausible that there is a distinct mechanism organizing or coupling activity in the network. If local $1/f^{\wedge\alpha}$ activity reflects network interaction or if correlation reflects passive propagation of this local activity through the network, correlation should be equally present at all frequencies. However, there is some evidence that correlation may have a distinct

spectral profile. [178, 179, 218, 219] Interpretation of these reports is limited by the narrow frequency range and limited spectral resolution possible with the BOLD data used.

We used oxygen polarography to directly evaluate the frequency dependence of network correlation. Polarography is an invasive alternative to blood oxygen level dependent (BOLD) fMRI that allows us to record local oxygen fluctuations with much higher temporal resolution, frequency specificity and range than can be achieved with standard fMRI techniques. We measured oxygen fluctuations in the default (bilateral posterior cingulate, PCC, area 23) and visual/attention (bilateral V3) networks in the awake resting macaque. We demonstrate that correlation of oxygen fluctuations follows the inter-regional pattern of BOLD fMRI correlation and find that this correlation is dependent on different frequencies than local activity. In particular correlation depends on a band limited set of frequencies. This implies that inter-regional correlation reflects a distinct mechanism from that reflected in local $1/f^{\wedge\alpha}$ activity. A band limited mechanism is reminiscent of EEG rhythms identified as peaks in an otherwise $1/f^{\wedge\alpha}$ spectra and may imply a pseudo-oscillatory mechanism [220-222]. Intriguingly, although local oxygen fluctuations show a predominantly a $1/f^{\wedge\alpha}$ spectrum we note deviations from this profile at the same frequencies that correlation relies on. This is further evidence of for the presence of the band-limited mechanism, and might imply that correlation depends on inter-regional synchronization of local rhythmic or resonant systems.

Methods:

Oxygen Recording:

Oxygen polarography is an electrochemical technique in which the current flowing between a noble metal cathode and a non-polarizable reference electrode across a fluid bridge, in this case the brain/CSF, becomes proportional to oxygen concentration. [49, 196]. We implemented this technique with specialized platinum microelectrodes (FHC instruments) as a cathode, polarized at -0.8 V compared to a high quality Ag/AgCl reference (anode) (Grass Technologies). A high quality purpose built ammeter (Unisense PA2000) supplied the polarizing voltage and measured current. Oxygen signal response time was limited to 50 ms (20 Hz) by capacitance in the system and was thus filtered at 20 Hz just prior to digitization (Frequency Devices). Our system allows simultaneous recording at 4 sites in awake macaques with a temporal resolution of 50 ms and a spatial specificity of 30-100 microns.

Control of stray current paths was achieved by electrically isolating the entire system using a custom built optical isolator. The anode was placed on the back of the head in an area with no visible muscle movement and the skin was abraded to avoid sweat and movement potentials. These techniques minimize the potential sources for correlated noise in our system.

This technique has a long and well validated history in neuroscience. [109, 195]. Oxygen polarography and BOLD fMRI are very different techniques and should not be considered the wholly interchangeable. However, since blood oxygen is in equilibrium with tissue oxygen, the blood oxygen level dependent (BOLD) fMRI signal is highly related to tissue oxygen concentration. Further, though there are differences, both

measures primarily reflect the same thing, changes in the supply and demand of oxygen.

Animals, Behavior, Stimulus:

2 macaques participated in this study. Animals were cared for and handled in accordance with the public health service guide for animal use and all procedures were approved by the Washington University Animal Studies Committee. During recording macaques were fully hydrated and sat head-fixed in a dark room with no expectation of a task or reward. Behavior was unconstrained and macaques naturally settled into a "default" state equivalent to the resting state used in human fMRI. Eye tracking and behavioral monitoring demonstrated that macaques were awake but drowsy and resting comfortably.

Recording:

The brain was accessed via bilateral 15 mm chronic recording chambers (Crist instruments). MRI images (Siemens Trio MPRAGE .5 mm isotropic voxels) were obtained including a specialized phantom that allows visualization of the chamber and projection of a chamber based coordinate system into the brain. In one monkey, 2 small manganese chloride injections were placed using this coordinate projection and he was re-imaged to confirm and refine site accuracy . For each recording session, 4 specialized platinum microelectrodes were inserted using the MRI projection into bilateral posterior cingulate (PCC) and area V3, using twin multi-electrode microdrives (NAN instruments). During penetration electrophysiology was recorded from the advancing electrodes. Placement in gray matter was confirmed by multi-unit activity.

We recorded from 16 V3-V3 pairs and 15 PCC-PCC pairs, and 62 across network pairs. Minimum recording length was 30 minutes. Most were at least 1 hour. Data from both monkeys was similar and thus combined. Data was stored at 1 kHz using the Plexon MAP system (Plexon Inc.). To confirm that our correlation results were not driven by systemic noise we also recorded from 27 pairs of electrodes in electrical contact with the monkey but outside the brain. The recordings chambers that allow electrode penetration are filled with saline. To estimate potential correlated systemic noise we recorded oxygen from this saline and estimated the correlation between signals recorded from chambers over each hemisphere (bilateral saline recordings parallel to bilateral cortical recordings). These recordings are sensitive to potential shared noise caused by, monkey movement, shared reference movement, room electrical noise, and any signal distortion occurring along the signal path. Thus they provide a reasonable control for potential non-physiological sources of correlated fluctuation.

Analysis:

All analyses were done in Matlab (Matlab Inc. Natick Ma). Since we were focused on correlation of low frequency oxygen fluctuations data was down-sampled from 1 kHz to 40 Hz. Correlation was assessed as Pearson's r using Matlab's built in functions. In order to evaluate frequency within specific frequency ranges, the oxygen signals were filtered using Chebyshev type two filters into the band of interest prior to correlation. For assessing correlation as a function of frequency 1/2 octave filters with 1/8 octave overlap were generated across the frequency range .001 to 20 Hz, and correlation assessed for each range. Filtering and assessing correlation avoids assumptions about

periodicity and/or waveform common to mean squared coherence measures of shared signal by frequency. However, since correlation requires a both matched amplitude and phase we also assessed coherence and synchrony. Wavelet-based mean-squared coherence estimates the degree to which the amplitude of fluctuations at a particular frequency is shared between two signals over time. Synchrony evaluates the degree to which the phase of fluctuations at a particular frequency is shared between two signals over time.

Power spectra were assessed using the linear taper method (PMTM in Matlab). The 1/f character of the spectra was assessed by linear regression on the spectrum in log log space. Deviations from this line were estimated by subtraction. However, subtraction in log space is akin to division in linear space. Thus the resulting value reflects the ratio of total power to power explained by a 1/f fit. This is similar to correlation in which the dot product of the two signals is divided by the square root of the product of variance of the two signals, an estimate of variance shared between two signals. We thus compared the deviation of power by frequency to correlation by frequency. Prior to comparison, units were matched by taking the square root and exponent of the power ratio.

The sampling frequency of our data also allowed us to directly address concerns about respiratory and heart rate (RR, HR) contamination. We estimated the time course of respiratory and heart rate by using a method modified from the one proposed by Fekete et al [223]. Briefly, we identified the time stamps of individual heart pulsations by matching a template of pulsation's influence on oxygen signal with the recorded oxygen signal. We used the time stamps to calculate the time course of HR. Next, RR

was estimated from respiratory induced modulations in HR. Respiratory sinus arrhythmia is a well-established physiological process[224]. Thus one can infer respiratory rate based on HR fluctuation at around 0.3Hz. We band-pass filtered the time course of HR between 0.2 to 0.4Hz, and the local peaks were recognized as the time stamps of each respiration, which were then used to calculate the time course of RR. Then, we removed the fundamental frequency effect of RR and HR from oxygen signals, by subtracting the timecourses of heartbeat-related and respiration-related artifacts, based on the mean heartbeat-related and respiration-related fluctuations. Finally, we low-pass filtered the RR and HR time series and regressed slow RR and HR fluctuations from the data.

Results:

We simultaneously recorded resting state oxygen fluctuations from bilateral posterior cingulate and bilateral area V3 in the awake macaque (Figure 1A). Our results demonstrate oxygen correlation between functionally related regions as predicted by BOLD fMRI functional connectivity. As can be seen in Figure 1B, polarographic oxygen recording captures higher frequencies than can be detected with fMRI. However, after the oxygen signals are filtered into the standard BOLD fMRI range, .01-.1 Hz, they look very similar to resting state BOLD fMRI fluctuations, despite the dramatically higher spatial specificity of our technique compared to BOLD fMRI (30-100 microns vs ~ 3 mm). Further, oxygen fluctuations in this frequency range are correlated across regions in the manner predicted by BOLD fMRI (Figure 1C). All pairs show non-zero correlation similar to the BOLD fMRI global signal (see discussion). However, PCC-PCC and V3-V3 pairs (in network) are more highly correlated than PCC-V3 pairs (out of network).

Functional network specific correlation is the primary finding and definition of fMRI based functional connectivity (In network r=0.41 ±0.03 p<.0001 and out of network r =0.29 ± 0.02 p<.0001 difference significant at p<.05). Given the spatial scale of our recording these results imply that BOLD fMRI functional connectivity represents a well-distributed signal that can be measured in micron scale volumes. System noise is not correlated (not shown, see methods for noise definition).

The higher frequency content of our polarographic recordings allows us to avoid a common artifact in analysis of BOLD fMRI fluctuations. As can be seen in Figure 1B, the high frequency content is highly stereotyped. In separate experiments we recorded simultaneous EKG and found that these pulsations reflect heartbeats. (Figure 2) Because BOLD fMRI typically samples at ~0.3 Hz, the 1-1.5 Hz fluctuations due to heart rate can be aliased into the measured signal. With the high sampling rate of polarography, we can both low-pass filter and/or regress out heart rate from our data. Directly identifying and regressing out the heart rate pulsations is preferable to low-pass filtering alone because regression, unlike low-pass filtering, also removes lower frequency modulations of heart rate. For example, respiratory sinus arrhythmia is a well described fluctuation of heart rate with breath rate. Regression of heart rate can thus also remove breath rate. Figure 1 shows in and out of network correlation after simply filtering our oxygen signals into the common BOLD fMRI frequency range (.01-.1 Hz). Removal of heart rate (not shown) has minimal impact on these findings, and does not impact the in/out difference, providing further evidence that extra-cortical physiological activity has minimal impact on functional connectivity. Heart rate was regressed prior to analysis shown in figures 3 and 4.

Since we are reporting correlation between functionally related regions and oxygen polarography is an electrochemical measurement, we felt it was possible that the brain's electrical activity could induce correlated signal fluctuations. In the voltage zone (-0.7 to-0.9 V) over which current is restricted by oxygen concentration, small voltage fluctuations should not drive significant current changes. Further, our system is optically isolated from ground and from all other equipment in lab. Thus no direct path exists for neurophysiological electrical potentials to drive current through our system and disrupt our measurement. However, since current is passing directly through the fluid of measure, CSF, a fluctuating voltage field in the current path could have a small impact on current stability. We directly assessed this by applying an external fluctuating voltage field during in vitro recording. We weighted the small resulting signal fluctuations by the ratio of the external voltage field (measured at the electrode tip) to the magnitude of LFP recorded with the same electrode and concluded that LFPs could at most drive 0.3 % of the total variance of our in brain oxygen recordings. Thus even if neural potentials were perfectly correlated between regions they could not account for enough signal variance to significantly influence the measured correlations.

Figure 3 evaluates oxygen correlation as a function of frequency. To generate figure 3, the post heart rate regression oxygen signal was filtered in ½ octave overlapping bands from .001-20 Hz. Correlation was assessed for each band. In addition we assessed synchrony and coherence (not shown) and identified the same frequency dependence. All three metrics show a band limited relationship between .01-.3 Hz with a peak at ~.06 Hz.

The presence of the same band limiting in all three metrics argues strongly that there is a specific linking mechanism or a specific shared signal operating in this frequency band. Correlation assesses the variance shared between two signals at 0 phase. It is possible that in a long-range network fluctuations at different frequencies experience different delays or interactions in the network and would have a variable of non-zero phase relationship. Band limited coherence rules out the possibility that band limited correlation could arise from different phase jitter at different frequencies. Band limited synchrony rules out the presence of non-zero phase coupling between regions at other frequencies. Together these metrics argue for a frequency limited mechanism orchestrating inter-regional correlation signal.

Band limiting is present within and across networks suggesting a general, and not network specific mechanism. Further, the band limited correlation profile is near identical in both networks (V3-V3 and PCC-PCC). However, in network relationships are significantly stronger for all 3 metrics suggesting that the frequency specific coupling mechanism is stronger within network. There is also a small network specific peak in correlation at ~10 Hz. Out of network correlation at 10 Hz is not different from zero. This correlation is not driven by measured recording noise (yellow trace), should not be driven by electrophysiological interference (see above) and we expect that it reflects a real correlated fluctuation in local oxygen.

The 0.3 and 1.3 Hz correlation peaks reflect respiratory and heart rate respectively (RR, HR). Before evaluating correlation, coherence, and synchrony, heart rate was regressed out of the raw signals. However, this regression does not fully remove HR driven correlation. HR significantly reduces the peak at 1.3 Hz. As mentioned above,

heart rate fluctuates in time with respiration, respiratory sinus arrhythmia. HR regression also significantly reduces the RR peak at 0.3 Hz as expected. Notably the magnitude and frequency dependence of correlation in the .01-.3 range are unchanged by HR regression arguing that low frequency fluctuations in HR and RR do not influence band limiting of correlation. Note that noise (yellow line) in our system does not show the .01-.3 Hz band limiting of correlation. Noise does show some correlation at the frequency of heart rate. This is expected as pulsation moves the chamber saline and slightly disrupts the oxygen gradient to the electrode.

The presence of band-limited activity is also detectable in the local oxygen power spectrum. Figure 4A shows that local oxygen fluctuations primarily have a $1/f^{\wedge\alpha}$ power spectrum consistent with BOLD fMRI signal fluctuations. However, the power spectrum also shows notable deviations from the $1/f^{\wedge\alpha}$ model. These deviations have a similar frequency profile as band-limited correlation. Figure 4B shows the average correlation in frequency space of the power deviations and interregional oxygen correlation frequency profiles across recording pairs. The frequency dependence of power and correlation are significantly related. ($p<.0001$) Further, consistent with a stronger presence of a band limited mechanism in compared to out of network, the similarity of power and correlation frequency profiles is significantly stronger in network than out of network ($p<.05$). The deviation from $1/f^{\wedge\alpha}$ is similar in both networks and similarly related to the profile of correlation. These data are consistent with the idea that a single band-limited mechanism drives both the long-range correlation and the deviations in power from the $1/f^{\wedge\alpha}$ model.

Since recording noise also often has a $1/f^{\wedge\alpha}$ spectra, we performed an additional set of controls to confirm that the similarity of the deviations in the local power spectrum and the frequency dependence of correlation did not simply reflect signal to noise. We generated white noise, adjusted the power spectrum and mean correlation of the noise to match the data, and evaluated correlation as a function of frequency. As expected band filtered correlation of this "mean correlated" noise showed no frequency dependence. In order to confirm that we were not missing cross frequency phase relationships in our generated noise we also examined correlation after shuffling signal pairs and after rotating one of the signals in anatomical pairs. After shuffling or rotation, signals were uncorrelated and correlation showed no dependence on frequency.

Discussion:

We recorded tissue oxygen fluctuations in two BOLD fMRI defined functional connectivity networks, the default-mode network (bi-lateral PCC) and the visual/attention network (bi-lateral V3.) [68, 147] Our results validate the use of oxygen polarographic recording of tissue oxygen in the awake macaque as an alternative means to study BOLD fMRI defined functional connectivity. Blood oxygen is in equilibrium with tissue oxygen, it is reasonable to assume that oxygen fluctuations we measure are the same phenomena studied with BOLD functional connectivity. Our tool is capable of detecting network specific correlation of oxygen fluctuations, the basic finding of fMRI functional connectivity.

This work has further value in evaluating functional connectivity in the awake but resting macaque. The loud and stimulating BOLD fMRI environment limits the collection

of BOLD fMRI in the awake resting macaque. While humans can fairly easily filter out the fMRI environment, and often even fall asleep during scanning, macaques cannot. The ability to implement our technique in a standard macaque recording environment, in which macaques enter a natural resting state, provides a new view on macaque functional connectivity.

Beyond validation, the ability to detect correlated fluctuations with our technique is informative about the organization of oxygen fluctuations. Our measurements have spatial specificity of 30-100 microns, far below that of BOLD fMRI. Further, our electrodes were only targeted to regions, PCC or V3. Within regions, bilateral sites were not matched by any other criteria. Thus, oxygen fluctuations must be fairly uniform within a region. If they were not, correlation would not be detectable at this level. It was possible that functional connectivity was a regional level phenomenon, requiring the regional level view of fMRI. Functional connectivity could have reflected the average of highly distinct local activity. Instead our results argue that functional connectivity reflects a more uniform signal

Since we can directly regress out heart rate, and to some degree breath rate, without changing our correlation findings, we argue that physiologic fluctuations in heart or breath rate are not a significant force in driving functional connectivity. In standard BOLD fMRI correlation analyses a common global signal is regressed before correlation and the default and attention networks have a residual negative correlation. Raw ongoing BOLD fMRI fluctuations are highly correlated across the whole brain reflecting a correlated “global” signal. There has been substantial argument about whether the regressed out global signal is measurement noise or a neural signal. In the absence of

correlated noise, or HR or RR driven correlation, the out of network correlation we report supports the idea that the global signal has a neural origin. [30, 225, 226] With only 4 recording sites we cannot directly separate network specific from global shared signals in the current data. Thus we cannot compare possible global positive vs. BOLD fMRI predicted negative correlation between the default and attention systems.

It is also worth noting that prior to any regression or filtering, the oxygen fluctuations are fairly smooth (ignoring the heart rate artifacts). It was possible that BOLD fMRI applied an artificial low-pass filter to abrupt transitions between oxygen levels, or system states. Our observations support the general belief the BOLD fluctuations reflect slowly varying activity. However, occasionally there appear to be abrupt shifts from positive to negative or vice versa that may be reflected in the 10 Hz correlation we report.

The spatial pattern of functional connectivity is highly related to known functional and anatomical architecture. This has led to the proposition that correlation may simply be a result of related functional information spreading, integrating and interfering, across an anatomical “wired” system. [227] In contrast, functional connectivity could result from a distinct mechanism organizing activity between regions. If the inter-regional relationship simply reflected activity propagating within the anatomically wired network, one would expect correlation to evenly reflect activity measured at nodes in that network. Correlation would not show frequency dependence.

The presence of the same frequency structure in coherence and synchrony further supports the idea of distinct mechanism. Transmission delays and filtering properties of

long-range connections could lead to phase changes in the underlying fluctuations during transmission. This could influence temporal dependence of signals in two regions at different frequencies and influence the frequencies over which zero phase correlation was present. However, the presence of the same frequency profile in coherence (phase independent) and synchrony (a specific test for phase alignment) argue that our results are not an artifact of the stringent limits (0 phase and amplitude matching) of correlation or a network filtering artifact. Together these results argue for a frequency specific, rhythmic, linking mechanism.

Clarifying the nature of this mechanism or finding the source of the rhythm will require future exploration. There are three main possibilities, a shared rhythmic input signal driving correlated activity in distant regions, local rhythmic circuitry that is coupled between regions, or network level dynamics leading to frequency limited resonance and a frequency dependence of shared activity or correlation. Brain activity with similar spectral profiles or neural structures that could provide rhythmic input, establish local rhythms or lead to network dynamics are present throughout the nervous system. [180-185, 187, 228-240] However, rhythms in the basal ganglia and thalamus make intriguing candidates.

Activity with the correct frequency structure has been identified in the basal ganglia. [241-243] This activity appears to originate locally in the basal ganglia. However, its frequency is tuned by network level interactions requiring the subthalamic nucleus. Given the role of the basal ganglia in filtering cortical activity and action selection, this rhythm seems a plausible source for cortical network integration. [244] Distinct rhythms with the correct frequency structure have also been identified in thalamic nuclei. [171,

245, 246] Intriguingly some of these thalamic fluctuations appear to depend at least in part on a specific ATP dependent hyperpolarizing ion channel [247]. It has been suggested that this rhythm may have a non-cortical origin or arise in the interplay between neurons and astrocytes or between neuronal metabolism and vascular supply of metabolites which make them an intriguing candidate for coordinating oxygen fluctuations. [248-251] For a brief review of infra-slow brain rhythms and a discussion of rhythmic vs aperiodic activity see [252].

These results reflect on recent discussions of criticality in the brain. A $1/f^{\wedge\alpha}$ power spectrum or scale free behavior is a hallmark of critical dynamic systems. Scale free features refer to a link between magnitude and frequency. Infrequent events are proportionally larger than frequent events. Thus, the magnitude or power of fluctuations in a signal are proportional to their frequency or follow a $1/f^{\wedge\alpha}$ scaling rule. Critical dynamic systems are systems poised at a critical point between phases. At this point the number of states the system can adopt, and thus the apparent amount of information it can represent can be maximized. The brain is often thought of heuristically as a critical dynamic system poised between global synchrony or global de-synchrony and resulting runaway excitation or inhibition. Neural behavior, for instance spiking avalanches, show scale free spatial and temporal properties. [253-255] The size of avalanches scales with their frequency. Functional connectivity also shows scale free features. [174] Network metrics of the pattern of correlation strength show scale free patterns of connections. In addition, over time the degree of global synchrony fluctuates with a 1/f character. The 1/f power spectrum of local BOLD fMRI fluctuations

have also been tied to the idea of a critical system underlying functional connectivity [217, 256-258]

Our distinctly band limited, not scale free, results argue that it may not be appropriate to link the 1/f local spectrum and the 1/f network features in arguing that functional connectivity is reflective of a critical system. Our results are not in direct conflict with specific hypothesis about critical organization on the local or global scale. However, they suggest that if critical processes are in fact driving local BOLD fluctuations and long-range BOLD correlation, they may not be the same process. If local and long-range synchrony/de-synchrony represent the same process, the scale free features would match, which is not supported by what we observe. Importantly critical dynamic systems theory and oscillatory or rhythmic coupling represent two very distinct models of information processing in the brain [186, 252, 259]. Our results are more consistent with the latter. However, oscillatory coupling among nodes in a network can drive critical behavior of the network as a whole. [256, 260, 261]

Intriguingly, we also observe network specific correlation at ~10 Hz. These results are in contrast with the general feeling that functional connectivity is a slow phenomenon. At the slow sampling rate of BOLD fMRI, fluctuations at this rate would be aliased into very low frequencies, and could impact evaluation of the spectral features of functional connectivity evaluated using BOLD fMRI. However, the actual fluctuations at this frequency represent a tiny signal compared to the overall oxygen signal. It is unlikely that the vasculature could show a coupled oscillation this fast. However it could be driven by correlated metabolic fluctuations in oxygen consumption

at this rate. These could relate to abrupt shifts in direction of the oxygen signal, although we did not directly test that here.

In total, our results demonstrate the viability of using oxygen polarography in the awake macaque to study functional connectivity. The higher temporal resolution and spatial specificity of oxygen polarography allow different insight into the fine scale structure of functional connectivity than is possible with BOLD fMRI. The technical implementation of oxygen polarography in the standard macaque electrophysiology setup allows investigation of functional connectivity under behavioral conditions not possible in the fMRI setting and in the future ready exploration of the neural correlates of functional connectivity. Finally, our spectral analysis of long-range correlated and local oxygen fluctuations suggests the need to incorporate a new mechanism into our understanding of functional connectivity, and suggests that heuristic descriptions of the brain as a complex dynamic system may need to assume different dynamic systems at different scales.

In the future, the high temporal resolution of our technique will allow analysis of the relative phase or directionality and the stationarity of the inter-regional relationships indicated by correlation. In the present case we do not expect a meaningful phase difference between bilateral regions and cannot adequately separate network from global signals to compare phases between networks. While we can evaluate correlation over time, we did not simultaneously measure noise correlation over time and cannot separate meaningful non-stationarity from fluctuations in signal to noise. In the future, these limits can be overcome by placing more electrodes in single networks and adding simultaneous noise recording.

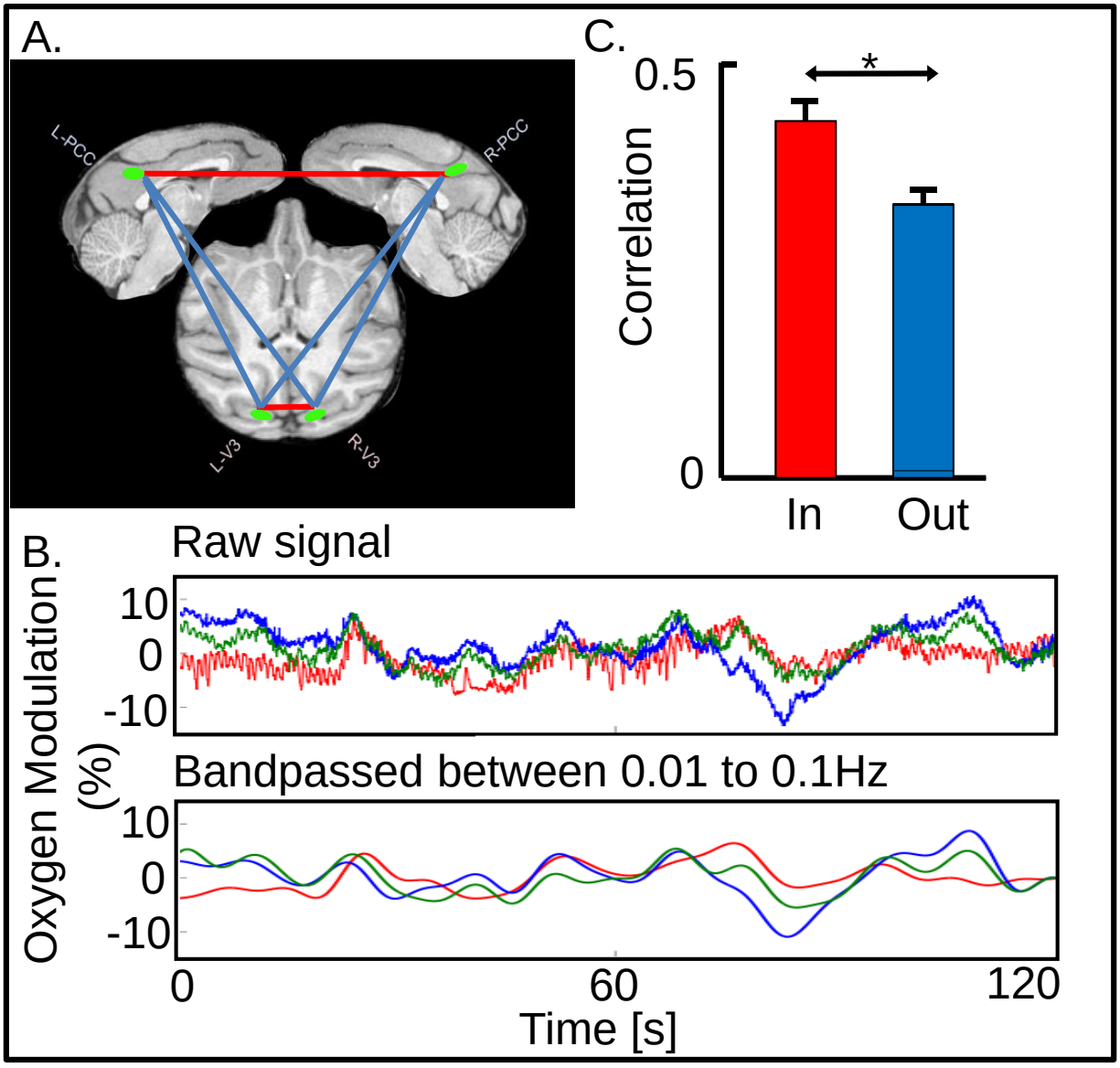

Figure 1 Network Correlated Oxygen Fluctuations in PCC and V3. Panel A shows assumed network relationships of approximate recording sites. Red links denote common (In); blue links denote different (out) network membership. Panel B shows raw and filtered oxygen signals recorded from 3 representative sites. The high frequency modulation in the raw recording is primarily heart rate, see figure 2, after filtering into the .01-.1 Hz range oxygen fluctuations look much like BOLD fMRI fluctuations. Panel C shows the correlation and standard error across pairs of filtered oxygen signals grouped.by network membership. Note that all oxygen fluctuations are correlated similar to the BOLD fMRI global signal, but that correlation of network matched oxygen fluctuations is significantly greater, * denotes p<.05. These results validate our use of polarography as a surrogate BOLD fMRI functional connectivity.

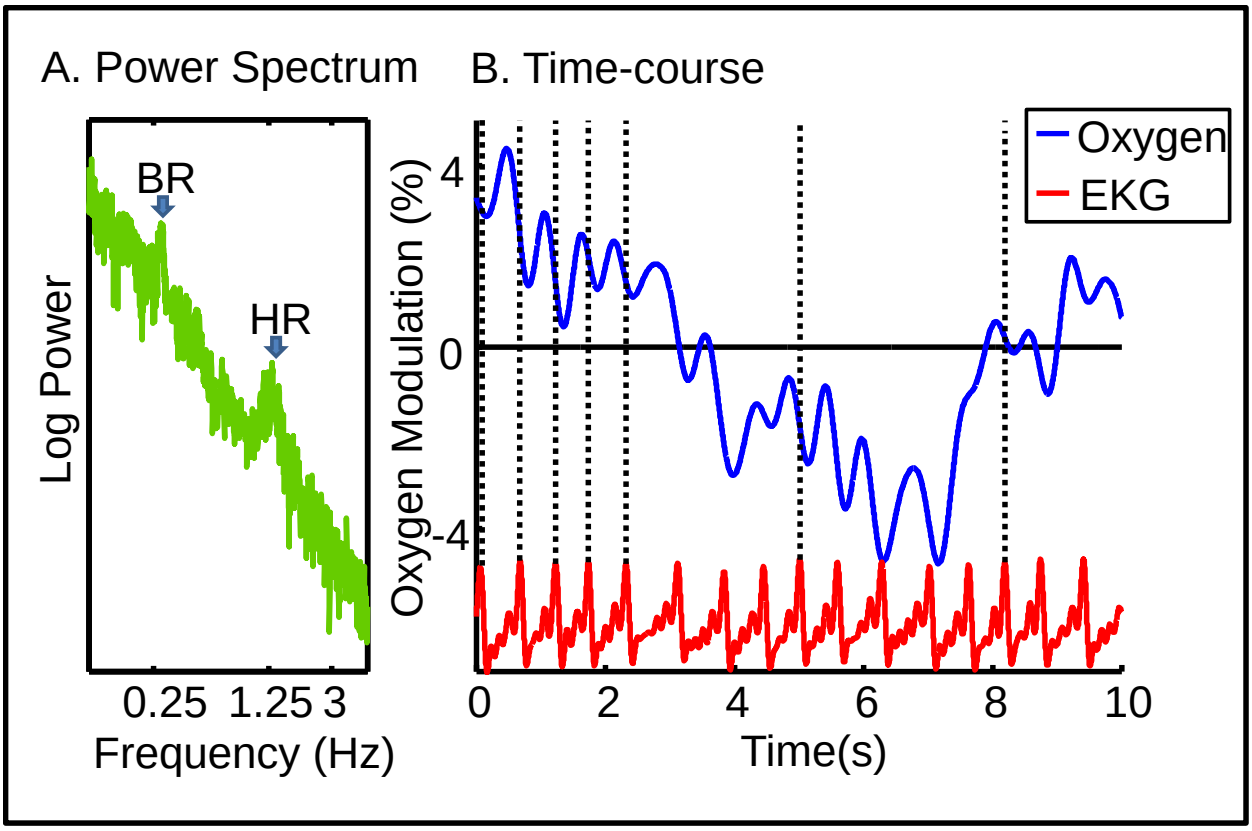

Figure 2 Heart Rate Detectable in Oxygen Recording. Panel A shows a sample power spectrum of oxygen fluctuations in log-log space, note the peaks at breath rate and heart rate. Panel B shows an example of simultaneous oxygen and EKG recording, note the trough in oxygen at each beat. Compared to BOLD fMRI oxygen fluctuations can be recorded at much higher temporal resolution. This allows HR to be directly visualized and breath rate to be estimated by respiratory sinus arrhythmia. At the sampling frequency of BOLD fMRI HR and BR are aliased into low frequencies.

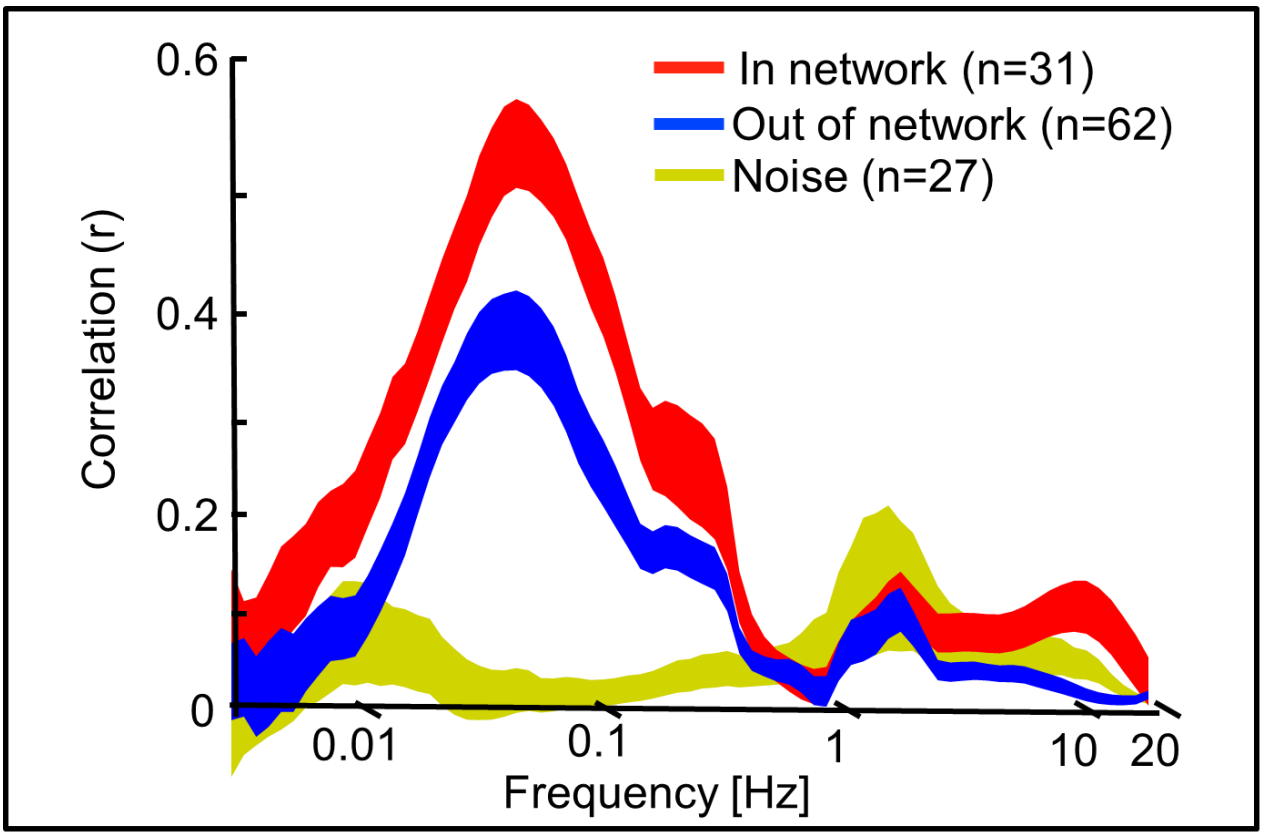

Figure 3 Band Limited Oxygen Correlation. Red blue and yellow lines show the dependence of in network, out of network and noise correlation on frequency. Oxygen signals were filtered into discrete frequency bands, ½ octave wide ⅛ octave overlap, prior to assessing correlation. Correlation between distant oxygen fluctuations is dependent on specific frequencies, i.e. correlation is band limited. Width of the lines indicates standard error of the mean correlation across pairs. Note that both in network and out of network pairs of oxygen show a similar band limiting but that in network is better correlated across the band. Further, note that separately recorded system noise does not show this band limiting. Heart rate induces movement in the chamber saline used for noise recordings drives some correlation. Also note that at ~10 Hz, in network oxygen pairs are significantly correlated while noise and out of network pairs are not. The dependence of correlation on specific frequencies of oxygen modulation is strong evidence that there is a mechanism coordinating this inter-regional relationship.

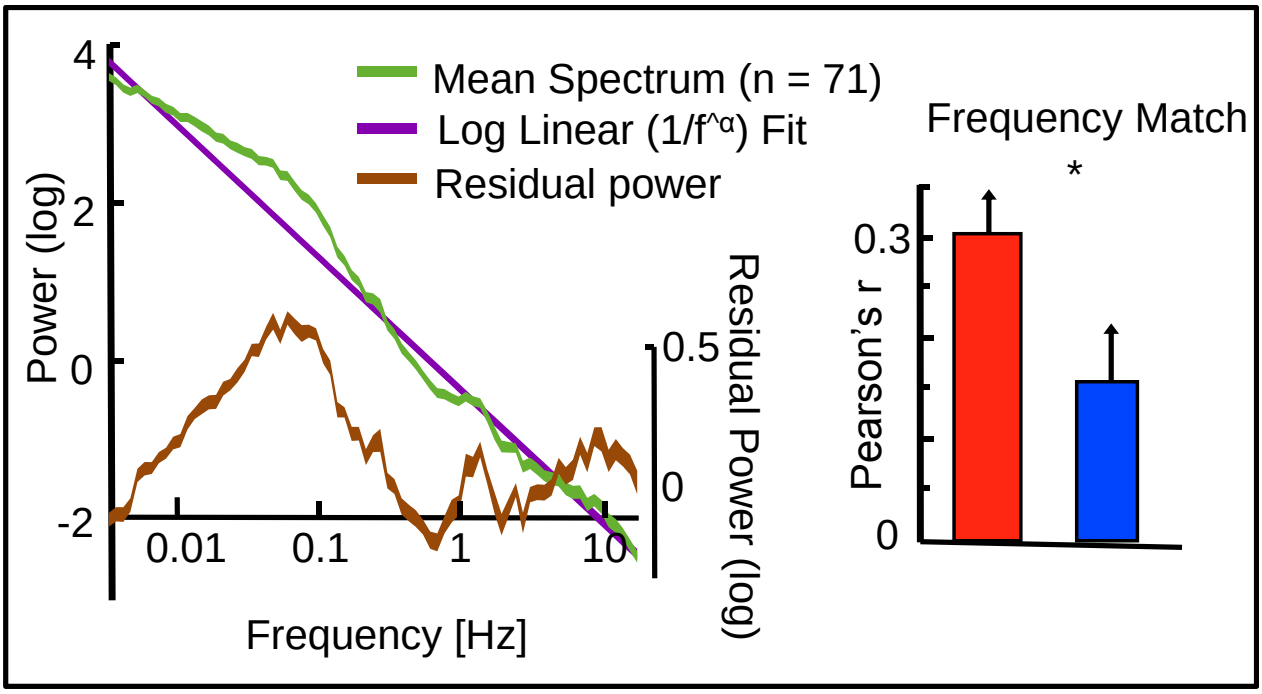

Figure 4 Local Oxygen Power Spectrum Relates to Band Limited Correlation The left panel shows the power spectrum of oxygen fluctuations(green) in log-log space, a linear fit to that spectrum explaining the log linear portion of the spectrums variance (purple), and the residual power around the fit (brown). Consistent with BOLD fMRI signal fluctuations, oxygen fluctuations have a primarily log linear, or scale free, power spectrum. By eye it is clear that the residual power not explained by the log linear fit is present at frequencies similar to the band limited correlation. The right panel quantifies this similarity. The correlation between the square root of the inverse log of the power deviation (to match units) and profile of correlation by frequency is shown. This relationship was assessed for average power and correlation between each pair of recordings and grouped by network membership. Note that both in and out of network oxygen pairs demonstrate this relationship, but that it is stronger in network.

Chapter 5: General Conclusions

The above chapters argued for the motivation, validity, and functional advantages of oxygen polarographic study in the awake macaque. Utilizing the advantages of this approach we provided evidence for a hemodynamically defined macaque default mode and related neural activity, a strong match in both default and stimulus driven cortex between neural and BOLD activity and an active mechanism organizing long-range oxygen correlation. The technical development, testing, and early applications of our oxygen polarographic system described above hopefully highlight not only its power, but inspire ideas for future experiments it enables. This work should be seen as proof of concept, early implementation of and the starting point for an ongoing body of research using the tools we have developed.

Chapter 1 discussed the need to bridge the large body of human BOLD fMRI and animal electrophysiology research. Chapter 2 discussed the development, testing and technical features of the oxygen polarographic system I developed. Simultaneous measurement and direct comparison of BOLD fMRI and electrophysiological views of the brain is exceedingly technically difficult. Oxygen polarography in the awake macaque is an ideal bridge between the two techniques. This tool measures tissue oxygen (a highly related signal to blood oxygen level dependent fMRI) at a resolution and in an environment far more conducive to matched electrophysiological recording in the awake macaque. The oxygen polarographic system developed in chapter 2 allows study of both stimulus driven and ongoing oxygen fluctuations and of their inter-regional

interaction. Thus, it can provide a surrogate for the main phenomena studied with BOLD fMRI.

Although four-site coverage is sufficient for many experiments, the basic template of the system we developed is scalable. The number of sites is only limited by the ability to place electrodes. The resolution of the system is well matched to electrophysiological study, however, there may be cases in which different or multiple resolutions might be valuable, for instance comparing voxel sized recordings to micro scale recordings. [46] The spatial specificity is dependent on electrode tip diameter, which could easily be modified without affecting the function of the system. Further, in cases in which concerns over the nuances of the BOLD fMRI signal arise, our system could be expanded to adjudicate. In addition to oxygen content, BOLD fMRI is influenced by blood flow and volume. While these are normally correlated, occasionally concern that one or the other dominates a particular measurement arises. Measures of blood flow, like thermal clearance, can be readily combined with polarography without affecting the polarographic system.

In chapters 3 and 4 we discussed assessment of stimulus driven and ongoing oxygen fluctuations. Our results validate our ability to study these phenomena and support the use of oxygen polarography as a surrogate for awake macaque BOLD fMRI. In addition, our results provide new evidence of a macaque default mode, the electrophysiology of default-mode network suppression, the link between hemodynamic and electrophysiological views of the brain, and the temporal structure of functional connectivity. The results presented in chapters 3 and 4 are both proof of concept with

our technique and interesting new science. However, they should be seen as merely the beginning.

The present results focused on the mean stimulus response by region or the mean correlation by network. However, there is substantial site by site variability in both the stimulus response and correlation. In the present study a uniform whole field stimulus was used and electrodes were targeted by MRI to disparate regions. These data do not provide much leverage to compare site by site response or correlation differences. In the future we plan to place multiple electrodes in single regions. This will allow comparison of nearby site by site response differences and exploration of their origin. Further it will allow direct evaluation of regional homogeneity of oxygen fluctuations. This will allow evaluation of the role of spatial averaging in detecting BOLD fMRI correlation, and may shed insight into the origin of pair by pair differences in correlation we observe. [46, 262, 263] In addition to cross cortical differences, in the future we will also investigate cross layer differences. [38] We cannot explicitly identify cortical layers. However, since we can record electrophysiology during penetration we can estimate whether we are recording in superficial, deep or midway through the cortical sheet.

In addition to site by site variability in correlation or stimulus response, ongoing oxygen levels and stimulus responses fluctuate with time (or trial by trial). Local BOLD fMRI fluctuations have been tied to fluctuations in threshold perception and continuous performance. [66, 69] This observation has led to the hypothesis that local oxygen level reflects fluctuations in cortical excitability. To test this, we are comparing local oxygen level in the frontal eye fields to the amount of current required to elicit a saccade. The frontal eye fields are an area on the anterior bank of the arcuate sulcus known to

participate in saccade generation. This region is often electrophysiologically defined by the low current, compared to surrounding tissue, required to elicit a saccade. However, the current required varies within the frontal eye fields and with time. Direct stimulation threshold is a clear marker of cortical excitability. If the threshold to elicit a saccade at sites in the frontal eye fields varies with oxygen level it will be direct proof that oxygen fluctuations reflect cortical excitability. Inter-regional correlation strength has been shown to correlate with inter-subject variability. [64] Within subjects correlation strength is known to fluctuate over time and may relate to inter-subject variability in correlation. [264] Given the apparent importance of correlation to brain function and the variability of correlation and function over time it is plausible that network level correlation, in addition to local oxygen level, affects behavioral output. In our stimulation experiments we can also ask if the correlation between right and left frontal eye fields in the time window around stimulation relates to saccade threshold or endpoint. We also expect to evaluate whether local oxygen level or inter-regional correlation predicts response variability, and given the potentially opposing roles of default and task active cortex, whether stimulus response variability is correlated between networks. Further, since we are recording at high temporal resolution, we expect to evaluate whether the results of these lines of inquiry depend on the frequency of oxygen fluctuations we focus on.

We also intend to add simultaneous electrophysiological recording. These recordings will allow us to evaluate the neural correlates of ongoing local oxygen fluctuations and the neural correlates of the portion of the oxygen fluctuations correlated between regions. Multi-site electrophysiological recording will allow us to examine inter-regional neural relationships that may relate to oxygen correlation, for example time

varying phase locking of particular LFP frequencies. We will also evaluate whether trial by trial oxygen response variability reflects neural response variability or variability in neural oxygen coupling. Multi-site within region recording will allow us to evaluate whether site-by-site variability is due to neural response or coupling variability. In all cases, simultaneous recording will allow us to go beyond mere evaluation of correlation or linear transform, and use probabilistic analyses, for example mutual information, to explore what neural features are informative about the oxygen response, or in reverse, what an oxygen response can reliably tell us about a neural response.

Finally, we intend to exploit the power of the macaque platform to explore the relationship between ongoing oxygen fluctuations, oxygen correlation, stimulus response and neural activity under different task conditions and under multiple states of arousal. For example we can evaluate inter-regional correlation or stimulation response of both oxygen and electrophysiological activity as we induce anesthesia, or in addition to the current stimulation vs rest comparison we can ask the monkey to perform a variety of tasks. Both directions, increased (or more specific) and decreased engagement with the world may provide disassociation of particular neural and oxygen activity. Further we expect to apply local drug manipulations. Currently we regularly examine the effects of small, local, injections of muscimol, a GABA antagonist that increases local inhibition and turns off local cortical activity, on behavior. We intend to evaluate the impacts of muscimol on both ongoing and stimulus driven oxygen and neural activity. Whether from these experiments, or a host of others enabled by this system, I expect an exciting future of oxygen polarography-based results to come from the Snyder lab.

Appendix: 1. Cathode Design

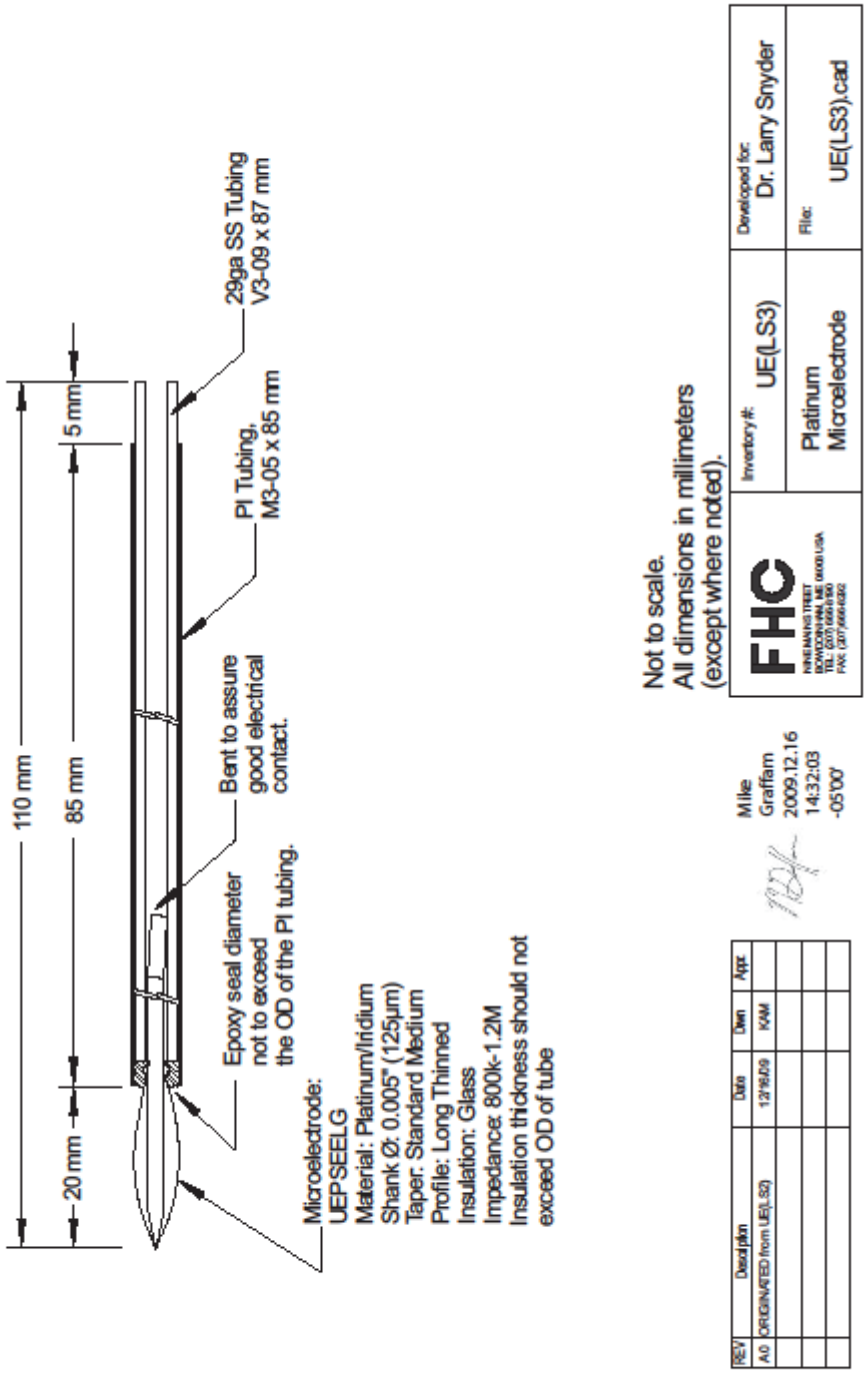

Appendix 2 Optical Isolator Design

Schematics

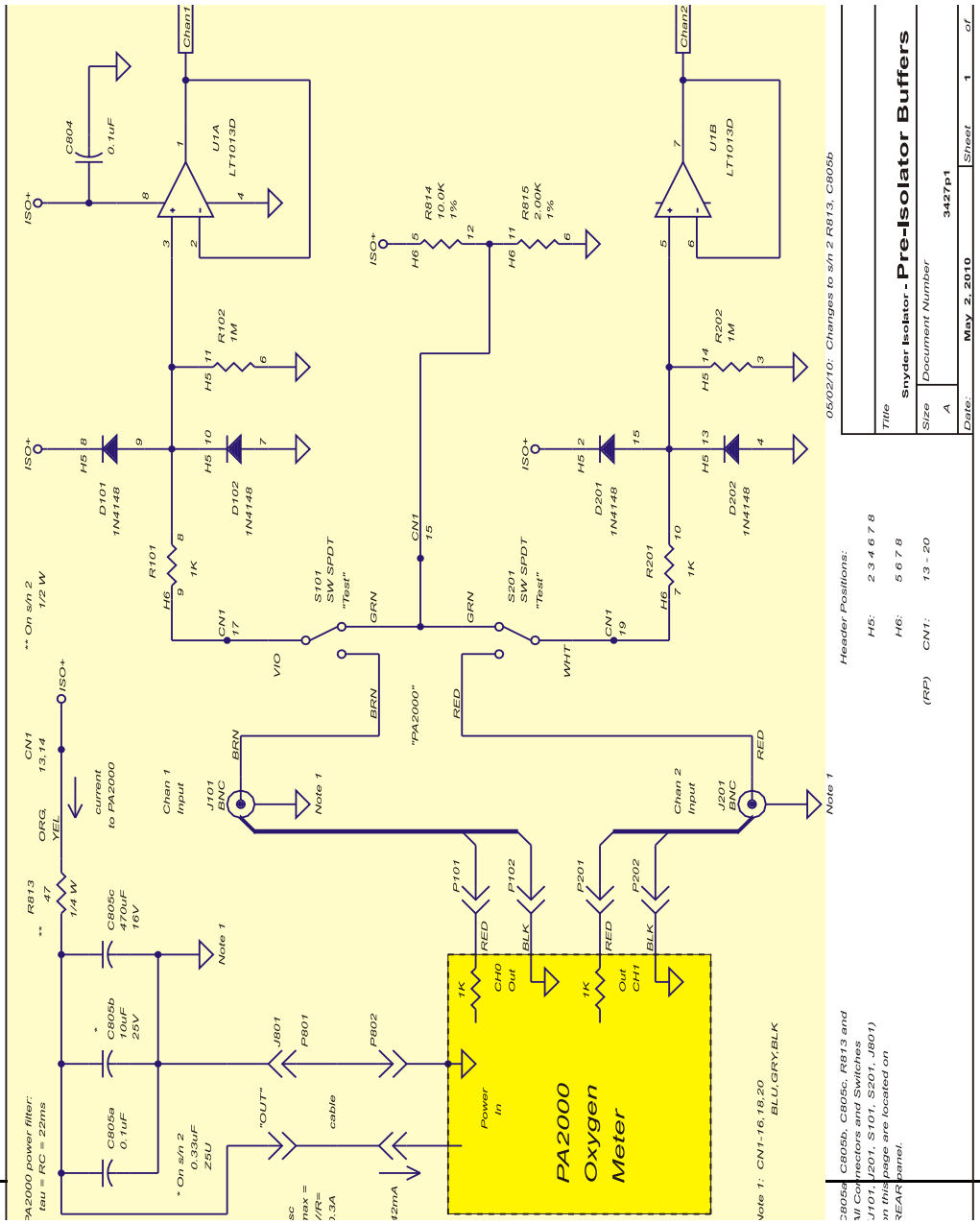

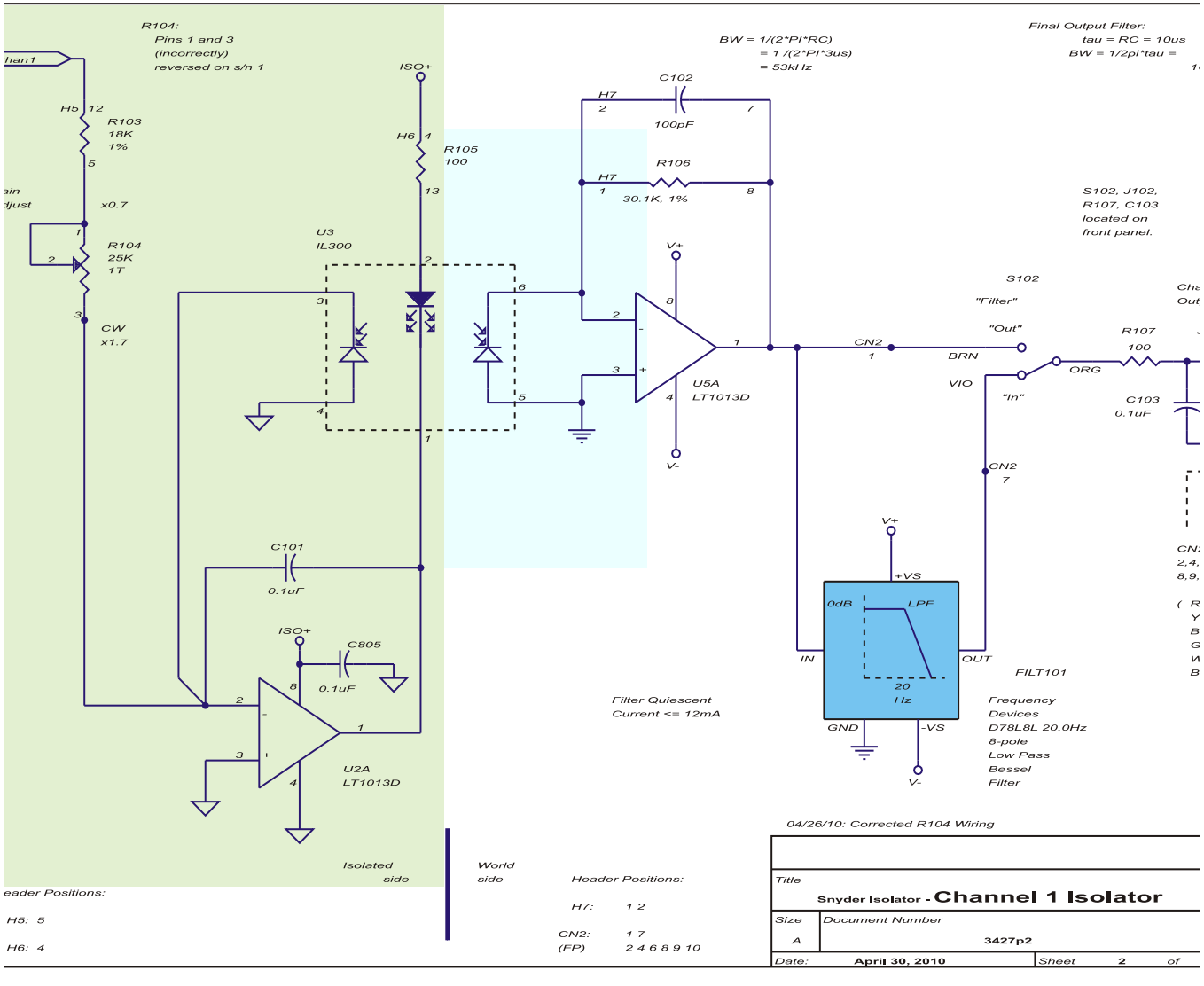
R104:
Pins 1 and 3
(incorrectly)
reversed on s/n 1
BW = 1/(2*PI*RC)
= 1 /(2*PI*3us)
= 53kHz
Final Output Filter:
tau = RC = 10us
BW = 1/2pi*tau =
ISO+
C102
100pF
H7
2
7
H5 12
R103
18K
1%
5
H6 4
R105
100
13
R106
30.1K, 1%
H7
1
8
S102, J102,
R107, C103
located on
front panel.
x0.7
1
R104
25K
1T
2
3
CW
x1.7
U3
IL300
2
6
3
4
1
5
V+
8
2
1
3
4
U5A
LT1013D
V-
S102
"Filter"
"Out"
"In"
CN2
1
BRN
VIO
ORG
R107
100
C103
0.1uF
CN2
7
C101
0.1uF
ISO+
C805
0.1uF
8
2
1
3
4
U2A
LT1013D
V+
+VS
0dB
LPF
IN
OUT
20
Hz
GND
-VS
V-
FILT101
Filter Quiescent
Current <= 12mA
Frequency
Devices
D78L8L 20.0Hz
8-pole
Low Pass
Bessel
Filter
04/26/10: Corrected R104 Wiring
Isolated
side
World
side
Header Positions:
H7: 1 2
CN2: 1 7
(FP) 2 4 6 8 9 10
eader Positions:
H5: 5
H6: 4
Title
Snyder Isolator - Channel 1 Isolator
Size
A
Document Number
3427p2
Date:
April 30, 2010
Sheet 2 of

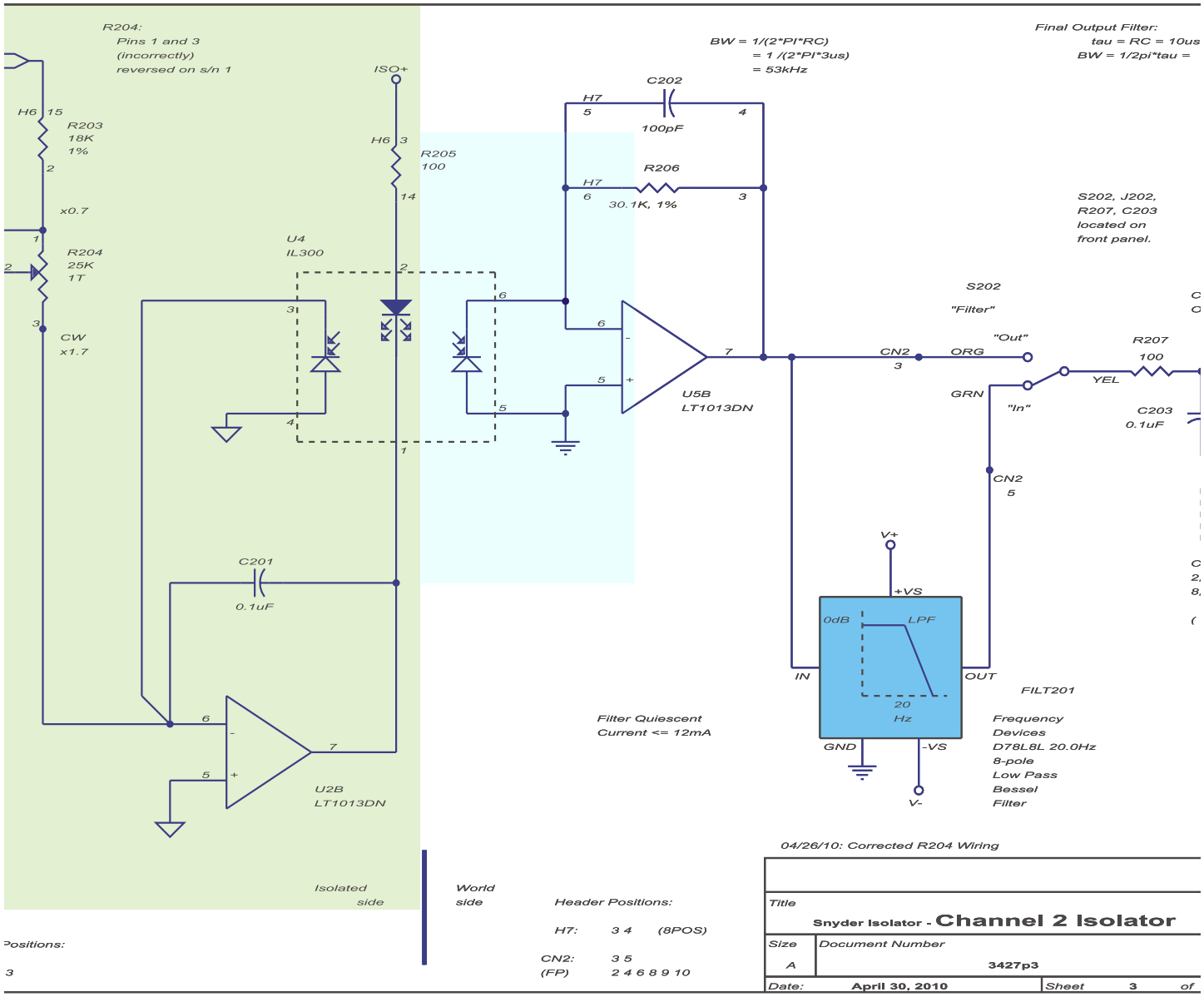
R204:
Pins 1 and 3
(incorrectly)
reversed on s/n 1
ISO+
H6 15
R203
18K
1%
2
x0.7
1
R204
25K
1T
2
3
CW
x1.7
H6 3
R205
100
14
U4
IL300
2
3
4
1
6
5
C201
0.1uF
6
7
5
U2B
LT1013DN
Isolated
side
BW = 1/(2*PI*RC)
= 1 /(2*PI*3us)
= 53kHz
H7
5
C202
100pF
4
R206
H7
6
30.1K, 1%
3
6
7
5
U5B
LT1013DN
Final Output Filter:
tau = RC = 10us
BW = 1/2pi*tau =
S202, J202,
R207, C203
located on
front panel.
S202
"Filter"
"Out"
CN2
3
ORG
R207
100
YEL
GRN
"In"
C203
0.1uF
CN2
5
V+
+VS
0dB
LPF
IN
OUT
20
Hz
GND
-VS
V-
FILT201
Filter Quiescent
Current <= 12mA
Frequency
Devices
D78L8L 20.0Hz
8-pole
Low Pass
Bessel
Filter
04/26/10: Corrected R204 Wiring
World
side
Header Positions:
H7: 3 4 (8POS)
CN2: 3 5
(FP) 2 4 6 8 9 10
Positions:
3
Title
Snyder Isolator - Channel 2 Isolator
Size
A
Document Number
3427p3
Date:
April 30, 2010
Sheet 3 of

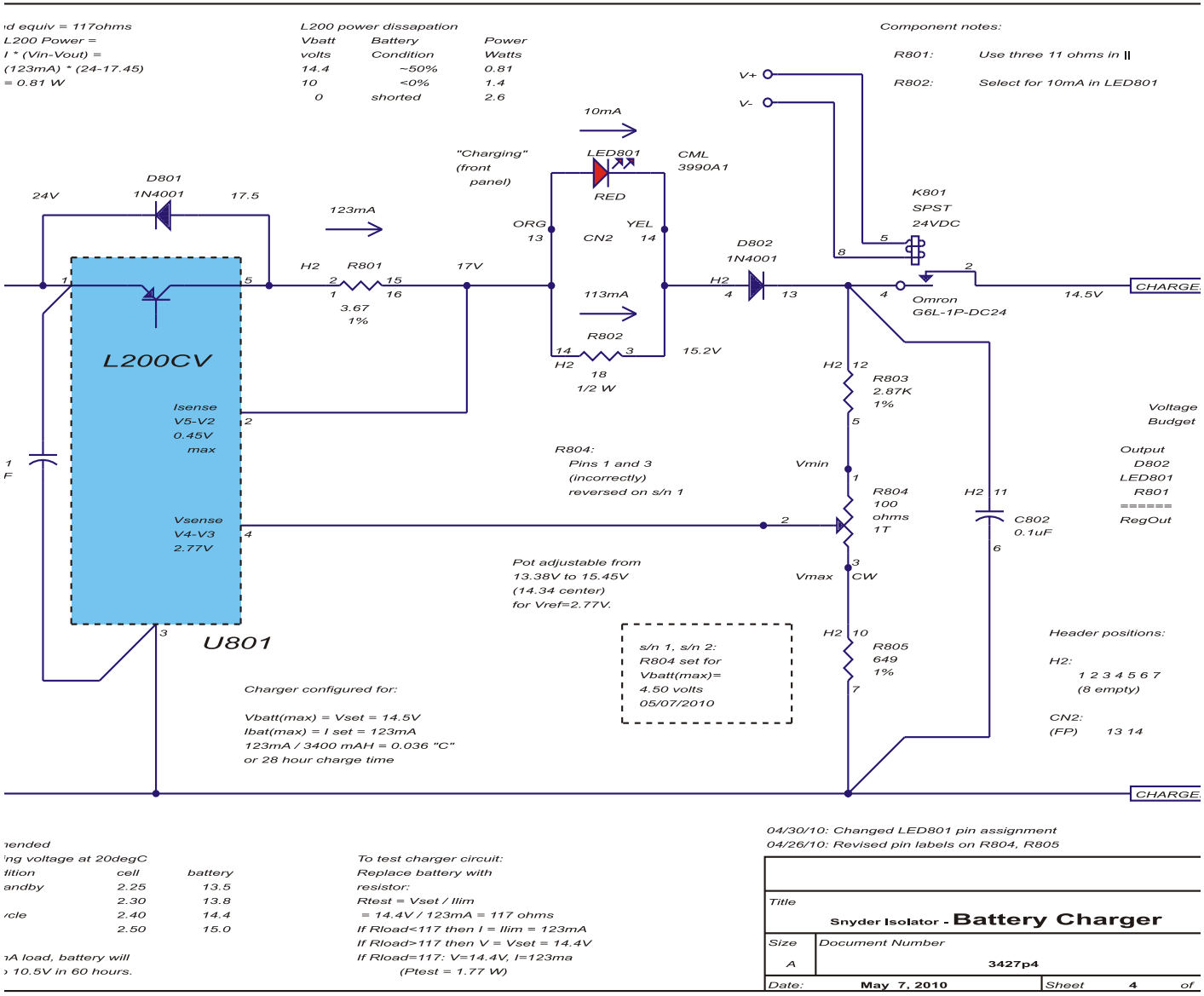
d equiv = 117ohms
L200 Power =
I * (Vin-Vout) =
(123mA) * (24-17.45)
= 0.81 W
L200 power dissapation
Vbatt Battery Power
volts Condition Watts
14.4 ~50% 0.81
10 <0% 1.4
0 shorted 2.6
Component notes:
R801: Use three 11 ohms in ||
R802: Select for 10mA in LED801
V+
V-
10mA
"Charging" (front panel)
LED801
CML 3990A1
RED
K801 SPST 24VDC
24V
D801 1N4001
17.5
123mA
ORG 13
CN2
YEL 14
D802 1N4001
H2 R801 2 1 15 16
3.67 1%
17V
113mA
H2 4 13
CHARGE
14.5V
Omron G6L-1P-DC24
L200CV
R802
14 H2 3
18 1/2 W
15.2V
H2 12
R803 2.87K 1%
Isense V5-V2 0.45V max
Voltage Budget
R804: Pins 1 and 3 (incorrectly) reversed on s/n 1
Vmin
R804 100 ohms 1T
H2 11
C802 0.1uF
Output D802 LED801 R801 ====== RegOut
Vsense V4-V3 2.77V
Pot adjustable from 13.38V to 15.45V (14.34 center) for Vref=2.77V.
Vmax CW
U801
s/n 1, s/n 2: R804 set for Vbatt(max)= 4.50 volts 05/07/2010
H2 10
R805 649 1%
Header positions:
H2: 1 2 3 4 5 6 7 (8 empty)
CN2: (FP) 13 14
Charger configured for:
Vbatt(max) = Vset = 14.5V
Ibat(max) = I set = 123mA
123mA / 3400 mAH = 0.036 "C"
or 28 hour charge time
CHARGE
ended
ng voltage at 20degC
dition cell battery
andby 2.25 13.5
2.30 13.8
rcle 2.40 14.4
2.50 15.0
nA load, battery will
> 10.5V in 60 hours.
To test charger circuit:
Replace battery with resistor:
Rtest = Vset / Ilim
= 14.4V / 123mA = 117 ohms
If Rload<117 then I = Ilim = 123mA
If Rload>117 then V = Vset = 14.4V
If Rload=117: V=14.4V, I=123ma
(Ptest = 1.77 W)
04/30/10: Changed LED801 pin assignment
04/26/10: Revised pin labels on R804, R805
Title
Snyder Isolator - Battery Charger
Size A
Document Number 3427p4
Date: May 7, 2010
Sheet 4 of

witches and Both LEDs
page are located on
T panel (CN2).

** R812 and C804 physically on s/n 1 and s/n 2 but connected only on s/n 2.

Header Positions:

H3: 1 2 3 4 (8POS)

H4: 1 2 3 4 5 6 7 8

CN2: 19 - 34 (FP)

Component notes:

R811/D804
Select for LED803
dim at Vbat = 10.5V,
bright at Vbat = 14V
Meas: lled = 18.8mA @13.5V

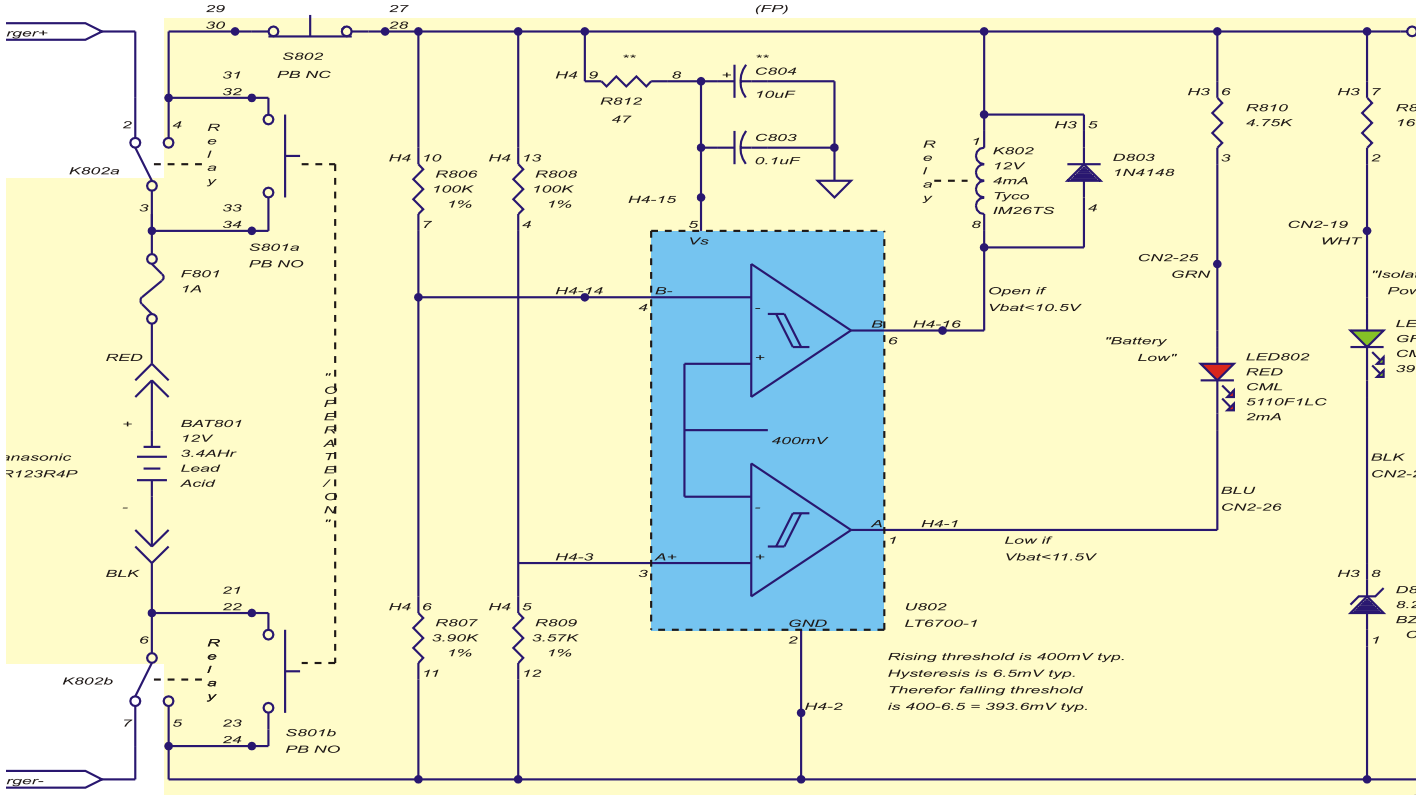

entarily pressing S801 connects battery to isolated
uitry and then disconnects battery from charger.

entarily pressing S802 disconnects battery from isolated
uitry and then reconnects it to the charger.

ttery voltage drops below 10.5 volts (100% discharge)
ery automatically disconnects from isolated circuitry
begins recharging.

04/30/10: Changed LED803 pin assignment
04/27/10: Added C804 and R812

Title: Snyder Isolator - Battery Management		
Size: A	Document Number: 3427p5	
Date: May 8, 2010	Sheet 5	of

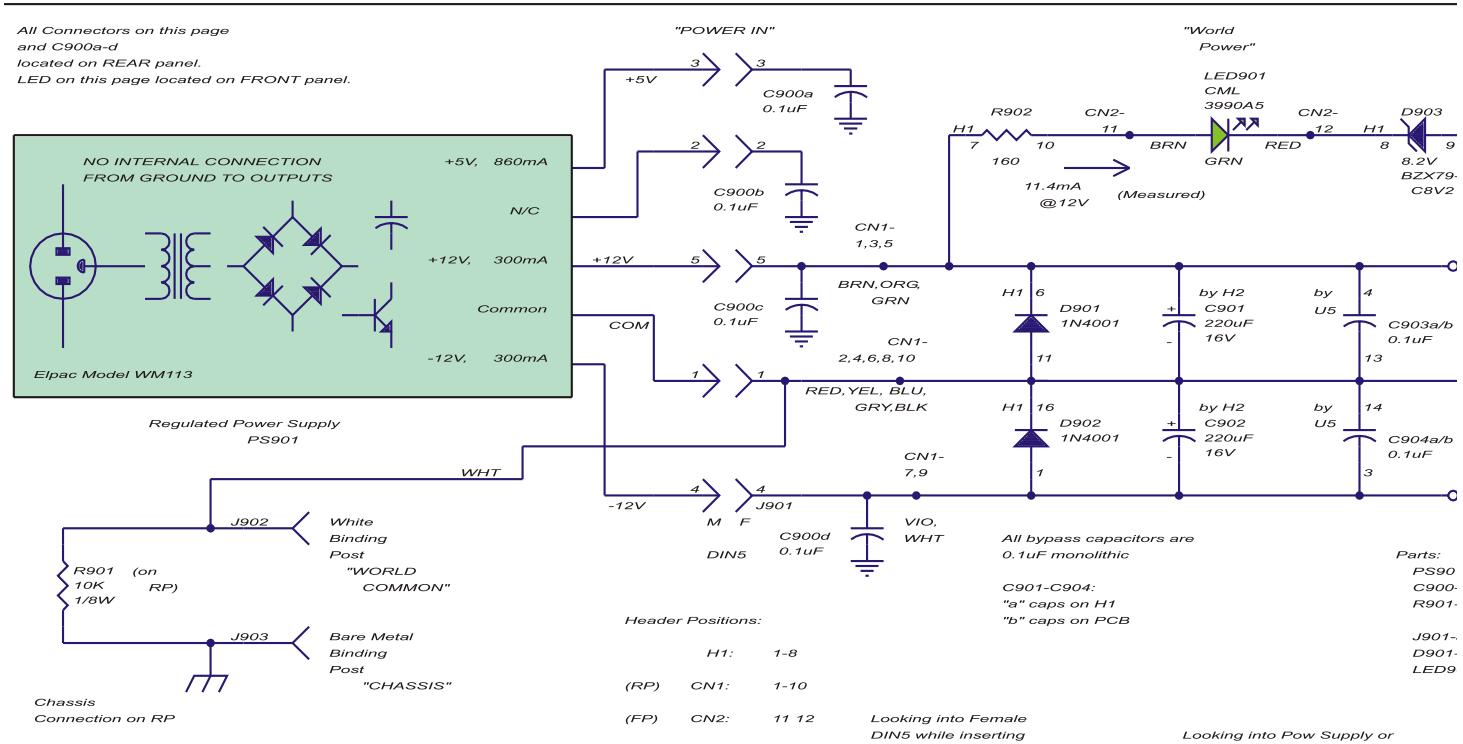

Power Table				Isolated		"World" side		
U#	Part #	Function	Pins	Iso +	⏚	V+	V-	⏚
U802	Linear Tech LT6700-1	Dual Comparator	SOT 6	5	2	--	--	--
U1 U2	Linear Tech LT1013D	Dual Op-amp	DIP 8	8	4	--	--	--
U3 U4	Vishay IL300	Analog Isolator	DIP	--	--	--	--	--
U5	Linear Tech LT1013D	Dual Op-amp	DIP 8	--	--	8	4	--
FILT 101 201	Freq Devices D78L8L 20.0Hz	LP Bessel Filter	SPEC 5	--	--	+VS	-VS	GND

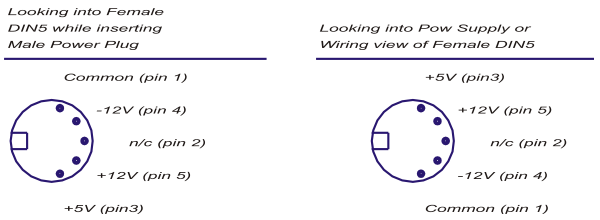

04/30/10: Deleted C901, C902 from H2
04/30/10: Moved R901 from CB to RP

Title	Snyder Isolator - **Input Power Supply**	
Size A	Document Number 3427p6	
Date: May 2, 2010	Sheet 6	of

Board Layout

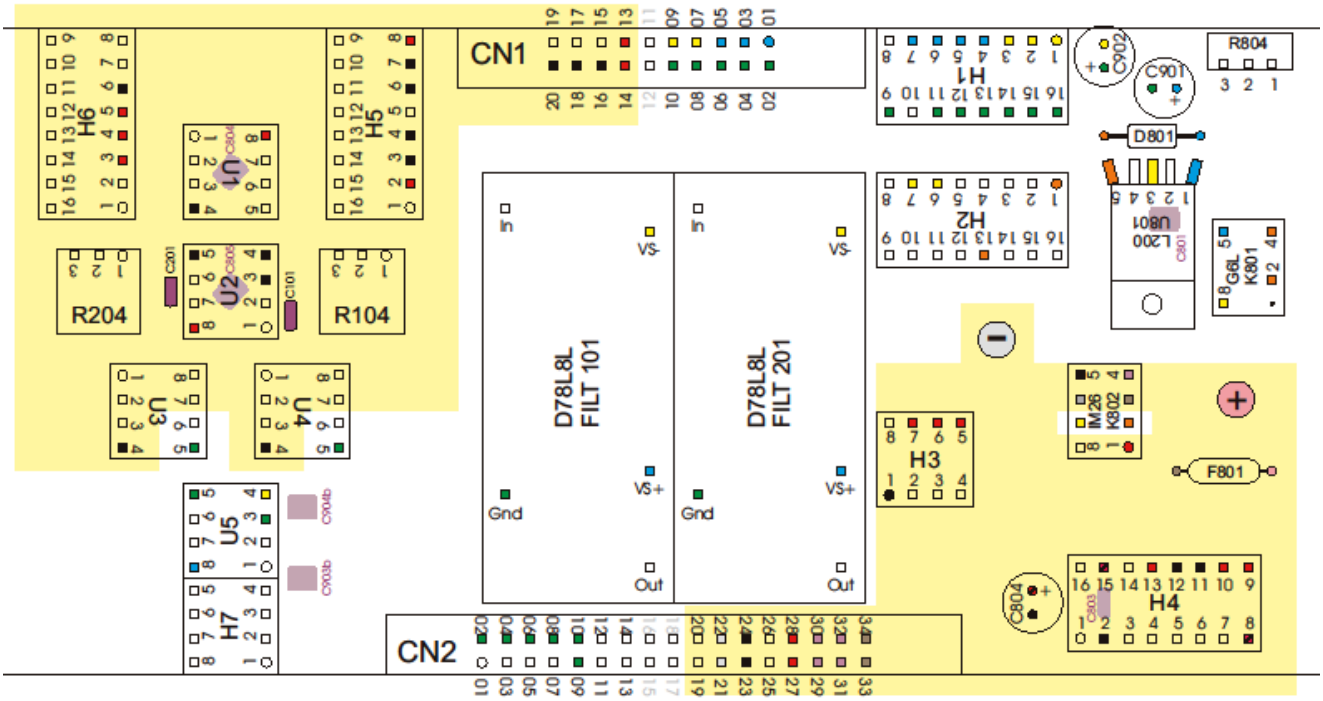

Optical Isolator Pictures

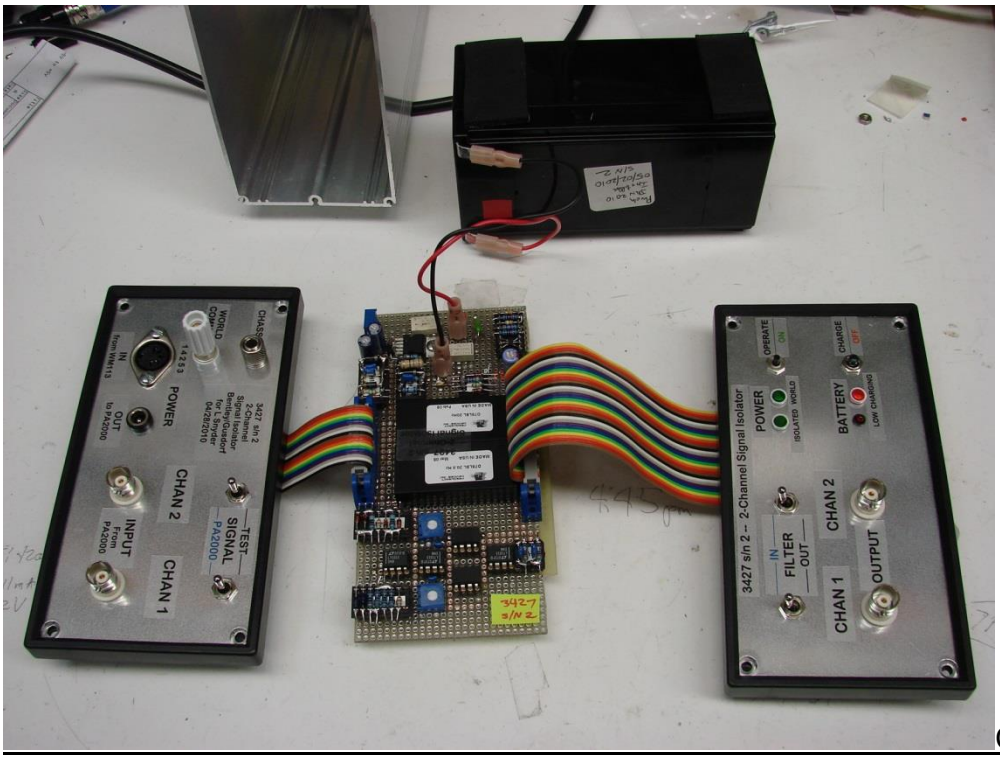

Case removed

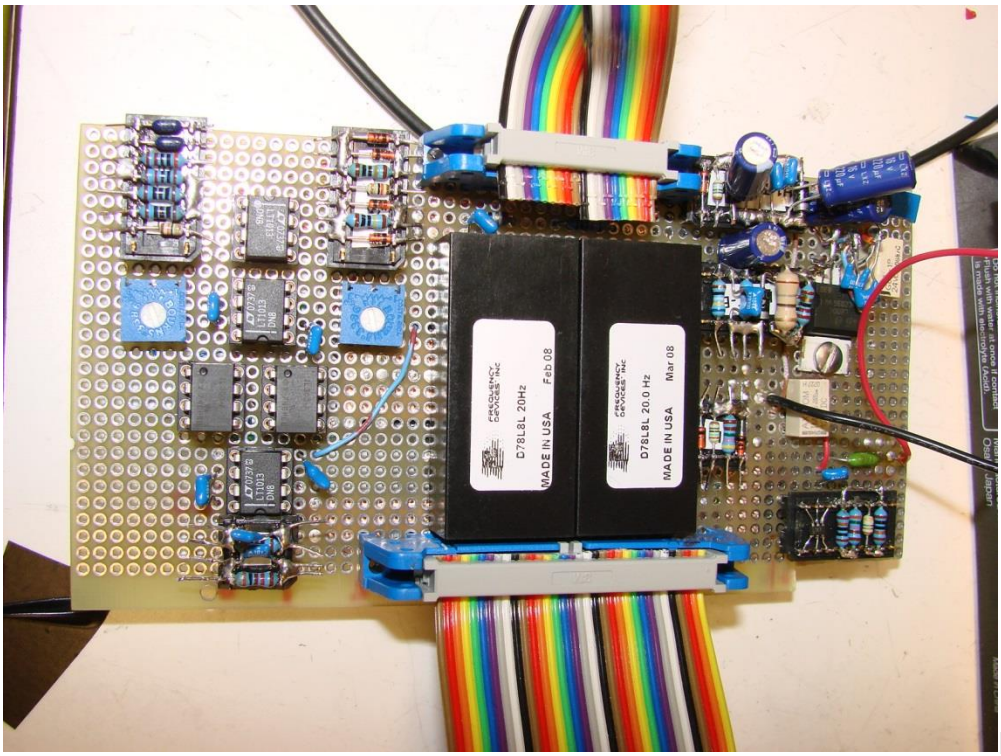

Main Board

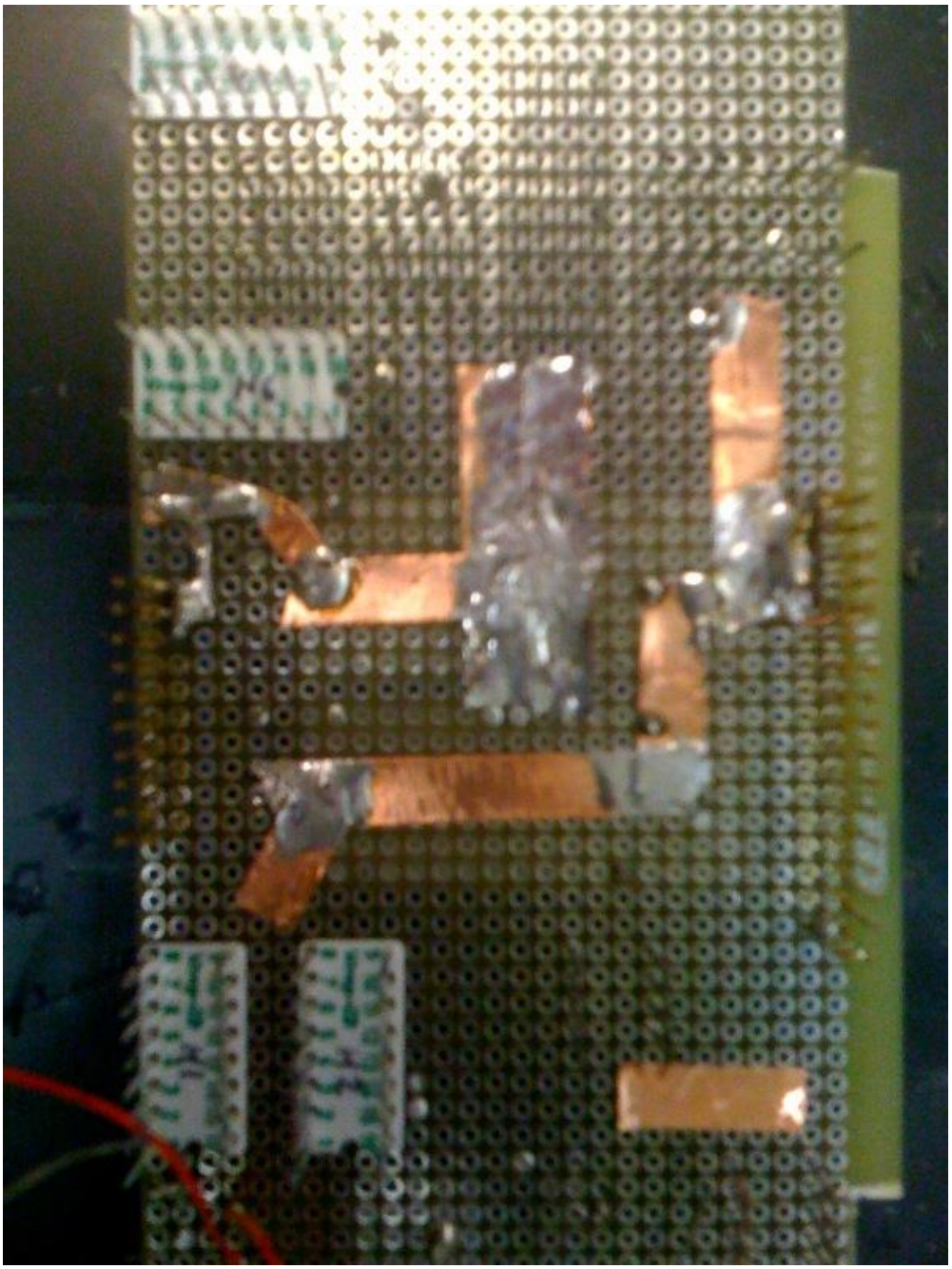

Separated Ground Planes

Rear Panel

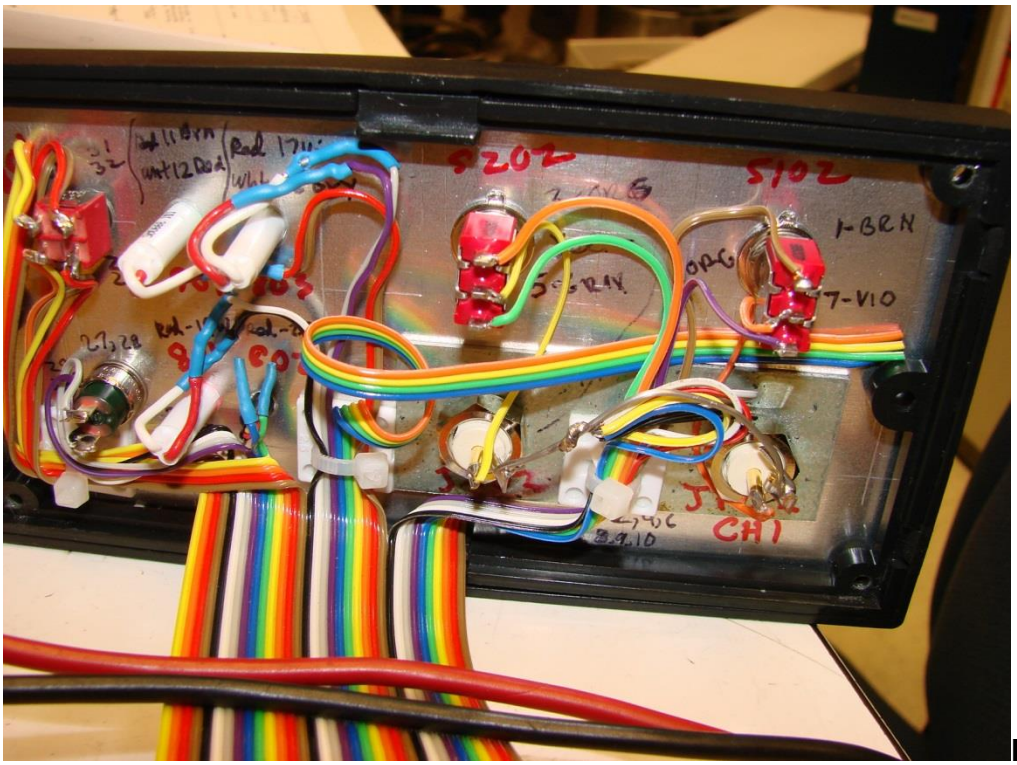

Front Panel

References

1. Raichle, M.E. and M.A. Mintun, *Brain work and brain imaging.* Annual Review of Neuroscience, 2006. **29**: p. 449-76.
2. Zhang, D. and M.E. Raichle, *Disease and the brain's dark energy.* Nature reviews. Neurology, 2010. **6**(1): p. 15-28.
3. Raichle, M.E. and M.A. Mintun, *Brain work and brain imaging.* Annu Rev Neurosci, 2006. **29**: p. 449-76.
4. Raichle, M.E., *Functional brain imaging and human brain function.* J Neurosci, 2003. **23**(10): p. 3959-62.
5. Buckner, R.L. and J.L. Vincent, *Unrest at rest: default activity and spontaneous network correlations.* Neuroimage, 2007. **37**(4): p. 1091-6; discussion 1097-9.
6. Fox, P.T. and M.E. Raichle, *Focal physiological uncoupling of cerebral blood flow and oxidative metabolism during somatosensory stimulation in human subjects.* Proceedings of the National Academy of Sciences of the United States of America, 1986. **83**(4): p. 1140-4.
7. Ogawa, S., et al., *Brain magnetic resonance imaging with contrast dependent on blood oxygenation.* Proc Natl Acad Sci U S A, 1990. **87**(24): p. 9868-72.
8. Fox, P.T., M.E. Raichle, and W.T. Thach, *Functional mapping of the human cerebellum with positron emission tomography.* Proceedings of the National Academy of Sciences of the United States of America, 1985. **82**(21): p. 7462-6.
9. Petersen, S.E., et al., *Positron emission tomographic studies of the cortical anatomy of single-word processing.* Nature, 1988. **331**(6157): p. 585-9.
10. Mintun, M.A., P.T. Fox, and M.E. Raichle, *A highly accurate method of localizing regions of neuronal activation in the human brain with positron emission tomography.* Journal of cerebral blood flow and metabolism : official journal of the International Society of Cerebral Blood Flow and Metabolism, 1989. **9**(1): p. 96-103.
11. Buxton, R.B., E.C. Wong, and L.R. Frank, *Dynamics of blood flow and oxygenation changes during brain activation: the balloon model.* Magnetic resonance in medicine : official journal of the Society of Magnetic Resonance in Medicine / Society of Magnetic Resonance in Medicine, 1998. **39**(6): p. 855-64.
12. Ogawa, S., et al., *Functional brain mapping by blood oxygenation level-dependent contrast magnetic resonance imaging. A comparison of signal characteristics with a biophysical model.* Biophys J, 1993. **64**(3): p. 803-12.
13. Ekstrom, A., *How and when the fMRI BOLD signal relates to underlying neural activity: the danger in dissociation.* Brain research reviews, 2010. **62**(2): p. 233-44.
14. Ekstrom, A., et al., *Correlation between BOLD fMRI and theta-band local field potentials in the human hippocampal area.* Journal of neurophysiology, 2009. **101**(5): p. 2668-78.
15. Rosa, M.J., et al., *Estimating the transfer function from neuronal activity to BOLD using simultaneous EEG-fMRI.* NeuroImage, 2010. **49**(2): p. 1496-1509.

16. Conner, C.R., et al., *Variability of the relationship between electrophysiology and BOLD-fMRI across cortical regions in humans.* The Journal of neuroscience : the official journal of the Society for Neuroscience, 2011. **31**(36): p. 12855-65.
17. Sloan, H.L., et al., *Regional differences in neurovascular coupling in rat brain as determined by fMRI and electrophysiology.* NeuroImage, 2010. **53**(2): p. 399-411.
18. Mishra, A.M., et al., *Where fMRI and electrophysiology agree to disagree: corticothalamic and striatal activity patterns in the WAG/Rij rat.* The Journal of neuroscience : the official journal of the Society for Neuroscience, 2011. **31**(42): p. 15053-64.
19. Bartolo, M.J., et al., *Stimulus-induced dissociation of neuronal firing rates and local field potential gamma power and its relationship to the resonance blood oxygen level-dependent signal in macaque primary visual cortex.* The European journal of neuroscience, 2011. **34**(11): p. 1857-70.
20. Sirotin, Y.B., et al., *Spatial homogeneity and task-synchrony of the trial-related hemodynamic signal.* NeuroImage, 2012. **59**(3): p. 2783-97.
21. Sirotin, Y.B. and A. Das, *Anticipatory haemodynamic signals in sensory cortex not predicted by local neuronal activity.* Nature, 2009. **457**(7228): p. 475-9.
22. Boynton, G.M., *Spikes, BOLD, attention, and awareness: a comparison of electrophysiological and fMRI signals in V1.* Journal of vision, 2011. **11**(5): p. 12.
23. Geukes, S., et al., *A Large N400 but No BOLD Effect - Comparing Source Activations of Semantic Priming in Simultaneous EEG-fMRI.* PloS one, 2013. **8**(12): p. e84029.
24. Devor, A., et al., *Suppressed neuronal activity and concurrent arteriolar vasoconstriction may explain negative blood oxygenation level-dependent signal.* J Neurosci, 2007. **27**(16): p. 4452-9.
25. Devor, A., et al., *Neuronal Basis of Non-Invasive Functional Imaging: From Microscopic Neurovascular Dynamics to BOLD fMRI.* 2012. **4**: p. 433-500.
26. Shmuel, A., et al., *Negative functional MRI response correlates with decreases in neuronal activity in monkey visual area V1.* Nature neuroscience, 2006. **9**(4): p. 569-77.
27. Magri, C., et al., *The amplitude and timing of the BOLD signal reflects the relationship between local field potential power at different frequencies.* The Journal of neuroscience : the official journal of the Society for Neuroscience, 2012. **32**(4): p. 1395-407.
28. Murayama, Y., et al., *Relationship between neural and hemodynamic signals during spontaneous activity studied with temporal kernel CCA.* Magnetic resonance imaging, 2010. **28**(8): p. 1095-103.
29. Shmuel, A. and D.A. Leopold, *Neuronal correlates of spontaneous fluctuations in fMRI signals in monkey visual cortex: Implications for functional connectivity at rest.* Hum Brain Mapp, 2008. **29**(7): p. 751-61.
30. Scholvinck, M.L., et al., *Neural basis of global resting-state fMRI activity.* Proceedings of the National Academy of Sciences of the United States of America, 2010. **107**(22): p. 10238-43.

31. Buxton, R.B., *Interpreting oxygenation-based neuroimaging signals: the importance and the challenge of understanding brain oxygen metabolism.* Frontiers in Neuroenergetics, 2010.
32. Shmuel, A. and D.A. Leopold, *Neuronal correlates of spontaneous fluctuations in fMRI signals in monkey visual cortex: Implications for functional connectivity at rest.* Human Brain Mapping, 2008. **29**(7): p. 751-61.
33. Maier, A., et al., *Divergence of fMRI and neural signals in V1 during perceptual suppression in the awake monkey.* Nature neuroscience, 2008. **11**(10): p. 1193-200.
34. Magri, C., et al., *The Amplitude and Timing of the BOLD Signal Reflects the Relationship between Local Field Potential Power at Different Frequencies.* Journal of Neuroscience, 2012. **32**(4): p. 1395-1407.
35. Goense, J., H. Merkle, and Nikos K. Logothetis, *High-Resolution fMRI Reveals Laminar Differences in Neurovascular Coupling between Positive and Negative BOLD Responses.* Neuron, 2012. **76**(3): p. 629-639.
36. Goense, J.B. and N.K. Logothetis, *Neurophysiology of the BOLD fMRI signal in awake monkeys.* Current biology : CB, 2008. **18**(9): p. 631-40.
37. Logothetis, N.K., et al., *Neurophysiological investigation of the basis of the fMRI signal.* Nature, 2001. **412**(6843): p. 150-7.
38. Goense, J.B. and N.K. Logothetis, *Laminar specificity in monkey V1 using high-resolution SE-fMRI.* Magn Reson Imaging, 2006. **24**(4): p. 381-92.
39. Tootell, R.B., D. Tsao, and W. Vanduffel, *Neuroimaging weighs in: humans meet macaques in "primate" visual cortex.* The Journal of neuroscience : the official journal of the Society for Neuroscience, 2003. **23**(10): p. 3981-9.
40. Cooper, R., *Local Chnages of Intra-Cerebral Blood Flow and Oxygen in Humans.* Med. Electron. Biol Engng, 1963. **1**: p. 539-536.
41. Moskalenko, Y.E., et al., *Variations in Blood Volume and Oxygen Availability in the Human Brain.* Nature, 1964. **202**: p. 159-61.
42. Cooper, R., et al., *Regional control of cerebral vascular reactivity and oxygen supply in man.* Brain Res, 1966. **3**(2): p. 174-91.
43. Davies, P.W.a.F.B., *Direct Measurement of the Brain Oxygen Concentration with a Platinum Electrode.* Fed Proc, 1942. **1**.
44. Davies, P.W. and D.W. Bronk, *Oxygen tension in mammalian brain.* Fed Proc, 1957. **16**(3): p. 689-92.
45. Thompson, J.K., M.R. Peterson, and R.D. Freeman, *Single-neuron activity and tissue oxygenation in the cerebral cortex.* Science, 2003. **299**(5609): p. 1070-2.
46. Thompson, J.K., M.R. Peterson, and R.D. Freeman, *Separate spatial scales determine neural activity-dependent changes in tissue oxygen within central visual pathways.* J Neurosci, 2005. **25**(39): p. 9046-58.
47. Li, B. and R.D. Freeman, *High-resolution neurometabolic coupling in the lateral geniculate nucleus.* J Neurosci, 2007. **27**(38): p. 10223-9.
48. Viswanathan, A. and R.D. Freeman, *Neurometabolic coupling in cerebral cortex reflects synaptic more than spiking activity.* Nat Neurosci, 2007.
49. Fatt, I., *Polarographic Oxygen Sensors.* CRC press, 1976. **Cleveland Ohio**.
50. Chapin, H., E. Bagarinao, and S. Mackey, *Real-time fMRI applied to pain management.* Neuroscience letters, 2012. **520**(2): p. 174-81.

51. Bruhl, A.B., et al., *Real-time Neurofeedback Using Functional MRI Could Improve Down-Regulation of Amygdala Activity During Emotional Stimulation: A Proof-of-Concept Study.* Brain topography, 2014. **27**(1): p. 138-48.
52. Buckner, R.L., F.M. Krienen, and B.T. Yeo, *Opportunities and limitations of intrinsic functional connectivity MRI.* Nature neuroscience, 2013. **16**(7): p. 832-7.
53. Deshpande, G. and X. Hu, *Investigating effective brain connectivity from fMRI data: past findings and current issues with reference to Granger causality analysis.* Brain connectivity, 2012. **2**(5): p. 235-45.
54. Mahmoudi, A., et al., *Multivoxel pattern analysis for FMRI data: a review.* Computational and mathematical methods in medicine, 2012. **2012**: p. 961257.
55. Fox, M.D. and M. Greicius, *Clinical applications of resting state functional connectivity.* Frontiers in systems neuroscience, 2010. **4**: p. 19.
56. Zhang, D., et al., *Preoperative sensorimotor mapping in brain tumor patients using spontaneous fluctuations in neuronal activity imaged with functional magnetic resonance imaging: initial experience.* Neurosurgery, 2009. **65**(6 Suppl): p. 226-36.
57. Shimony, J.S., et al., *Resting-state spontaneous fluctuations in brain activity: a new paradigm for presurgical planning using fMRI.* Academic radiology, 2009. **16**(5): p. 578-83.
58. Nelson, S.M., et al., *The critical roles of localization and physiology for understanding parietal contributions to memory retrieval.* The Neuroscientist : a review journal bringing neurobiology, neurology and psychiatry, 2013. **19**(6): p. 578-91.
59. Raichle, M.E., *Two views of brain function.* Trends in Cognitive Sciences, 2010. **14**(4): p. 180-90.
60. Menon, R.S., et al., *Functional brain mapping using magnetic resonance imaging. Signal changes accompanying visual stimulation.* Invest Radiol, 1992. **27 Suppl 2**: p. S47-53.
61. Raichle, M.E., *Functional brain imaging and human brain function.* The Journal of neuroscience : the official journal of the Society for Neuroscience, 2003. **23**(10): p. 3959-62.
62. Raichle, M.E., *A paradigm shift in functional brain imaging.* The Journal of neuroscience : the official journal of the Society for Neuroscience, 2009. **29**(41): p. 12729-34.
63. Fox, M.D. and M.E. Raichle, *Spontaneous fluctuations in brain activity observed with functional magnetic resonance imaging.* Nature reviews. Neuroscience, 2007. **8**(9): p. 700-11.
64. Song, M., et al., *Brain spontaneous functional connectivity and intelligence.* Neuroimage, 2008. **41**(3): p. 1168-76.
65. Smith, S.M., et al., *Correspondence of the brain's functional architecture during activation and rest.* Proceedings of the National Academy of Sciences of the United States of America, 2009. **106**(31): p. 13040-5.
66. Fox, M.D., et al., *Intrinsic fluctuations within cortical systems account for intertrial variability in human behavior.* Neuron, 2007. **56**(1): p. 171-84.
67. Fox, M.D., et al., *Spontaneous neuronal activity distinguishes human dorsal and ventral attention systems.* Proc Natl Acad Sci U S A, 2006. **103**(26): p. 10046-51.

68. Fox, M.D., et al., *The human brain is intrinsically organized into dynamic, anticorrelated functional networks.* Proc Natl Acad Sci U S A, 2005. **102**(27): p. 9673-8.
69. Boly, M., et al., *Baseline brain activity fluctuations predict somatosensory perception in humans.* Proc Natl Acad Sci U S A, 2007. **104**(29): p. 12187-92.
70. Biswal, B.B., et al., *Toward discovery science of human brain function.* Proceedings of the National Academy of Sciences of the United States of America, 2010. **107**(10): p. 4734-9.
71. Hampson, M., et al., *Connectivity-behavior analysis reveals that functional connectivity between left BA39 and Broca's area varies with reading ability.* Neuroimage, 2006. **31**(2): p. 513-9.
72. Hampson, M., et al., *Brain connectivity related to working memory performance.* J Neurosci, 2006. **26**(51): p. 13338-43.
73. Biswal, B., et al., *Functional connectivity in the motor cortex of resting human brain using echo-planar MRI.* Magn Reson Med, 1995. **34**(4): p. 537-41.
74. Sakmann, B. and E. Neher, *Patch clamp techniques for studying ionic channels in excitable membranes.* Annual review of physiology, 1984. **46**: p. 455-72.
75. Corporation, M.D., *The Axon CNS Guide to Electrophysiology & Biophysics Laboratory Techniques.* Molecular Devices, 2006.
76. Mutoh, H. and T. Knopfel, *Probing neuronal activities with genetically encoded optical indicators: from a historical to a forward-looking perspective.* Pflugers Archiv : European journal of physiology, 2013. **465**(3): p. 361-71.
77. Turaga, D. and T.E. Holy, *Organization of vomeronasal sensory coding revealed by fast volumetric calcium imaging.* The Journal of neuroscience : the official journal of the Society for Neuroscience, 2012. **32**(5): p. 1612-21.
78. Pesaran, B., *Uncovering the mysterious origins of local field potentials.* Neuron, 2009. **61**(1): p. 1-2.
79. Pan, W.J., et al., *Simultaneous FMRI and electrophysiology in the rodent brain.* Journal of visualized experiments : JoVE, 2010(42).
80. Logothetis, N.K., *The neural basis of the blood-oxygen-level-dependent functional magnetic resonance imaging signal.* Philos Trans R Soc Lond B Biol Sci, 2002. **357**(1424): p. 1003-37.
81. Laufs, H., et al., *Electroencephalographic signatures of attentional and cognitive default modes in spontaneous brain activity fluctuations at rest.* Proc Natl Acad Sci U S A, 2003. **100**(19): p. 11053-8.
82. Mantini, D., et al., *Electrophysiological signatures of resting state networks in the human brain.* Proc Natl Acad Sci U S A, 2007. **104**(32): p. 13170-5.
83. Larson-Prior, L., *Does alpha-band EEG activity in eyes-closed rest index a unitary state over time?* Human Brain Mapping Poster, 2006.
84. Thompson, G.J., et al., *Neural correlates of time-varying functional connectivity in the rat.* NeuroImage, 2013. **83**: p. 826-36.
85. Pan, W.J., et al., *Infraslow LFP correlates to resting-state fMRI BOLD signals.* NeuroImage, 2013. **74**: p. 288-97.
86. Goense, J.B., K. Whittingstall, and N.K. Logothetis, *Functional magnetic resonance imaging of awake behaving macaques.* Methods, 2010. **50**(3): p. 178-88.

87. Goense, J.B.M., K. Whittingstall, and N.K. Logothetis, *Functional magnetic resonance imaging of awake behaving macaques.* Methods, 2010. **50**(3): p. 178-188.
88. Passingham, R., *How good is the macaque monkey model of the human brain?* Current Opinion in Neurobiology, 2009. **19**(1): p. 6-11.
89. Kim, S.A. and S.B. Jun, *Optical Measurement of Neural Activity in the Brain.* Experimental neurobiology, 2013. **22**(3): p. 158-166.
90. Strangman, G., et al., *A quantitative comparison of simultaneous BOLD fMRI and NIRS recordings during functional brain activation.* Neuroimage, 2002. **17**(2): p. 719-31.
91. Franceschini, M.A., et al., *Hemodynamic evoked response of the sensorimotor cortex measured noninvasively with near-infrared optical imaging.* Psychophysiology, 2003. **40**(4): p. 548-60.
92. Bluestone, A., et al., *Three-dimensional optical tomography of hemodynamics in the human head.* Optics express, 2001. **9**(6): p. 272-86.
93. Brian R. White1, Adam Q. Bauer2., Abraham Z. Snyder2,3, Bradley L. Schlaggar2,3,4,5, Jin-Moo Lee3, and Joseph P. Culver1, 6, *Imaging of Functional Connectivity in the Mouse Brain.* Plos One, 2011.
94. Ts'o, D.Y., et al., *Functional organization of primate visual cortex revealed by high resolution optical imaging.* Science, 1990. **249**(4967): p. 417-20.
95. Arieli, A., et al., *Dynamics of ongoing activity: explanation of the large variability in evoked cortical responses.* Science, 1996. **273**(5283): p. 1868-71.
96. Grinvald, A., et al., *High-resolution optical imaging of functional brain architecture in the awake monkey.* Proceedings of the National Academy of Sciences of the United States of America, 1991. **88**(24): p. 11559-63.
97. Fuster, J., et al., *Near-infrared spectroscopy (NIRS) in cognitive neuroscience of the primate brain.* NeuroImage, 2005. **26**(1): p. 215-20.
98. Meyer, J.S., H.C. Fang, and D. Denny-Brown, *Polarographic study of cerebral collateral circulation.* AMA Arch Neurol Psychiatry, 1954. **72**(3): p. 296-312.
99. Halsey, J.H., Jr. and L.C. Clark, Jr., *Polarographic study of experimental cerebral infarction.* Neurology, 1968. **18**(3): p. 282.
100. Meyer, J.S. and J. Hunter, *Polarographic study of cortical blood flow in man.* J Neurosurg, 1957. **14**(4): p. 382-99.
101. Rice, E., *Polarographic Studies of Cats Auditory Cortex.* J. Neurophysiol, 1960. **23**(4): p. 350-362.
102. Jamieson, D. and H.A. Vandenbrenk, *Measurement of Oxygen Tensions in Cerebral Tissues of Rats Exposed to High Pressures of Oxygen.* J Appl Physiol, 1963. **18**: p. 869-76.
103. Cross, B.A.a.I.A.S., *Some Factors Affecting Oxygen Tension in the Brain and Other Organs.* Proceedings of the Royal Society of London - Series B: Biological Sciences, 1962. **156**.
104. Meyer, J.S. and J. Hunter, *Effects of hypothermia on local blood flow and metabolism during cerebral ischemia and hypoxia.* J Neurosurg, 1957. **14**(2): p. 210-27.
105. Crockard, H.A., et al., *Measurements of oxygen tension in the cerebral cortex of baboons.* J Neurol Sci, 1976. **27**(1): p. 17-28.

106. Ingvar, D.H., D.W. Lubbers, and B. Siesjo, *Measurement of oxygen tension on the surface of the cerebral cortex of the cat during hyperoxia and hypoxia.* Acta Physiol Scand, 1960. **48**: p. 373-81.
107. Cooper, C.E., D.T. Delpy, and E.M. Nemoto, *The relationship of oxygen delivery to absolute haemoglobin oxygenation and mitochondrial cytochrome oxidase redox state in the adult brain: a near-infrared spectroscopy study.* Biochem J, 1998. **332 (Pt 3)**: p. 627-32.
108. Crockard, H.A., et al., *Changes in regional cortical tissue oxygen tension and cerebral blood flow during temporary middle cerebral artery occlusion in baboons.* J Neurol Sci, 1976. **27**(1): p. 29-44.
109. Lowry, J.P., et al., *Real-time electrochemical monitoring of brain tissue oxygen: A surrogate for functional magnetic resonance imaging in rodents.* NeuroImage, 2010. **52**(2): p. 549-555.
110. Jennifer Li, D.S.B., 2 A. Louise Upton,2 Gary Gilmour,1 Mark D. Tricklebank,1 Marianne Fillenz,2 Chris Martin,3 and D.M.B.a.S.B.M. John P. Lowry, *Close temporal coupling of neuronal activity and tissue*

oxygen responses in rodent whisker barrel cortex. European Journal of Neuroscience, 2011. **34**: p. 1983-1996.
111. McHugh, S.B., et al., *Brain tissue oxygen amperometry in behaving rats demonstrates functional dissociation of dorsal and ventral hippocampus during spatial processing and anxiety.* European Journal of Neuroscience, 2011. **33**(2): p. 322-337.
112. McHugh, S.B., et al., *Brain tissue oxygen amperometry in behaving rats demonstrates functional dissociation of dorsal and ventral hippocampus during spatial processing and anxiety.* The European journal of neuroscience, 2011. **33**(2): p. 322-37.
113. Li, J., et al., *Close temporal coupling of neuronal activity and tissue oxygen responses in rodent whisker barrel cortex.* The European journal of neuroscience, 2011. **34**(12): p. 1983-96.
114. Bazzu, G., et al., *Real-time monitoring of brain tissue oxygen using a miniaturized biotelemetric device implanted in freely moving rats.* Analytical chemistry, 2009. **81**(6): p. 2235-41.
115. Manil, J., et al., *Properties of the spontaneous fluctuations in cortical oxygen pressure.* Advances in experimental medicine and biology, 1984. **169**: p. 231-9.
116. Burgess, D., *correlation Between Oxygen Cycels in Contralateral Regions of the Brain (Abstract).* Stroke, 1973. **4**: p. 374.
117. Linden, H., et al., *Modeling the spatial reach of the LFP.* Neuron, 2011. **72**(5): p. 859-72.
118. Leopold, D.A., Y. Murayama, and N.K. Logothetis, *Very slow activity fluctuations in monkey visual cortex: implications for functional brain imaging.* Cereb Cortex, 2003. **13**(4): p. 422-33.
119. Salvador, R., et al., *Undirected graphs of frequency-dependent functional connectivity in whole brain networks.* Philos Trans R Soc Lond B Biol Sci, 2005. **360**(1457): p. 937-46.
120. Shulman, G.L., et al., *Searching for activations that generalize over tasks.* Human Brain Mapping, 1997. **5**(4): p. 317-22.

121. Raichle, M.E., et al., *A default mode of brain function.* Proceedings of the National Academy of Sciences of the United States of America, 2001. **98**(2): p. 676-82.
122. Raichle, M.E. and A.Z. Snyder, *A default mode of brain function: a brief history of an evolving idea.* Neuroimage, 2007. **37**(4): p. 1083-90; discussion 1097-9.
123. Buckner, R.L., *The brain's default network: origins and implications for the study of psychosis.* Dialogues in clinical neuroscience, 2013. **15**(3): p. 351-8.
124. Gusnard, D.A., et al., *Medial prefrontal cortex and self-referential mental activity: relation to a default mode of brain function.* Proceedings of the National Academy of Sciences of the United States of America, 2001. **98**(7): p. 4259-64.
125. Spreng, R.N. and C.L. Grady, *Patterns of brain activity supporting autobiographical memory, prospection, and theory of mind, and their relationship to the default mode network.* Journal of cognitive neuroscience, 2010. **22**(6): p. 1112-23.
126. Schilbach, L., et al., *Minds at rest? Social cognition as the default mode of cognizing and its putative relationship to the "default system" of the brain.* Consciousness and cognition, 2008. **17**(2): p. 457-67.
127. Li, W., X. Mai, and C. Liu, *The default mode network and social understanding of others: what do brain connectivity studies tell us.* Frontiers in human neuroscience, 2014. **8**: p. 74.
128. Broyd, S.J., et al., *Default-mode brain dysfunction in mental disorders: a systematic review.* Neuroscience and Biobehavioral Reviews, 2009. **33**(3): p. 279-96.
129. Buckner, R.L., *The serendipitous discovery of the brain's default network.* Neuroimage, 2012. **62**(2): p. 1137-45.
130. Andrews-Hanna, J.R., et al., *Functional-anatomic fractionation of the brain's default network.* Neuron, 2010. **65**(4): p. 550-62.
131. Buckner, R.L., J.R. Andrews-Hanna, and D.L. Schacter, *The brain's default network: anatomy, function, and relevance to disease.* Annals of the New York Academy of Sciences, 2008. **1124**: p. 1-38.
132. Sheline, Y.I., et al., *The default mode network and self-referential processes in depression.* Proceedings of the National Academy of Sciences of the United States of America, 2009. **106**(6): p. 1942-7.
133. Brewer, J.A., K.A. Garrison, and S. Whitfield-Gabrieli, *What about the "Self" is Processed in the Posterior Cingulate Cortex?* Frontiers in human neuroscience, 2013. **7**: p. 647.
134. Garrison, K.A., et al., *Effortless awareness: using real time neurofeedback to investigate correlates of posterior cingulate cortex activity in meditators' self-report.* Frontiers in human neuroscience, 2013. **7**: p. 440.
135. Pearson, J.M., et al., *Posterior cingulate cortex: adapting behavior to a changing world.* Trends in cognitive sciences, 2011. **15**(4): p. 143-51.
136. Pearson, J.M., et al., *Neurons in posterior cingulate cortex signal exploratory decisions in a dynamic multioption choice task.* Current biology : CB, 2009. **19**(18): p. 1532-7.
137. Hayden, B.Y., D.V. Smith, and M.L. Platt, *Cognitive control signals in posterior cingulate cortex.* Frontiers in human neuroscience, 2010. **4**: p. 223.

138. Hayden, B.Y., D.V. Smith, and M.L. Platt, *Electrophysiological correlates of default-mode processing in macaque posterior cingulate cortex.* Proceedings of the National Academy of Sciences of the United States of America, 2009. **106**(14): p. 5948-53.
139. Ossandon, T., et al., *Transient suppression of broadband gamma power in the default-mode network is correlated with task complexity and subject performance.* The Journal of neuroscience : the official journal of the Society for Neuroscience, 2011. **31**(41): p. 14521-30.
140. Jerbi, K., et al., *Exploring the electrophysiological correlates of the default-mode network with intracerebral EEG.* Frontiers in systems neuroscience, 2010. **4**: p. 27.
141. Foster, B.L. and J. Parvizi, *Resting oscillations and cross-frequency coupling in the human posteromedial cortex.* NeuroImage, 2012. **60**(1): p. 384-91.
142. Foster, B.L., M. Dastjerdi, and J. Parvizi, *Neural populations in human posteromedial cortex display opposing responses during memory and numerical processing.* Proceedings of the National Academy of Sciences of the United States of America, 2012. **109**(38): p. 15514-9.
143. Dastjerdi, M., et al., *Differential electrophysiological response during rest, self-referential, and non-self-referential tasks in human posteromedial cortex.* Proceedings of the National Academy of Sciences of the United States of America, 2011. **108**(7): p. 3023-8.
144. Fox, M.D. and M.E. Raichle, *Spontaneous fluctuations in brain activity observed with functional magnetic resonance imaging.* Nat Rev Neurosci, 2007. **8**(9): p. 700-11.
145. Dosenbach, N.U., et al., *Distinct brain networks for adaptive and stable task control in humans.* Proc Natl Acad Sci U S A, 2007. **104**(26): p. 11073-8.
146. Vincent, J.L., et al., *Coherent spontaneous activity identifies a hippocampal-parietal memory network.* J Neurophysiol, 2006. **96**(6): p. 3517-31.
147. Vincent, J.L., et al., *Intrinsic functional architecture in the anaesthetized monkey brain.* Nature, 2007. **447**(7140): p. 83-6.
148. Biswal, B.B. and S.S. Kannurpatti, *Resting-state functional connectivity in animal models: modulations by exsanguination.* Methods Mol Biol, 2009. **489**: p. 255-74.
149. Pawela, C.P., et al., *Resting-state functional connectivity of the rat brain.* Magn Reson Med, 2008. **59**(5): p. 1021-9.
150. Boly, M., et al., *Intrinsic brain activity in altered states of consciousness: how conscious is the default mode of brain function?* Ann N Y Acad Sci, 2008. **1129**: p. 119-29.
151. Cordes, D., et al., *Mapping functionally related regions of brain with functional connectivity MR imaging.* AJNR Am J Neuroradiol, 2000. **21**(9): p. 1636-44.
152. Sun, F.T., et al., *Functional connectivity of cortical networks involved in bimanual motor sequence learning.* Cereb Cortex, 2007. **17**(5): p. 1227-34.
153. Harrison, B.J., et al., *Modulation of brain resting-state networks by sad mood induction.* PLoS ONE, 2008. **3**(3): p. e1794.
154. Dhond, R.P., et al., *Acupuncture modulates resting state connectivity in default and sensorimotor brain networks.* Pain, 2008.

155. Cherkassky, V.L., et al., *Functional connectivity in a baseline resting-state network in autism.* Neuroreport, 2006. **17**(16): p. 1687-90.
156. Toni, I., et al., *The time course of changes during motor sequence learning: a whole-brain fMRI study.* Neuroimage, 1998. **8**(1): p. 50-61.
157. Villalobos, M.E., et al., *Reduced functional connectivity between V1 and inferior frontal cortex associated with visuomotor performance in autism.* Neuroimage, 2005. **25**(3): p. 916-25.
158. Bluhm, R.L., et al., *Spontaneous low-frequency fluctuations in the BOLD signal in schizophrenic patients: anomalies in the default network.* Schizophr Bull, 2007. **33**(4): p. 1004-12.
159. Zhou, Y., et al., *Functional dysconnectivity of the dorsolateral prefrontal cortex in first-episode schizophrenia using resting-state fMRI.* Neurosci Lett, 2007. **417**(3): p. 297-302.
160. Wolf, D.H., et al., *Alterations of fronto-temporal connectivity during word encoding in schizophrenia.* Psychiatry Res, 2007. **154**(3): p. 221-32.
161. Greicius, M.D., et al., *Resting-state functional connectivity in major depression: abnormally increased contributions from subgenual cingulate cortex and thalamus.* Biol Psychiatry, 2007. **62**(5): p. 429-37.
162. He, B.J., et al., *Breakdown of functional connectivity in frontoparietal networks underlies behavioral deficits in spatial neglect.* Neuron, 2007. **53**(6): p. 905-18.
163. Moore, C.I. and R. Cao, *The Hemo-Neural Hypothesis: On The Role of Blood Flow in Information Processing.* J Neurophysiol, 2007.
164. Golanov, E.V., S. Yamamoto, and D.J. Reis, *Spontaneous waves of cerebral blood flow associated with a pattern of electrocortical activity.* Am J Physiol, 1994. **266**(1 Pt 2): p. R204-14.
165. Vern, B.A., et al., *Interhemispheric synchrony of slow oscillations of cortical blood volume and cytochrome aa3 redox state in unanesthetized rabbits.* Brain Res, 1997. **775**(1-2): p. 233-9.
166. Halsey, J.H., Jr. and S. McFarland, *Oxygen cycles and metabolic autoregulation.* Stroke, 1974. **5**(2): p. 219-25.
167. Bero, A.W., et al., *Bidirectional Relationship between Functional Connectivity and Amyloid- Deposition in Mouse Brain.* Journal of Neuroscience, 2012. **32**(13): p. 4334-4340.
168. White, B.R., et al., *Bedside optical imaging of occipital resting-state functional connectivity in neonates.* Neuroimage, 2012. **59**(3): p. 2529-38.
169. White, B.R., et al., *Resting-state functional connectivity in the human brain revealed with diffuse optical tomography.* Neuroimage, 2009. **47**(1): p. 148-56.
170. Magnuson, M.E., et al., *Effects of severing the corpus callosum on electrical and BOLD functional connectivity and spontaneous dynamic activity in the rat brain.* Brain connectivity, 2013.
171. Albrecht, D., G. Royl, and Y. Kaneoke, *Very slow oscillatory activities in lateral geniculate neurons of freely moving and anesthetized rats.* Neuroscience research, 1998. **32**(3): p. 209-20.
172. Pan, W.-J., et al., *Broadband Local Field Potentials Correlate with Spontaneous Fluctuations in Functional Magnetic Resonance Imaging Signals in the Rat*

Somatosensory Cortex Under Isoflurane Anesthesia. Brain Connectivity, 2011. **1**(2): p. 119-131.
173. Honey, C.J., et al., *Predicting human resting-state functional connectivity from structural connectivity.* Proceedings of the National Academy of Sciences of the United States of America, 2009. **106**(6): p. 2035-40.
174. He, B.J., *Scale-Free Properties of the Functional Magnetic Resonance Imaging Signal during Rest and Task.* Journal of Neuroscience, 2011. **31**(39): p. 13786-13795.
175. Baria, A.T., et al., *Anatomical and functional assemblies of brain BOLD oscillations.* The Journal of neuroscience : the official journal of the Society for Neuroscience, 2011. **31**(21): p. 7910-9.
176. Chang, C. and G.H. Glover, *Time-frequency dynamics of resting-state brain connectivity measured with fMRI.* NeuroImage, 2010. **50**(1): p. 81-98.
177. Zuo, X.N., et al., *The oscillating brain: complex and reliable.* NeuroImage, 2010. **49**(2): p. 1432-45.
178. Beckmann, C.F., et al., *Investigations into resting-state connectivity using independent component analysis.* Philosophical transactions of the Royal Society of London. Series B, Biological sciences, 2005. **360**(1457): p. 1001-13.
179. Wu, C.W., et al., *Frequency specificity of functional connectivity in brain networks.* Neuroimage, 2008. **42**(3): p. 1047-55.
180. Steriade, M. and M. Deschenes, *[Fluctuations in excitability of precentral cortex interneurons in the monkey free of its movements during slow sleep and awakening].* Journal de physiologie, 1972. **65**: p. Suppl 3:507A.
181. Steriade, M., R.C. Dossi, and A. Nunez, *Network modulation of a slow intrinsic oscillation of cat thalamocortical neurons implicated in sleep delta waves: cortically induced synchronization and brainstem cholinergic suppression.* The Journal of neuroscience : the official journal of the Society for Neuroscience, 1991. **11**(10): p. 3200-17.
182. Steriade, M., *Cholinergic blockage of network- and intrinsically generated slow oscillations promotes waking and REM sleep activity patterns in thalamic and cortical neurons.* Progress in brain research, 1993. **98**: p. 345-55.
183. Steriade, M., et al., *The slow (< 1 Hz) oscillation in reticular thalamic and thalamocortical neurons: scenario of sleep rhythm generation in interacting thalamic and neocortical networks.* The Journal of neuroscience : the official journal of the Society for Neuroscience, 1993. **13**(8): p. 3284-99.
184. Contreras, D., I. Timofeev, and M. Steriade, *Mechanisms of long-lasting hyperpolarizations underlying slow sleep oscillations in cat corticothalamic networks.* The Journal of physiology, 1996. **494 (Pt 1)**: p. 251-64.
185. Steriade, M., *Synchronized activities of coupled oscillators in the cerebral cortex and thalamus at different levels of vigilance.* Cerebral cortex, 1997. **7**(6): p. 583-604.
186. Ward, L.M., *Synchronous neural oscillations and cognitive processes.* Trends in cognitive sciences, 2003. **7**(12): p. 553-9.
187. Buzsaki, G. and A. Draguhn, *Neuronal oscillations in cortical networks.* Science, 2004. **304**(5679): p. 1926-9.

188. Pletzer, B., H. Kerschbaum, and W. Klimesch, *When frequencies never synchronize: the golden mean and the resting EEG.* Brain research, 2010. **1335**: p. 91-102.
189. Kim, S.-G. and P.A. Bandettini, *Principles of BOLD Functional MRI*, 2011, Springer US: Boston, MA. p. 293-303.
190. Rabrait, C., et al., *High temporal resolution functional MRI using parallel echo volumar imaging.* J Magn Reson Imaging, 2008. **27**(4): p. 744-53.
191. Huettel, S.A., *Functional magnetic resonance imaging ; Scott A. Huettel, Allen W. Song, Gregory McCarthy.* Sunderland, Mass. : Sinauer Associates, 2004.
192. Heyrovsky, J., *The fundamental laws of polarography.* The Analyst, 1947. **72**(855): p. 229-34.
193. Heyrovsky, M., *JAROSLAV HEYROVSKY AND POLAROGRAPHY* The Jaroslav Heyrovsky Institute of Physical Chemistry, Academy of Sciences of the Czech Republic 182 23 Prague 8, Czech Republic 2005. **http://electrochem.cwru.edu/encycl/art-p03-polarography.htm**.
194. Thompson, J.K., M.R. Peterson, and R.D. Freeman, *Separate spatial scales determine neural activity-dependent changes in tissue oxygen within central visual pathways.* The Journal of neuroscience : the official journal of the Society for Neuroscience, 2005. **25**(39): p. 9046-58.
195. Bronk, D.W., M.G. Larrabee, and P.W. Davies, *The rate of oxygen consumption in localized regions of the nervous system: in presynaptic endings and in cell bodies.* Fed Proc, 1946. **5**(1): p. 11.
196. Clark, L.C., Jr., et al., *Continuous recording of blood oxygen tensions by polarography.* J Appl Physiol, 1953. **6**(3): p. 189-93.
197. Clark, L.C., Jr. and G. Sachs, *Bioelectrodes for tissue metabolism.* Ann N Y Acad Sci, 1968. **148**(1): p. 133-53.
198. Vanderkooi, J.M., M. Erecinska, and I.A. Silver, *Oxygen in mammalian tissue: methods of measurement and affinities of various reactions.* Am J Physiol, 1991. **260**(6 Pt 1): p. C1131-50.
199. Heeger, D.J. and D. Ress, *What does fMRI tell us about neuronal activity?* Nature reviews. Neuroscience, 2002. **3**(2): p. 142-51.
200. Nir, Y., et al., *Coupling between neuronal firing rate, gamma LFP, and BOLD fMRI is related to interneuronal correlations.* Current biology : CB, 2007. **17**(15): p. 1275-85.
201. Lustig, C., et al., *Functional deactivations: change with age and dementia of the Alzheimer type.* Proceedings of the National Academy of Sciences of the United States of America, 2003. **100**(24): p. 14504-9.
202. Shmuel, A., et al., *Negative functional MRI response correlates with decreases in neuronal activity in monkey visual area V1.* Nat Neurosci, 2006. **9**(4): p. 569-77.
203. Logothetis, N.K., C. Kayser, and A. Oeltermann, *In vivo measurement of cortical impedance spectrum in monkeys: implications for signal propagation.* Neuron, 2007. **55**(5): p. 809-23.
204. Mantini, D., et al., *Default mode of brain function in monkeys.* The Journal of neuroscience : the official journal of the Society for Neuroscience, 2011. **31**(36): p. 12954-62.

205. Kojima, T., et al., *Default mode of brain activity demonstrated by positron emission tomography imaging in awake monkeys: higher rest-related than working memory-related activity in medial cortical areas.* The Journal of neuroscience : the official journal of the Society for Neuroscience, 2009. **29**(46): p. 14463-71.
206. Martindale, J., et al., *Long duration stimuli and nonlinearities in the neural-haemodynamic coupling.* Journal of cerebral blood flow and metabolism : official journal of the International Society of Cerebral Blood Flow and Metabolism, 2005. **25**(5): p. 651-61.
207. Raichle, M.E. and D.A. Gusnard, *Intrinsic brain activity sets the stage for expression of motivated behavior.* J Comp Neurol, 2005. **493**(1): p. 167-76.
208. McAvoy, M., et al., *Resting states affect spontaneous BOLD oscillations in sensory and paralimbic cortex.* J Neurophysiol, 2008. **100**(2): p. 922-31.
209. Collin, G., et al., *Structural and Functional Aspects Relating to Cost and Benefit of Rich Club Organization in the Human Cerebral Cortex.* Cerebral Cortex, 2013.
210. Bullmore, E. and O. Sporns, *Complex brain networks: graph theoretical analysis of structural and functional systems.* Nature reviews. Neuroscience, 2009. **10**(3): p. 186-98.
211. Damoiseaux, J.S. and M.D. Greicius, *Greater than the sum of its parts: a review of studies combining structural connectivity and resting-state functional connectivity.* Brain structure & function, 2009. **213**(6): p. 525-33.
212. Honey, C.J., et al., *Network structure of cerebral cortex shapes functional connectivity on multiple time scales.* Proceedings of the National Academy of Sciences of the United States of America, 2007. **104**(24): p. 10240-5.
213. van den Heuvel, M.P. and O. Sporns, *An anatomical substrate for integration among functional networks in human cortex.* The Journal of neuroscience : the official journal of the Society for Neuroscience, 2013. **33**(36): p. 14489-500.
214. Sporns, O. and C.J. Honey, *Topographic dynamics in the resting brain.* Neuron, 2013. **78**(6): p. 955-6.
215. Sporns, O., *Structure and function of complex brain networks.* Dialogues in clinical neuroscience, 2013. **15**(3): p. 247-62.
216. Suthana, N., et al., *Dissociations within human hippocampal subregions during encoding and retrieval of spatial information.* Hippocampus, 2011. **21**(7): p. 694-701.
217. He, B.J., et al., *The temporal structures and functional significance of scale-free brain activity.* Neuron, 2010. **66**(3): p. 353-69.
218. Obrig, H., et al., *Spontaneous low frequency oscillations of cerebral hemodynamics and metabolism in human adults.* Neuroimage, 2000. **12**(6): p. 623-39.
219. Cordes, D., et al., *Frequencies contributing to functional connectivity in the cerebral cortex in "resting-state" data.* AJNR. American journal of neuroradiology, 2001. **22**(7): p. 1326-33.
220. Compston, A., *The Berger rhythm: potential changes from the occipital lobes in man.* Brain : a journal of neurology, 2010. **133**(Pt 1): p. 3-6.

221. Steriade, M., A. Nunez, and F. Amzica, *A novel slow (< 1 Hz) oscillation of neocortical neurons in vivo: depolarizing and hyperpolarizing components.* J Neurosci, 1993. **13**(8): p. 3252-65.
222. Berger, H., *Über das Elektroenkephalogram des Menschen.* Arch. f. Psychiat, 1929. **87**: p. 527-70. .
223. Fekete, T., et al., *The NIRS Analysis Package: noise reduction and statistical inference.* PLoS One, 2011. **6**(9): p. e24322.
224. Yasuma, F. and J. Hayano, *Respiratory sinus arrhythmia: why does the heartbeat synchronize with respiratory rhythm?* Chest, 2004. **125**(2): p. 683-90.
225. Chang, C., J.P. Cunningham, and G.H. Glover, *Influence of heart rate on the BOLD signal: the cardiac response function.* Neuroimage, 2009. **44**(3): p. 857-69.
226. Chang, C. and G.H. Glover, *Effects of model-based physiological noise correction on default mode network anti-correlations and correlations.* Neuroimage, 2009. **47**(4): p. 1448-59.
227. Honey, C.J., et al., *Network structure of cerebral cortex shapes functional connectivity on multiple time scales.* Proc Natl Acad Sci U S A, 2007. **104**(24): p. 10240-5.
228. Oakson, G. and M. Steriade, *Slow rhythmic rate fluctuations of cat midbrain reticular neurons in synchronized sleep and waking.* Brain research, 1982. **247**(2): p. 277-88.
229. Steriade, M., A. Nunez, and F. Amzica, *Intracellular analysis of relations between the slow (< 1 Hz) neocortical oscillation and other sleep rhythms of the electroencephalogram.* The Journal of neuroscience : the official journal of the Society for Neuroscience, 1993. **13**(8): p. 3266-83.
230. Contreras, D. and M. Steriade, *Synchronization of low-frequency rhythms in corticothalamic networks.* Neuroscience, 1997. **76**(1): p. 11-24.
231. Steriade, M. and F. Amzica, *Slow sleep oscillation, rhythmic K-complexes, and their paroxysmal developments.* Journal of sleep research, 1998. **7 Suppl 1**: p. 30-5.
232. Hutcheon, B. and Y. Yarom, *Resonance, oscillation and the intrinsic frequency preferences of neurons.* Trends in neurosciences, 2000. **23**(5): p. 216-22.
233. Compte, A., et al., *Cellular and network mechanisms of slow oscillatory activity (<1 Hz) and wave propagations in a cortical network model.* Journal of neurophysiology, 2003. **89**(5): p. 2707-25.
234. Vanhatalo, S., et al., *Infraslow oscillations modulate excitability and interictal epileptic activity in the human cortex during sleep.* Proceedings of the National Academy of Sciences of the United States of America, 2004. **101**(14): p. 5053-7.
235. Filippov, I.V., et al., *Dynamics of infraslow potentials in the primary auditory cortex: component analysis and contribution of specific thalamic-cortical and non-specific brainstem-cortical influences.* Brain research, 2008. **1219**: p. 66-77.
236. Hughes, S.W., et al., *Novel modes of rhythmic burst firing at cognitively-relevant frequencies in thalamocortical neurons.* Brain research, 2008. **1235**: p. 12-20.
237. Monto, S., et al., *Very slow EEG fluctuations predict the dynamics of stimulus detection and oscillation amplitudes in humans.* The Journal of neuroscience : the official journal of the Society for Neuroscience, 2008. **28**(33): p. 8268-72.

238. Ko, A.L., et al., *Quasi-periodic fluctuations in default mode network electrophysiology.* The Journal of neuroscience : the official journal of the Society for Neuroscience, 2011. **31**(32): p. 11728-32.
239. Zanatta, P., et al., *The human brain pacemaker: Synchronized infra-slow neurovascular coupling in patients undergoing non-pulsatile cardiopulmonary bypass.* NeuroImage, 2013. **72**: p. 10-9.
240. Hiltunen, T., et al., *Infra-slow EEG fluctuations are correlated with resting-state network dynamics in fMRI.* The Journal of neuroscience : the official journal of the Society for Neuroscience, 2014. **34**(2): p. 356-62.
241. Ruskin, D.N., et al., *Multisecond oscillations in firing rate in the basal ganglia: robust modulation by dopamine receptor activation and anesthesia.* Journal of neurophysiology, 1999. **81**(5): p. 2046-55.
242. Ruskin, D.N., D.A. Bergstrom, and J.R. Walters, *Multisecond oscillations in firing rate in the globus pallidus: synergistic modulation by D1 and D2 dopamine receptors.* The Journal of pharmacology and experimental therapeutics, 1999. **290**(3): p. 1493-501.
243. Ruskin, D.N., et al., *Correlated multisecond oscillations in firing rate in the basal ganglia: modulation by dopamine and the subthalamic nucleus.* Neuroscience, 2003. **117**(2): p. 427-438.
244. Leisman, G. and R. Melillo, *The basal ganglia: motor and cognitive relationships in a clinical neurobehavioral context.* Reviews in the neurosciences, 2013. **24**(1): p. 9-25.
245. Hughes, S.W., et al., *Infraslow (<0.1 Hz) oscillations in thalamic relay nuclei basic mechanisms and significance to health and disease states.* Progress in brain research, 2011. **193**: p. 145-62.
246. He, J., *Slow oscillation in non-lemniscal auditory thalamus.* The Journal of neuroscience : the official journal of the Society for Neuroscience, 2003. **23**(23): p. 8281-90.
247. Lorincz, M.L., et al., *ATP-dependent infra-slow (<0.1 Hz) oscillations in thalamic networks.* PloS one, 2009. **4**(2): p. e4447.
248. Moore, C.I. and R. Cao, *The hemo-neural hypothesis: on the role of blood flow in information processing.* Journal of neurophysiology, 2008. **99**(5): p. 2035-47.
249. Cunningham, M.O., et al., *Neuronal metabolism governs cortical network response state.* Proceedings of the National Academy of Sciences of the United States of America, 2006. **103**(14): p. 5597-601.
250. Parri, H.R., T.M. Gould, and V. Crunelli, *Spontaneous astrocytic Ca2+ oscillations in situ drive NMDAR-mediated neuronal excitation.* Nature neuroscience, 2001. **4**(8): p. 803-12.
251. Parri, H.R. and V. Crunelli, *Pacemaker calcium oscillations in thalamic astrocytes in situ.* Neuroreport, 2001. **12**(18): p. 3897-900.
252. Palva, J.M. and S. Palva, *Infra-slow fluctuations in electrophysiological recordings, blood-oxygenation-level-dependent signals, and psychophysical time series.* NeuroImage, 2012. **62**(4): p. 2201-11.
253. Rubinov, M., et al., *Neurobiologically realistic determinants of self-organized criticality in networks of spiking neurons.* PLoS computational biology, 2011. **7**(6): p. e1002038.

254. Friedman, N., et al., *Universal critical dynamics in high resolution neuronal avalanche data.* Physical review letters, 2012. **108**(20): p. 208102.
255. Beggs, J.M. and N. Timme, *Being critical of criticality in the brain.* Frontiers in physiology, 2012. **3**: p. 163.
256. Kitzbichler, M.G., et al., *Broadband criticality of human brain network synchronization.* PLoS computational biology, 2009. **5**(3): p. e1000314.
257. Boonstra, T.W., B.J. He, and A. Daffertshofer, *Scale-free dynamics and critical phenomena in cortical activity.* Frontiers in physiology, 2013. **4**: p. 79.
258. He, B.J., *Scale-free properties of the functional magnetic resonance imaging signal during rest and task.* The Journal of neuroscience : the official journal of the Society for Neuroscience, 2011. **31**(39): p. 13786-95.
259. Muramoto, K., et al., *Frequency of synchronous oscillations of neuronal activity increases during development and is correlated to the number of synapses in cultured cortical neuron networks.* Neuroscience letters, 1993. **163**(2): p. 163-5.
260. Yuan, D., M. Zhang, and J. Yang, *Dynamics of the Kuramoto model in the presence of correlation between distributions of frequencies and coupling strengths.* Physical review. E, Statistical, nonlinear, and soft matter physics, 2014. **89**(1-1): p. 012910.
261. Meier, M., R. Haschke, and H.J. Ritter, *Perceptual grouping by entrainment in coupled kuramoto oscillator networks.* Network, 2014. **25**(1-2): p. 72-84.
262. Yaseen, M.A., et al., *Microvascular oxygen tension and flow measurements in rodent cerebral cortex during baseline conditions and functional activation.* Journal of Cerebral Blood Flow & Metabolism, 2010. **31**(4): p. 1051-1063.
263. Kim, D.S., et al., *Spatial relationship between neuronal activity and BOLD functional MRI.* Neuroimage, 2004. **21**(3): p. 876-85.
264. Jones, D.T., et al., *Non-stationarity in the "resting brain's" modular architecture.* Plos One, 2012. **7**(6): p. e39731.